Characterisation, Interpretation and Implications of the Adelaide Urban Heat Island

Huade Guan[1, 2], John Bennett[1], Cäcilia Ewenz[1], Simon Benger[1], Vinodkumar[1, 2], Shanyou Zhu[1], Roger Clay[3], Veronica Soebarto[4]

[1]School of the Environment, Flinders University

[2]National Centre for Groundwater Research and Training

[3]School of Chemistry and Physics, University of Adelaide

[4]School of Architecture and Built Environment, University of Adelaide

June 2013

Adelaide, Australia

ACKNOWLEDGEMENTS

This research has been funded by the following organisations through three projects:

(1) Joint research project "Investigation of the Parkland Impacts on the Urban Heat-island Intensity in the Adeladie Metropolitan Area" between Flinders Universtiy and the Department of Planning and Local Government , 2009-2010.
   - Funded by the Department of Planning Transport and Infrastructure (then Department of Planning and Local Government), and
   - Flinders University through the Flinders Research Centre for Coast and Catchment, Flinders Water, and Flinders Collaborative Research Grant Scheme (seed grant in 2008).

(2) Adelaide Urban Heat Island Research, 2010-2011
   - Funded by the Department of the Premier and Cabinet through the Capital City Committee Project Team.

(3) Joint research project "City of Adelaide Urban Heat Island Micro-Climate Study" between Flinders University and the Adelaide City Council, 2011-2012
   - Funded by the Department of Environment, Water and Natural Resources, through the University Sector Agreement Research Fund, and
   - Adelaide City Council
   - Managed by the Environment Research Hub, Flinders University

Many organisations have kindly provided data or facility support. They are: SA Power Networks, the Bureau of Meteorology (Kent Town Office), the Environment Protection Authority, the Adelaide City Council, Airborne Research Australia, and The University of Adelaide.

Prof. Craig Simmons, Emeritus Professor Peter Schwerdtfeger, and Mr. Graeme Hopkins are thanked for providing assistance with project ideas at an early stage. Kathryn Bellette, Prof. Criag Simmons, and Prof. Andrew Millington are appreciated for their efforts to liaise with governmental agencies and industrial partners for the project.

Many Honours and PhD students have assisted in data collection and analyses. They are Chris Kent, Chuanyu Zhu, Yunhui Guo, Robert Andrew, Ñorman Rößger, Saeedeh Gharib, and Alex Waldron.

The University Sector Agreement Research Fund project steering committee (Kathryn Bellette, Marnie Hope, Olessya Vitkovskaya, Ray Sweeting and Richard Day) are greatly

appreciated for their time and advice for the project. Our thanks also go to Adrian Stokes, David Chick, Peter Nattrass, Karen Rouse, Tim Horton, John Mercer, Bruce Perkin, Paul Smith, Lois Boswell, Peter Rebellato, Gabriella Vikor, Paul Davy, Sergey Zhukovskiy, Paul Cooper, Paul Lemmey, Francois Koch, Jack Mazek, Josh Roberts, Rob Mitchell, Andrew Partridge, Greg Ingleton, Warwick Grace, Adrian Marshall, Andrew McGrath, Darren Ray, John Nairn, Mark Moses, and Brenton Perkins, for the help they provided in various aspects of the research. We appreciate the help rendered by the administrative staff of the School of Environment, Flinders University, in administrative matters.

The editorial input to this document by John Bennett and Kathryn Bellette is appreciated.

The image on the Report's cover was taken and supplied by Chris Kent, formerly of Flinders University.

Executive Summary

Various methods, including field observations, remote sensing, and statistical, analytical and numerical models, have been applied to characterise and interpret the Adelaide urban heat island (UHI) since 2009.

Major findings: Below are the major findings resulting from this three-year project, and implications for urban planning and building design in Adelaide.

(1) The urban heat island is clearly observed in the Adelaide central business district (CBD). The locations and magnitudes of hot spots in the CBD vary diurnally. In the daytime, a hot spot occurs in the northwest corner of the CBD, while in the night, a hotspot occurs in the northern section of King William Street, between Waymouth/Pirie Street and North Terrace. These broad UHI characteristics provide information useful for future development and urban-heat mitigation planning.

(2) The air temperature in the Adelaide parklands is effectively cooler than the CBD by about 1.5^{o}C in the night time, and 0.5^{o}C in the daytime. With parkland irrigation, the cooling effect may be larger. The numerical modelling results indicate that the parklands can also help reduce air temperatures in the CBD, with a magnitude yet to be more firmly established.

(3) A sea breeze significantly reduces the CBD air temperature in the afternoon during summer. Such cooling improves human comfort levels, and may be used to reduce cooling energy consumption. Harnessing its effects should be considered more intentionally in future urban planning.

(4) Office building energy performance varies substantially in the CBD. A 2- to 3-times reduction in office building daytime base electricity consumption, and its associated CO_2 emissions, can be achieved by improving building energy performance. Climate change and the urban heat island have strong implications for energy consumption and associated CO_2 emissions. A warming of 1^{o}C daytime temperature may increase cooling electricity consumption by 1.5 million kWh per year for the sum of office

buildings in the Adelaide CBD. The increase of equivalent CO_2 emissions will be in the order of one thousand tonnes per year.

(5) Office building energy consumption responds sensitively to heat waves. For an event similar to the early 2009 heat wave, the daytime office building electricity demand may increase by 50% from the base daytime electricity use. This information will be useful for the electricity company (SA Power Networks) to better plan and allocate electricity during a heat wave period.

(6) With the projected increases in building height provided by the Adelaide City Council, the night-time temperature in some parts of the CBD may increase by one degree. However, tall buildings may reduce near-surface air temperature in the daytime by decreasing solar exposure of the surface.

(7) The night-time UHI intensity in the CBD can be largely interpreted by an effective sky view factor (ESVF), a new concept developed in this study. The ESVF is a measure of the efficiency of surface radiative cooling, which is dependent on the surrounding building height and density, and cloud-cover conditions. The ESVF can be used to predict the change of UHI intensity with future development in the CBD, and to provide reference data by which to prioitise the nature and location of UHI mitigation and evaluate the efficiency of heat-mitigation solutions post installation.

(8) A good foundation of instrumentation, field observations, modelling, and remote sensing has been established, and can be employed to conduct further research into the Adelaide UHI and associated water, energy, and human health issues. A network of 45 temperature observation points and some wind and humidity stations are in operation over the Adelaide metropolitan area. Thermal cameras and mobile traverse equipment have operated as required. Atmospheric models for examining meter-scale, and kilometre-scale processes are available at Flinders University, and a building energy performance model is at the University of Adelaide. These latter have been used in preparing various chapters in this report.

Recommendations for future work: Suggestions for future work are included at the end of many chapters of this report. The primary areas are highlighted here.

(1) To upgrade the current UHI monitoring network to include more meteorological variables (particuarly wind for its effect on CBD ventilation rates, and humidity for its role in heating and cooling processes, both in the environment and in buildings, as well as other variables), and to add real-time monitoring capacity. An improved monitoring network will provide information to further understand and interpret the Adelaide urban climate. From real-time monitoring, spatial temperature distributions will be accessible that would very useful in informing management of and resilience to heat waves.

(2) To quantify sea breeze effects on CBD and suburban temperatures in more depth, to explore possibilities for optimization of its daytime cooling effects in summer. This will provide quantitative evidence to support the design of future urban development, such as orientation, spacing and heights of building blocks.

(3) To improve parkland monitoring and management to achieve environmental benefits, in particular those relating to urban heat mitigation and CO_2 sequestration. This work will examine the parkland environmental benefits together with water and electricity consumption.

(4) To comprehensively examine the responses of both residential and commercial building energy consumption to climate, considering both heating and cooling energy use. The outcome of this work will be useful for predicting energy demands under future climate scenarios. It is also useful for the electricity supply company in planning and allocating electricity supply prior to and during a heat wave period.

(5) To develop models to more robustly evaluate the impacts of the form of urban development on urban thermal climate and its social-economic consequences, to inform urban planning and design policies.

(6) To develop sustainable urban heat island mitigation solutions, considering energy, water, and human health effects together.

Guide to the chapters:

A summary of the chapters in which the above conclusions are based are described next to help readers quickly locate detailed information.

Chapter 1 provides an overview of the urban heat island phenomenon and its social-economic connections, and related issues in Adelaide.

A significant urban heat island is observed (Chapters 2, 3, 4 and 6). On average (throughout the year), the Adelaide CBD is 1.5^{o}C warmer in the night time, and about 0.5^{o}C warmer in the daytime, than the surrounding parklands, with some variations between seasons, and with weather conditions. The urban-park thermal contrasts are influenced by cloud cover and wind speeds, with overcast conditions and high wind speeds limiting the growth of urban-park temperature difference. The critical wind speed for which the thermal effects are nullified is found to be about 5 m.s^{-1} (measured at Kent Town, 10 metres above ground). During warm, calm nights, it is not uncommon to observe over 5-degree night-time temperature difference between the CBD and the Park Lands.

Warm spots in the CBD vary between day and night (Chapters 2 and 3). The locations of peak warm spots in the CBD vary between day and night. During the night time, a warm centre is located in the northern section of King William Street, while in the daytime, a warm centre appears in the northwestern corner of the CBD.

Spatial variations in the morphology and composition of Adelaide's urban environment have a strong influence on temperature variation across the city (Chapters 3, 5, 6). Urban heat island intensity is strongly influenced by how much sky, solar radiation, and wind are blocked by buildings. With the projected building height increase provided by the Adelaide City Council, the night-time temperature in some parts of the CBD may increase by one degree. The narrow streets surrounded by high buildings, known as urban canyons, have their own micro-climates which can vary spatially. The surroundings of buildings (footpaths and roads) contribute greatly to the UHI effect, depending on materials used, areas, and surrounding urban structure.

The unique **Adelaide CBD parklands help to reduce CBD air temperature (Chapter 4)**. Parklands not only reduce local air temperature, they can contribute to reducing air temperature in the surrounding building areas. Modelling results on one selected winter day

indicate that without the current Adelaide parklands, spatially averaged air temperatures within the CBD would increase by about 0.2^{o}C.

Electricity consumption in office buildings in the Adelaide CBD is sensitive to urban weather conditions (Chapters 7 and 8), in particular, air temperature. Results indicate a daytime mean temperature threshold of about 17^{o}C, above which, electricity consumption increases with air temperature, below which, any temperature dependency is weak or absent. The weather dependency of office building electricity consumption can be modelled by linear regression, with both air temperature and humidity being significant predictor variables. The regression model is useful for examining the change of electricity demand with future climate projections, and with heat wave conditions. Façade materials and the geometric environment of buildings also influence electricity consumption.

Office building energy performance varies substantially in the CBD (Chapter 7). The base electricity consumption and temperature dependency vary by a factor of 2 to 3 between three examined buildings. This suggests there is substantial capacity to improve building energy performance. A 2- to 3-times reduction in office building electricity consumption in the Adelaide CBD, and associated CO_2 emission, can be achieved by improving building energy performance **(Chapters 6, 8)**.

Climate change and the urban heat island have strong implications for energy consumption and associated CO_2 emission (Chapters 7 and 8). A warming of 1^{o}C daytime temperature may increase electricity consumption for cooling by 1.5 million kWh per year for the sum of office buildings in the Adelaide CBD. The increase of equivalent CO_2 emissions will be in the order of one thousand tonnes per year. Meanwhile, a warmer climate decreases heating energy consumption in winter, which partly offsets the increase in equivalent CO_2 emissions due to the increasing cooling energy consumption in summer. Heat waves strongly influence electricity demand. For an event similar to the early 2009 heat wave, the daytime office building electricity demand may increase on average by 50% from the daytime base electricity consumption.

Table of Contents

Table of figures

Tables

GLOSSARY of ACRONYMS:

ACC	Adelaide City Council
ACH	Air changes per hour.
ASE	Absorbed solar exposure
BCA	Building Code of Australia
BMS	Building management systems.
BoM	Bureau of Meteorology
CBD	Central Business District, Adelaide.
CHP	Combined heat and power
CIE	Centre for International Economics
COP	Coefficient of performance
CStdT	Central standard time (UTC+9h30m)
DCCEE	Department of Climate Change and Energy Efficiency (Canberra, Australia)
DMS	Data management system.
EPA	Environment Protection Authority –South Australia, or Environment Protection Agency, USA, depending on context.
ESVF	Effective sky-view factor
FAI	Frontal area index
GHG	Greenhouse gases.
GHG-e	Greenhouse gas emission equivalents of CO2.
GIS	Geographical information system
GPS	Global positioning system
HVAC	Heating, ventilation and air-conditioning.
IPCC	Intergovernmental Panel on Climate Change.
SFP	Specific fan power
SVF	Sky view factor
TAS	Thermal Analysis Software from EDSL
TRY	Test reference year
UHI	Urban heat island
UHII	Urban heat island intensity
UCM	Urban canopy model
UTC	Coordinated Universal Time.
UBN	Unique building number.
VAV	Variable air volume
WRF	Weather Research Forecasting

Chapter 1 - Introduction to the Adelaide Urban Heat Island Study

Huade Guan, Simon Benger, John Bennett

1.1 Climate change, the urban heat island, and social-economic connections.

The temperature of an urban area is often higher than the surrounding rural areas. It is analogous to a hot island standing out in a relatively cool sea. This phenomenon is referred to as the urban heat island (**UHI**) effect, an anthropogenically induced climate feature.

Climate change and an increasing urban population with associated demands for space, water, energy and other resources, have increased pressures on urban environments. The urban microclimate is one important aspect strongly influencing human health and comfort (*Golden et al.*, 2008; *Nitschke et al.*, 2007), water consumption (*Guhathakurta and Gober, 2007*), and electricity usage (*Golden et al.*, 2008). The urban microclimate occurs within the regional climate system, and is influenced by global warming (*Parker*, 2004). But urbanisation itself generates an additional microclimate influence, one aspect of which is the urban heat island phenomenon. A large city of at least one million people can experience increases in annual mean temperature of 1 to 3˚C *(Oke, 1997)*. It is possible for the UHI to be as large as 12˚C *(Oke, 1987)*. Smaller urban centres also exhibit the effects of an UHI but as the size of the urban area decreases the UHI effect decreases *(Oke, 1982)*.

Global warming is found to have caused about a 1°C increase in the worldwide average daily minimum temperature over the 1950-2000 period, independent of urban warming (*Parker*, 2004, 2010). The current rate is about 0.15°C/decade *(Hansen et al, 2010).* On this positive trend of global temperatures are superimposed urban temperature increases from the growth in urban size and population. A study in Phoenix, Arizona, USA, suggests a 1.4 °C increase in June (summer) monthly minimum temperature per 1000 home completions in the area surrounding a weather station (*Brazel et al.*, 2007). In 2011, 50% of the world's population were urban dwellers (*PRB*, 2010), increasing from 45% in 2000, so further increases in urban temperatures will occur.

The growth in urban population and size, rergardless of global warming trend, has inevitably altered urban microclimatic conditions, leading to problems and issues of increasing water and energy consumption, and impacting upon human comfort and health. It is well documented that the amount of both urban water and energy consumption responds to microclimatic conditions. Another study in Phoenix found that a one-degree increase in summer night-time temperatures due to the urban heat island effect, will increase individual residential water consumption by nearly 2000 litres per month (*Guhathakurta and Gober*, 2007). Studies by *Akbari et al (1992)* have found that peak urban electricity demand in five American cities (Los Angeles, CA; Washington, DC, Phoenix, AZ, Tucson, AZ; and Colorado Springs, CO) rises by 2-4% for each 1˚C rise in daily maximum temperature. The temperature increase created by UHIs is responsible for 5-10% of urban peak electricity demand, at a cost of several billion dollars annually *(Rosenfeld et al, 1995*). In the business districts of Tokyo, Japan, it is found that electricity consumption is sensitive to day-time air temperature, at around 1W per m^2 floor area for both winter (decreasing heating energy consumption with temperature) and summer (increasing cooling energy usage with temperature) (*Ihara et al.*, 2008). Electricity consumption within residential houses is also sensitive to climate conditions, as shown in several studies in Australia (*Wang et al.*, 2010). In that study on several cities across various climate zones in Australia, in which Adelaide was not included, the authors state that for a region "with an H/C (hot and cold) balanced temperate climate such as Sydney, the increase in the total H/C energy requirement is projected up to 120% and 530% for a 7 star house when the global temperature increases 2^{o}C and 5^{o}C respectively". In Chapter 7 of this report, the response of office building energy consumption to both weather and climate in Adelaide is shown and discussed.

UHIs also affect urban air quality. Increased demand for energy from air-conditioning requires additional generating capacity, which can contribute to urban air pollution (*Rosenfeld et al, 1995*). Also, higher temperatures from UHIs accelerate the formation of smog. The probability of smog increases by 6% per 1˚C rise in maximum daily temperature (*Rosenfeld et al, 1995*). Increased temperatures and higher air pollution levels associated with UHIs can be related to health problems such as general discomfort, respiratory

difficulties, heat cramps and exhaustion, non-fatal heat stroke, and heat-related mortality (*EPA, 2008*).

The UHI exacerbates heat wave intensities in urban areas. Heat waves have caused more deaths in USA than hurricanes, tornados, earthquakes, and floods combined (*Golden et al.*, 2008). In 1995, a heat wave in the Midwest USA caused more than 1,000 deaths (*NOAA, 1995*). Heat-wave related health problems are of increasing concern in Australia too (*Hansen et al.*, 2008; *Nitschke et al.*, 2007). Based on the data between 1994 and 2006 in Adelaide, *Nitschke et al*. (2007) reported that during the heatwave periods, total hospital admissions increased by 7%, total mental health admissions increased by 7%, and total renal admissions by 13%. A recent Australia Climate Commission report states that the UHI exacerbates serious health problems resulting from heat waves in cities, in particular for the elderly, the young, and those within lower socio-economic groups (*Hughes and McMichael*, 2011, *EPA, 2008*.). The increasing electricity demand for air conditioning during heat waves often challenges the electricity distribution systems and exacerbates health problem from blackout accidents and other electricity allocation practices due to shortages in the total electricity supply.

Runoff from surfaces with high temperatures may impair water quality if it flows into waterways. Field measurements showed that runoff from an urban area exposed to the summer's sun was 11-17˚C warmer than from a nearby rural area, on a day when pavements surfaces were 11-19˚C above air temperature. Runoff from shaded urban surfaces was only 2˚C warmer than from rural areas (*EPA, 2008*). Such runoff may compromise aquatic life through stressing metabolism and reproduction rates of aquatic species (*EPA, 2008*).

1.2 Questions and issues for the urban heat island in Adelaide.

80% of the South Australian population resides in the Greater Adelaide region. This population is projected to grow by up to 0.56 million in the next 30 years (*Government-SA*, 2007). Adelaide has long, hot and dry summers, in which heat waves are common (*Hansen et al.*, 2008). It is located on the coast, adjacent to Gulf St Vincent on the west, and has the Mount Lofty Ranges to the east. Daytime sea breezes and night-time gully winds make its UHI development different from most other cities for which a UHI has been investigated.

In addition, a unique feature of Adelaide is the approximately 500-meter wide parkland belt (the Adelaide parklands) which encircles the central business district (CBD). An important aspect of this study is the extent to which the parklands help mitigate the UHI effect in Adelaide. If its UHI mitigation function is proved, the Adelaide parklands may provide a good model for future urban develop internationally. For the city itself, it is important to manage the current parklands to optimize their beneficial environmental function. To this end it is important to collect baseline data and to understand the functioning of these unique parklands in improving urban environmental quality.

An observationally limited study in 1974 reported a minor UHI in Adelaide (*Lyons*, 1974), with an intensity of 1-2°C. Has the UHI intensity changed in Adelaide since then? At present, how does the Adelaide UHI vary seasonally and spatially? How will it change with the future development in Adelaide? Will it be impacted by the recent modification of Adelaide CBD building height limits? By how much do the Adelaide parklands modify the local temperature? Do the parklands influence the air temperature in the CBD? How sensitively does building energy consumption respond to urban weather? What are the implications of this weather-dependent building energy consumption in terms of carbon emissions? Answers to these questions are critical for evaluating the consequences of, and solutions to, urban thermal stress in a more economically, socially and environmentally sensitive way. They provide evidence-based support for urban planning and design in Adelaide.

1.3 Project history: monitoring, modelling and understanding the Adelaide UHI.

The project research team started the examination of the Adelaide urban heat island using remote sensing images in 2008, with a seed grant from Flinders University. The participants were Dr. Huade Guan and Mr. Chris Lee.

With assistance from Prof. Craig Simmons in communication with governmentl and industry partners, we obtained funding from the Department of Planning and Local Government and Flinders University for a joint project entitled “Investigation of the

Parkland Impacts on the Urban Heat-island Intensity in the Adelaide Metropolitan Area". The objectives of this project were to establish the Adelaide parkland effects on urban heat island mitigation. The participants of this project were Dr. Huade Guan, Dr. Vinodkumar, Mr. Chris Kent, Dr. John Bennett, Prof. Roger Clay, Dr. Caecilia Ewenz, A/Prof. Graeme Hopkins, and Prof. Craig Simmons.

With this project funding and the support from Department of the Premier and Cabinet through Capital City Committee Project Team, we set up a field monitoring network in the Metropolitan Adelaide in 2010. Some preliminary results from this monitoring network, together with atmospheric modelling, and remote sensing analysis, were summarized in two progress reports (*Vinodkumar, et al.* 2010a, and 2010b), which were submitted to the Department of Planning and Local Government.

Capitalising on the foundation of the UHI monitoring network, a joint project between Flinders University and Adelaide City Council, entitled "City of Adelaide Urban Heat Island Micro-Climate Study", was started in June 2011, primarily funded by the University Sector Agreement Research Fund administered at that time by the SA Department of the Premier and Cabinet, and currently by the Department of Environment Water and Natural Resources. The primary objectives of this project were: (1) Identify Urban Heat Island (UHI) 'hot spots'; (2) Examine and quantify contributing factors to selected UHI 'hot spots'; and (3) To quantify the implications of UHI micro-climates upon energy consumption in commercial office buildings and occupant comfort in the public realm. Participants of this project were Dr. Huade Guan, Dr. John Bennett, Dr. Caecilia Ewenz, Dr. Simon Benger, Dr. Shanyou Zhou, Prof. Roger Clay, A/Prof. Veronica Soebarto, Dr. Andrew McGrath, Mr. Chuanyu Zhu, and Ms. Yunhui Guo. The project was supervised by a project steering committee, co-chaired by Ms. Kathryn Bellette and Ms. Marnie Hope, with members from Flinders University, Adelaide City Council, and Department of Environment, Water and Natural Resources.

The results from the above funded projects are summarized in this report. The field monitoring network was established in 2010, and has been in operation and expanded as the project progressed (Chapter 2). Analytical models have been developed to interpret the distribution of the Adelaide urban heat island intensity (Chapter 3). Two types of numerical models, one at meter scale, the other at kilometre scale, have been adapted to study the Adelaide urban climate (Chapters 4 and 5). Satellite, airborne and ground-based remote

sensing techniques have been used in the study to characterise Adelaide's thermal environments at different spatial scales (Chapters 3 and 6). In addition to characterising and interpreting the Adelaide UHI, we have looked at some social-economic aspects, such as building energy consumption and associated CO2 emission issues (Chapters 7 and 8).

Results of this study have been presented at several national and international conferences (*Guan et al.*, 2011; *Guan et al.*, 2012; *Vinodkumar et al.*, 2012; *Zhu et al.*, 2012). Manuscripts resulting from the project are in preparation for peer-review journal publication, with one in press on International Journal of Climatology (*Zhu et al.* 2013).

1.4. Basic aspects of the urban heat island effect.

The magnitude of the urban heat island effect depends upon surface properties and structure, on solar radiation, and on properties of the atmosphere. This is because heating and cooling of any surface depends upon its net energy gains or losses. If more energy enters a surface than leaves, the surface warms, and vice versa. During the day, more energy from the sun is usually absorbed than is lost by thermal (infrared) radiation, convection, and conduction, so the surface warms. Under heat-wave conditions, advection of hot air past buildings by wind adds significant energy too. In an urban area, traffic adds thermal energy, and building operations add energy from lighting, heating and cooling. During the night, more energy is usually lost in the three energy exchange processes, so a surface cools. When surfaces or buildings gain more energy over 24 hours than they lose, they warm from one day to the next, and vice versa. As buildings warm, they contribute to a warmer environment. The urban landscape is one which, through its structure restricting energy losses, tends to maintain that warmer environment.

The major energy input is from the sun during the day, but electrical and gas heating and cooling, lighting, transportation, and industrial processes contribute significantly in urban areas. Also thermal radiation emitted by the walls of buildings and surfaces contributes to energy gains at any point in the urban landscape. The solar energy that is absorbed by surfaces goes to warming them, and to providing energy for transpiration when the surface is vegetated, or for evaporation if bare and moist. The fraction of solar energy that is absorbed is greater for dark coloured surfaces, and for rougher surfaces, these having low albedos (reflective properties – refer to chapter 3). The urban surface with its buildings

and streets, some forming “canyons”, is a much dissected surface, and thus absorbs more solar energy than an open site, and warms up more (*Taha et al, 1992*). Trees and vegetation help cool an area through shading and evapotranspiration. Replacing “green-space” by buildings (*EPA, 2008*) then leads to elevated surface and air temperatures (*Taha, 1997*).

Energy losses from a surface occur through thermal energy being radiated away, and by convection from cooler air flowing past a surface. Conduction from deeper below a surface also can play a role. Thermal radiation to the sky is the main loss mechanism at night, since the surface is usually much warmer than the equivalent sky temperature. In an urban environment, any losses skywards are restricted by adjacent buildings, so high building densities maintain higher temperatures at night. For a deeper appreciation of processes involved in the urban heat island, consult *Arnfield (2003)*, *Johnson et al (1991)* and *Oke (1982)*. Aspects of the energy budget of urban regions are investigated in some depth and findings are discussed throughout this report.

References for Chapter 1.

Akbari H., W. Bos, S. Bretz, J. Hanford, A. Rosenfeld, D. Sailor, and H. Taha. 1992. “Monitoring Peak Power and Cooling Energy Savings of Shade Trees and White Surfaces in the Sacramento Municipal Utility District (SMUD) Service Area: Project Design and Preliminary Results”, *Lawrence Berkeley National Laboratory Report No. LBL-33342, Berkeley, CA.*

Arnfield, A.J., 2003, “Two decades of urban heat island research: a review of turbulence, exchanges of energy and water, and the urban heat island”, *Int.J.Climatol, 2003, 23,1-26, DOI:10,1002/joc.859.*

Brazel, A., P. Gober, S. J. Lee, S. Grossman-Clarke, J. Zehnder, B. Hedquist, and E. Comparri (2007), "Determinants of changes in the regional urban heat island in metropolitan Phoenix (Arizona, USA) between 1990 and 2004", *Clim. Res.*, *33*(2), 171-182.

EPA (2008) Environmental Protection Agency (U.S) 2008, "Reducing Urban Heat Islands: Compendium of Strategies", Washington DC, USA.

Golden, J. S., D. Hartz, A. Brazel, G. Luber, and P. Phelan (2008), "A biometeorology study of climate and heat-related morbidity in Phoenix from 2001 to 2006", *Int. J. Biometeorol.*, *52*(6), 471-480.

Government-SA (2007), "The 30-Year Plan for Greater Adelaide", edited by D. o. P. a. L. Government, p. 226, Government of South Australia, Adelaide.

Guan, H., A. McGrath, R. Clay, C. Zhu, J. Bennett, C. Ewenz, Vinodkumar, and J. Hacker (2011), "Examination of high-resolution aerial thermal imagery with ground and

satellite measurements in Adelaide and its implications", in *International Workshop on Urban Weather and Climate: Observation and Modeling*, Beijing, China.

Guan, H., V. Soebarto, J. Bennett, C. Ewenz, R. Andrew, C. Zhu, S. Zhukovskiy, P. Davy, and K. Bellett (2012), "Consequences for energy consumption from building and environment heat exchanges" in *International Conference on Urban Climate*,Dublin, Ireland.

Guhathakurta, S., and P. Gober (2007), "The impact of the Phoenix urban heat island on residential water use", *J. Am. Plan. Assoc.*, *73*(3), 317-329.

Hansen, A., P. Bi, M. Nitschke, P. Ryan, D. Pisaniello, and G. Tucker (2008), "The effect of heat waves on mental health in a temperate Australian city", *Environ. Health Perspect.*, *116*(10), 1369-1375.

Hansen, J., Ruedy, R., Sato, M., and Lo, K., (2010), "Global Surface Temperature Change", *Rev.Geophys., 48, RG 4004*

Hughes, L. and T. McMichael (2011). "The Critical Decade: Climate Change and Health". Department of Climate Change and Energy Efficiency, The Climate Commission Secretariat.

Ihara, T., Y. Genchi, T. Sato, K. Yamaguchi, and Y. Endo (2008), "City-block-scale sensitivity of electricity consumption to air temperature and air humidity in business districts of Tokyo, Japan", *Energy*, *33*(11), 1634-1645.

Johnson, G.T., Oke,T.R., Lyons, T.J., Steyn, D.G., Watson, I.D., 1991, "Simulation of urban heat islands under "ideal" conditions at night: Part 1: Theory and tests against field data.", *Boundary Layet Meteorol, 56, 275-294, DOI: 10.1007/BF00120424.*

Lyons, T. J. (1974), "A climatic survey of the Adelaide region", *Rep. Report 14*, 213 pp, The Flinders Institute for Atmospheric and Marine Sciences, Adelaide.

Nitschke, M., G. R. Tucker, and P. Bi (2007), "Morbidity and mortality during heat waves in metropolitan Adelaide", *Med. J. Aust.*, *187*(11-12), 662-665.

NOAA. 1995. "Natural Disaster Survey Report: July 1995 Heat Wave". Retrieved 10 August 2011 from <http://www.nws.noaa.gov/om/assessments/pdfs/heat95.pdf>.

Oke.T.R. 1987."Boundary Layer Climates". New York, Routledge.

Oke, T.R. 1982. "The Energetic Basis of the Urban Heat Island", *Quarterly Journal of the Royal Meteorological Society. 108:1-24.*

Oke, T.R. 1997. "Urban Climates and Global Environmental Change". In: Thompson, R.D. and A. Perry (eds.) *Applied Climatology: Principles & Practices*. New York, NY: Routledge. pp. 273-287.

Parker, D. E. (2004), "Climate - Large-scale warming is not urban", *Nature*, *432*(7015), 290-290.

Parker, D.E., (2010), "Urban heat island effects on estimates of observed climate change", *WIRES Clim .Change 1,123-133.*

PRB (2010), 2010 World Population Data Sheet, edited by P. R. Bureau.

Rosenfeld A., H. Akbari, S. Bretz, B. Fishman, D. Kurn, D, Sailor, and H. Taha. 1995. "Mitigation of Urban Heat Islands: Material, Utility Programs, Updates", *Energy and Buildings, 22;255–265.*

Taha, H., D. Sailor, and H. Akbari. 1992. "High-Albedo Materials for Reducing Building Cooling Energy Use", Presented at the 1st CIEE R&D Conference, August 27–29, 1991, University of California at San Diego. Also Report No. LBL-31721, Lawrence Berkeley

National Laboratory, Berkeley, CA.

Taha H. 1997. "Urban Climates and Heat Islands: Albedo, Evapotranspiration, and Anthropogenic Heat", Energy & Buildings - Special Issue on Urban Heat Islands", *Volume 25, Number 2 (1997), pp. 99-103.*

Vinodkumar, H. Guan, C. Kent, J. Bennett, R. Clay, C. Ewenz, C.T. Simmons and G. Hopkins (2010), "Adelaide Urban Heat Island Project Interim Report: Characterizing the Urban Heat Island Phenomenon over Adelaide". Flinders University, Adelaide.

Vinodkumar, C. Kent, H. Guan, J. Bennett, C. Ewenz, R. Clay, C.T. Simmons and G. Hopkins (2010),"Adelaide Urban Heat Island Project Interim Report: Characterizing the Urban Heat Island Phenomenon over Adelaide", Flinders University, Adelaide.

Vinodkumar, H. Guan, C. T. Simmons, J. Bennett, C. Ewenz, and R. Clay (2012), "Influence of parks on urban environment: a real case and numerical study using WRF mesoscale model", in *International Conference on Urban Climate*, Dublin.

Wang, X. M., D. Chen, and Z. G. Ren (2010), "Assessment of climate change impact on residential building heating and cooling energy requirement in Australia", *Building and Environment*, *45*(7), 1663-1682.

Zhu, S., H. Guan, J. Bennett, R. Clay, C. Ewenz, A. McGrath, S. Benger, Vinodkumar, and V. Soebarto (2012), "Relationship of urban thermal environments and its morphometric parameters: a case study of Adelaide CBD", in *Research in urban meteorology and climatology: current activities and future prospects*, Melbourne.

Zhu, S., H. Guan, J. Bennett, R. Clay, C. Ewenz, S. Benger, A. Maghrabi, A. C. Millington (2013), "Influence of sky temperature distribution on sky view factor and its applications in urban heat island", *International Journal of Climatology, DOI: 10.1002/joc.3660 .*

Chapter 2 - Adelaide Urban Heat Island Observation Network

John Bennett, Caecilia Ewenz, Roger Clay, Huade Guan, Vinodkumar, Chris Kent

2.1 Fixed sensor network.

Spatial and temporal variations of near-surface air temperatures within and beyond the Adelaide CBD have been established using a network of instrumentation spread across the region (Figure 2.1). The network provided data from 50 sites. Of these, 39 were chosen especially to cover both detailed CBD and broader aspects of a study into the urban heat island of the Adelaide metropolitan area. Fourteen sites were set up within the CBD, eight were placed in the parklands that surround the CBD, and the remainder were spread across the suburban area of the Adelaide Plains. The latter area extended from Seaview Downs in the south to Wingfield and Dry Creek in the North, and from Modbury in the north east to Glengowrie in the south west. Budgetary limitations meant not all areas could be covered with equal density of instrumentation. Data from the other 10 sites was very generously provided by two organisations, five by the State Environment Protection Authority, and five by the Commonwealth Bureau of Meteorology. These sites extend the coverage from Christies Beach to Elizabeth, and also filled some spaces in the network. The locations of all sites are shown in Figure 2.1.

As can be seen in the following chapters, the network coverage has been adequate for establishing spatial temperature patterns with reasonable detail. However, the coverage is not without gaps in the suburban area. Even in the CBD, where the sensor density is highest, there are some spaces where delineating the thermal patterns has been less than ideal –in the NE and SE corners particularly, the eastern CBD and along the Torrens River, where it might be expected that a clearer pattern might emerge relating to the existence of cool zones in reducing temperature extremes.

The sites chosen, and instrument locations at the sites, were designed to provide temperatures that represented a significant zone around each one. In such studies, it is important to minimise very local effects caused by site idiosyncrasies, and instead, pick up the broader scale characteristics of the air that flows past each site. To that end, sites were

chosen away from the walls of buildings, with an unobstructed airflow, and away from the ground surface (where temperature gradients are often strongest). At each of the 39 occupied sites, air temperatures were measured at 4 metres height above the local surface. These have been monitored at 30 minutes intervals throughout each day and night, for over two years.

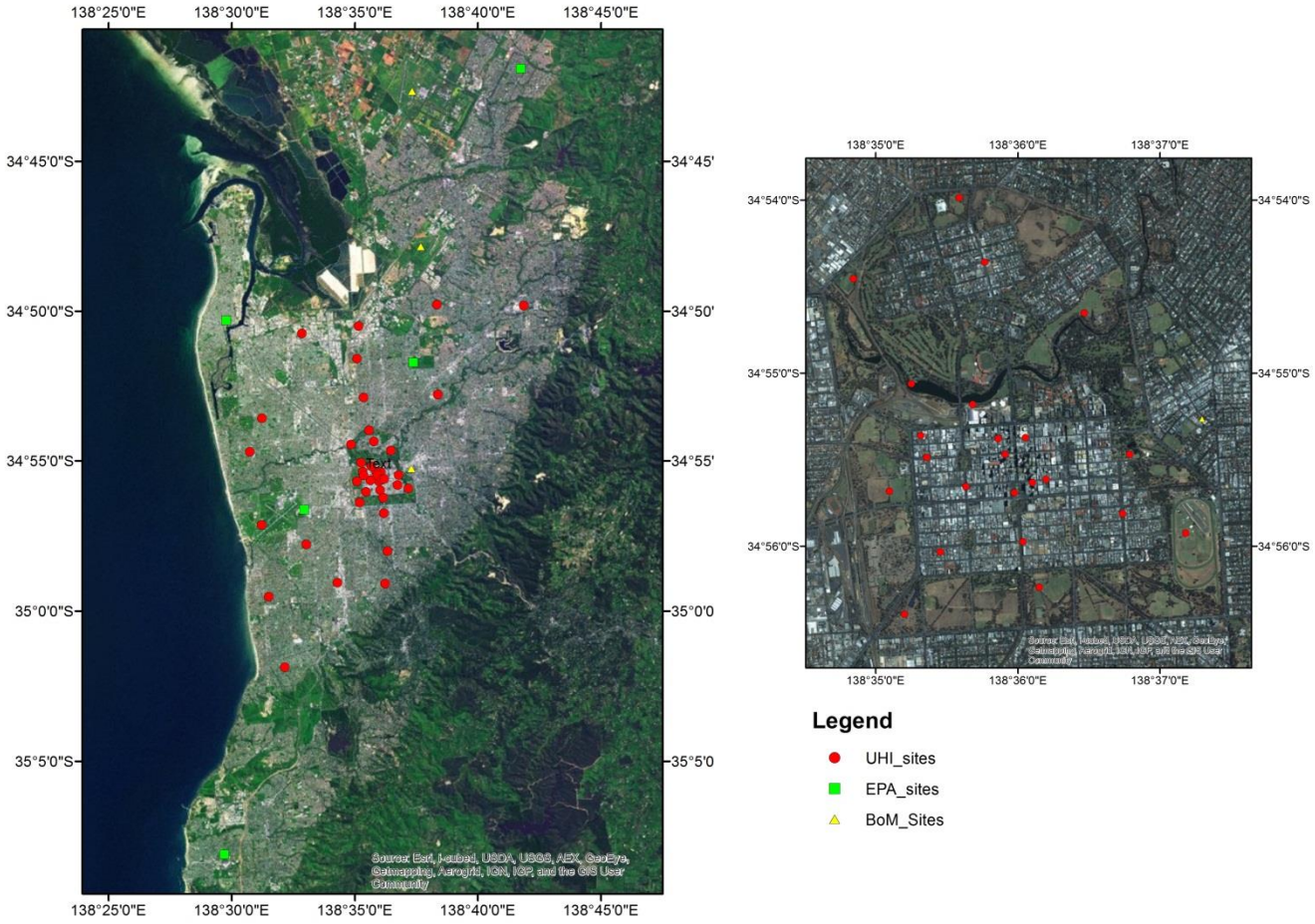

Figure 2.1 Image of the Adelaide region showing all temperature monitoring sites (left). The Central Business District contains the greatest density of sensors (expanded image, right).

The instrumentation (Maxim Integrated Products ThermoChron IButtons) combines a temperature sensor with a data logger, with a temperature resolution of ±0.0625°C for

recent sensors, or 0.125°C for ones used in the earliest deployments and since replaced. An image of a group of such sensors prepared for calibration is shown in figure 2.2.

Figure 2.2 Maxim Thermochron IButton sensors used in the sensor network of 39 sites in this study.

These sensors do not provide real-time monitoring capabilities, so in operation, they were deployed for periods of up to 81 days, depending upon the sampling interval, and downloaded at the end of that time.

To minimise solar and thermal radiation effects on the sensors themselves, and to protect them from rain but not airflow, they were placed inside louvred radiation shields. These were mounted from 0.5 to 0.9 m from their support structure, usually on a street lighting standard or electricity supply support pole. A CBD example is shown in figure 2.3. The shields were painted white to backscatter incident solar radiation, and were made of thermally insulating material, both to minimise heating from solar radiation during the day, and cooling during the night by thermal emission of radiation.

Comparisons of the temperatures measured in these radiation shields alongside Bureau of Meteorology temperatures measured in a standard Stevenson screen show excellent agreement, so no bias has been introduced via their use. Thus temperatures across the network have the same datum and are directly comparable, and with the data from other calibrated sources. This provides confidence in the patterns that are shown elsewhere in this report.

Figure 2.3 A typical CBD temperature measuring site, with the sensor inside a louvred radiation shield placed at the end of a mounting arm to distance it from its main support.

All sensors were calibrated against a precision quartz crystal thermometer to yield temperatures to a calibrated accuracy of better than 0.12°C. They thus yield temperature gradients and spatial patterns accurate to this degree across the study area. The data set is almost continuous and complete for all the sites, apart from the permanent loss of one site in Victoria Park, and sensor losses at 2 sites in the CBD, since replaced.

Sites were visited to download data and service equipment at 3 month intervals or shorter, to maintain performance standards of each. Those visits also provided opportunity to check changes to the surroundings to the sites as buildings were demolished, rebuilt or changed.

In addition to temperature alone, wind speed and direction, water vapour humidity, sunshine, and rainfall have been monitored at automatic weather stations at four parkland sites for a more limited period, at 6 m height, but sampled at 10 minute intervals. Data contributed from the two other organisations also covered the wider range of parameters, apart from sunshine, at various sampling intervals. That data provided early insights into the broader aspects of the Adelaide urban climate, and has contributed substantially to modelling aspects in more recent efforts to understand urban climate variations and changes.

2.2 Mobile instrumentation and traverse data.

As well as the above fixed installations, traverses through the streets of the CBD and out into the suburbs have been undertaken to obtain data with greater spatial resolution, but at limited times. These were run at night or early morning, under mostly clear skies, occasions when thermal effects on near-surface temperatures were expected to be largest in the CBD compared to open sites. These times also coincided with light to very light street traffic, thus minimising the effect of transient sources of heat. Instruments were mounted on vehicles that were driven along city and suburban streets. Two instrumental arrangements have been used. One, used at frequent intervals, consisted of an infra-red radiometer aimed towards the zenith and an air-temperature sensor mounted directly on the side of the vehicle. For the other set-up (Figure 2.4), sensors were mostly mounted on a boom extending in front of the vehicle, with up- and down- pointing radiometers, and thermometers at different levels.

Each sky-looking infrared sensor consists of a Heimann TPS 534 thermopile behind a 'standard' Perkin Elmer IR window, which detects thermal radiation in a wavelength interval from 7-14 micrometres, centred on 10 micrometres, a wavelength band where the surface can radiate almost freely to space. The devices have a 3° field of view, limited by a Fresnel lens, so only pick up radiation from a small patch of sky (or of whatever they are aimed at). Most details can be found in Clay et al (1998). The surface-pointing radiometer (item 1 in figure 2.4) was a similar Heimann KT15 instrument, sensitive over the wavelength band of 8-14 micrometres. These instruments respond rapidly to changing radiation levels, so are ideal for using in vehicle and airborne applications.

Other parameters that were measured with boom-mounted instruments were temperatures at nominally 30 cm and 1.8 m above the ground (using copper-constantan fine-wire thermocouples with rapid response times), humidity and duplicate temperature at approximately 1.6 m height (with two slower responding Digitek sensor/logger systems), and net long wave hemispheric radiation (with a shielded Swissteco net radiometer with approximately a 0.4-100 micrometre wavelength sensitivity). These parameters were logged at 1 second intervals, along with air pressure (for height information), on a Campbell-

Scientific CR10X logger, while the vehicle traversed various roadways. Each measurement was accompanied by a GPS position.

Figure 2.4. Sensors used in some night-time vehicle traverses of the CBD and suburbs. The roof-mounted boom supports (1) downwards pointing surface temperature radiometer, (2) air temperature thermocouple at 1.8 m, (3) upwards pointing sky temperature radiometer, (3) downwelling thermal radiation from whole sky, and (4) air temperature at 0.3 m, mounted on the traverse vehicle. Not shown are two relative humidity/air temperature sensors usually mounted on the boom, an air pressure sensor, and thermocouple reference sensor with its iButton comparison sensor all in a thermally isolated enclosure inside the vehicle.

From these data sets, GPS based maps of spatial variations of temperature (and other parameters) have been constructed which reveal details not possible with the more

dispersed and fixed installations alone. This in conjunction with data from overflights of the CBD by Airborne Research Australia, and the network data has provided a basis for much of the results presented in different chapters of the report.

2.3 Timing aspects.

In collecting and processing data, it was important to maintain good accuracy in timekeeping, so temperatures at each sites are directly comparable at essentially one time. Basic changes in time standards, as occurs between Daylight Saving Time and Central Standard Time twice a year were accomodated, so that diurnal and seasonal changes can be established on a common time base.. For all the results presented in this report, times and dates are in Central Standard Time (UTC+9.5 hr).

References for Chapter 2.

Clay, R.W., N.R. Wild, D.J. Bird, B.R. Dawson, M. Johnston, R. Patrick, and A. Sewell (1998) "A cloud moniotoring system for remote sites". Publ. Astron. Soc. Aust. 15 332-335.

Heimann IR thermometers: http://www.heimannsensor.com/products.php

Maxim Integrated Products, Inc. 160 Rio Robles San Jose, CA 95134 USA http://www.maxim-ic.com/products/ibutton/ *[30 June 2012].*

Chapter 3 - Morphological examination of the urban heat island intensity in the Adelaide CBD

Huade Guan, Shanyou Zhu, John Bennett, Roger Clay
Chuanyu Zhu, Yunhui Guo, Caecilia Ewenz, Simon Benger, and Andrew McGrath

3.1 Introduction.

In this chapter we characterize hot spots in the Adelaide Central Business District (CBD), and their diurnal and seasonal variations. The occurrence of these hot spots is interpreted in relation to urban morphology (i.e building density, heights, and orientation). An empirical relationship has been developed for estimating urban heat island intensity (UHII: how much warmer it will be at a given location by comparison with an open parkland site) for all weather conditions. The work contributes to (1) understanding why and by how much the Adelaide CBD is warmer than its surroundings, (2) estimating UHII for current urban forms, (3) predicting UHII for future urban developments, and (4) providing benchmark data to evaluate the effects of UHI mitigation measures.

Temperature at the Earth's surface is controlled by thermal energy inputs and outputs. Input is dominated by solar energy. During daytime, absorbed solar radiation heats up the ground surface which then warms the adjacent air mostly by convection. **Solar exposure** is a quantity often used to represent how much solar energy reaches the surface during a specific time interval (e.g., a day). Part of this solar energy is reflected back to the sky or adjacent walls immediately, with the remaining energy absorbed by the surface. The fraction of incoming solar radiation reflected by a surface is the surface **albedo**. Absorbed solar exposure (ASE, solar exposure multiplied by (1-albedo)) quantifies the solar energy that is used mostly to evaporate water and/or heat up the surface and the air. If the surface is moist, evaporation consumes significant energy, leaving less energy available to increase the surface and air temperatures. If the surface is covered by growing vegetation, transpiration will have similar effects as evaporation in reducing the surface temperature during the daytime. High solar exposure is found to contribute most of the heat stress to urban streets during hot summer days (*Ali-Toudert and Mayer*, 2007).

During night time, a surface loses energy by emitting thermal radiation to the sky, and under clear skies, receiving little radiation back. Because the energy input from below the surface is usually small, the surface cools and hence the air above cools. The efficiency of surface thermal radiation cooling depends on how much of the sky can be seen from a particular point on a surface. The fraction of sky visible compared with an unobstructed site is called the **Sky-view factor**. A value of one means the surface can "see" the sky completely, while a value of zero indicates that the sky is completely blocked. In urban areas, the sky-view factor is often small. Small sky-view factors are associated with significant UHII (*Gal et al.*, 2009; *Svensson*, 2004; *Unger*, 2009), and are examined shortly.

Wind is another important factor influencing air temperatures, because it moves thermal energy by forced convection from or towards a surface, depending on whether the air is cooler or warmer than the surface. Such advection changes air temperature at a point in the urban environment and also the rate at which buildings exchange thermal energy with their environment. In urban areas, buildings often reduce wind speeds at street level, and also affect wind direction. Lower winds may reduce rates of urban cooling during night time.

Reduction of windspeeds from building concentration in coastal cities like Adelaide, subject to sea breezes during daytime, may reduce their convective cooling effects (see also EPA 2008). A **Frontal area index** (defined as the ratio of the area of all buildings facing the wind from a particular direction, to the plan area those buildings occupy) is often used to quantify the effects of building-induced wind reduction in urban areas on UHII (*Wong et al.*, 2010). Large values (>1) correspond to high blockage.

In this chapter, we examine the dependence of hot spots in the Adelaide CBD with the above mentioned morphological quantities: sky-view factor (SVF), frontal area index (FAI), and absorbed solar exposure (ASE). Organisation of the remainder of this chapter is as follows: In Part 3.2 the hot spots in the CBD are characterised, based on the temperature monitoring network and an airborne thermal image. In Part 3.3, an interpretation of these hot spots is made, using the morphological factors. In Part 3.4, estimates are made of the mean UHII for current CBD and future building projections in Adelaide, and Part 3.5 provides conclusions and recommendations.

3.2 Warm spots in the Adelaide CBD and the diurnal and seasonal variations.

The Adelaide CBD is encircled by a unique green belt of Park Lands, designed by Colonel William Light in 1837 (Figure 3.1). The Park Lands are about 500 meters wide. They provide a contrasting surface to the CBD. Because of that contrast, in this chapter, we define the CBD urban heat island intensity as the difference between the CBD temperature and that of the surrounding Park Lands.

Figure 3.1 The parkland structure of the Adelaide CBD. Left: the original design by Colonel Light (*Whitelock*, 1985), and right: remote sensing image from Google Earth (accessed in 2011) showing the mostly vegetated area surrounding both the CBD and the North Adelaide urban area.

A typical diurnal variation of the heat island intensity has a maximum value near 10PM and a minimum value near 2PM (Oke, 1982). Based on our temperature network in the CBD and surrounding Park Lands, and Oke's (1987) work, seasonal mean night-time (at 10 PM) and daytime (at 2 PM) temperature contours are shown in Figure 3.2 and 3.3 for summer and winter. These are based on one year's data from September 2010 through to August 2011.

At night time at 10 PM, hot spots appear on both sides of the northern section of King William Street, between Waymouth/Pirie Street and North Terrace, for both summer

and winter (Figure 3.2). The temperature of this hot spot is about 1.8^{o}C warmer than the Park Lands for summer, and 1.5^{o}C warmer for winter. A local warm centre occurs in North Adelaide for both seasons, with a temperature 0.5^{o}C warmer than the surrounding Park Lands.

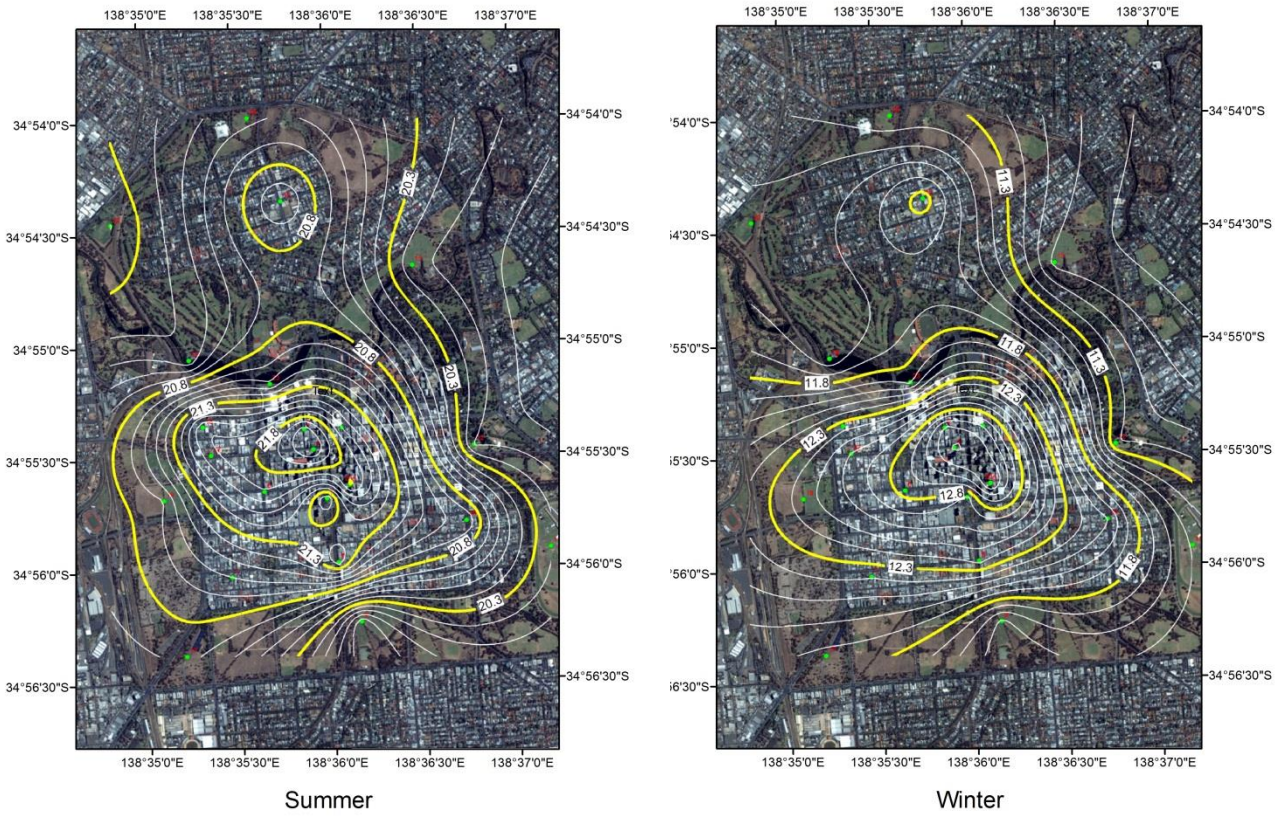

Figure 3.2 Contour maps of seasonal average night-time (10 PM CStdT) air temperature (measured at 4 m above ground) for summer and winter, showing the warming over the CBD and North Adelaide.

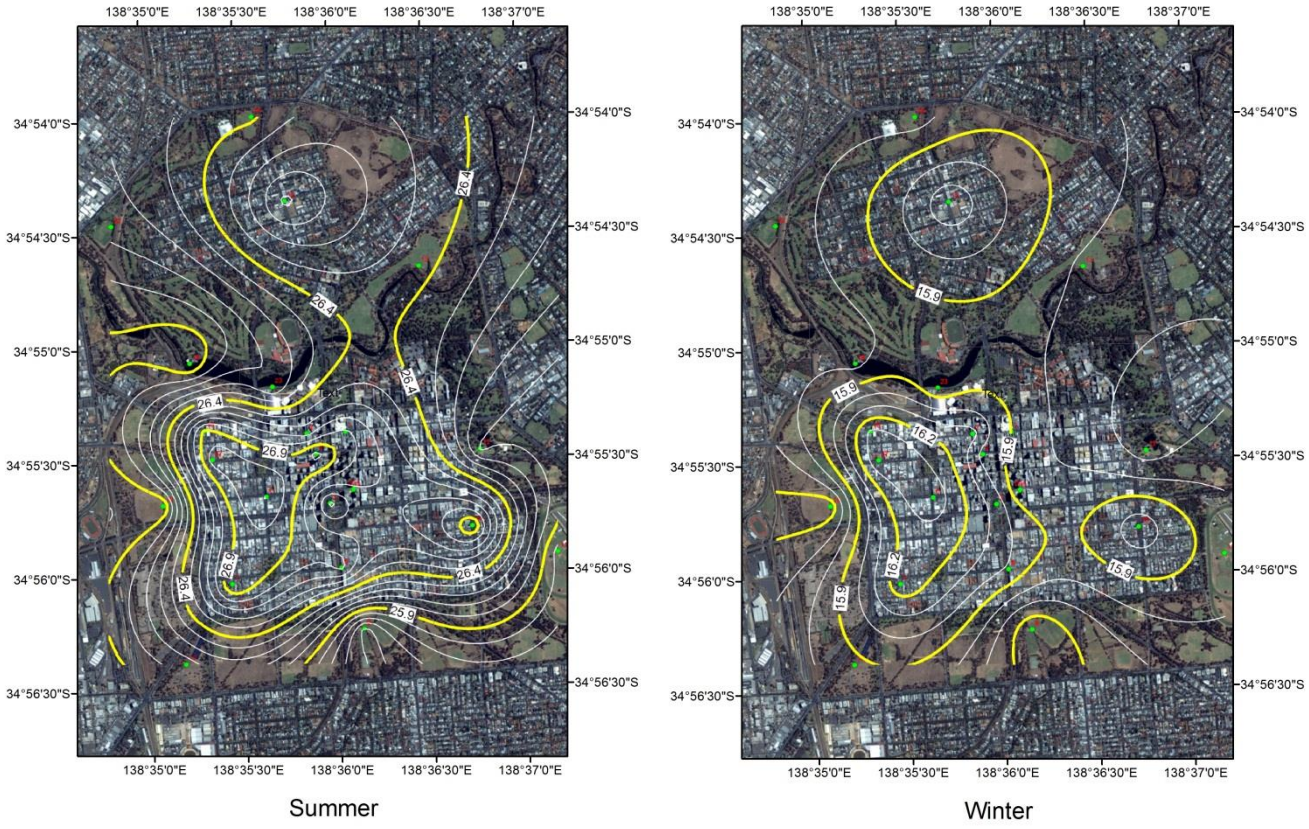

Figure 3.3 Contour maps of seasonal average daytime (2 PM, CStdT) air temperature (measured at 4 m above ground) for summer and winter.

At 2 PM, the hot spot appears in the north-western corner of the CBD, and is 0.8^{o}C warmer than the surrounding Park Lands for summer, and 0.5^{o}C warmer for winter (Figure 3.3). This is likely related to a larger solar exposure in this corner owing to an absence of tall buildings and a larger proportion of open car park areas. By contrast, the north-eastern corner is the coolest in the CBD. This may be caused by its proximity to the well-vegetated Botanic Gardens, and more extensive and well-watered surfaces outside the CBD in that direction.

A local warm centre appears in North Adelaide, with a temperature 0.6^{o}C warmer than the surrounding Park Lands for summer, and 0.4^{o}C warmer for winter.

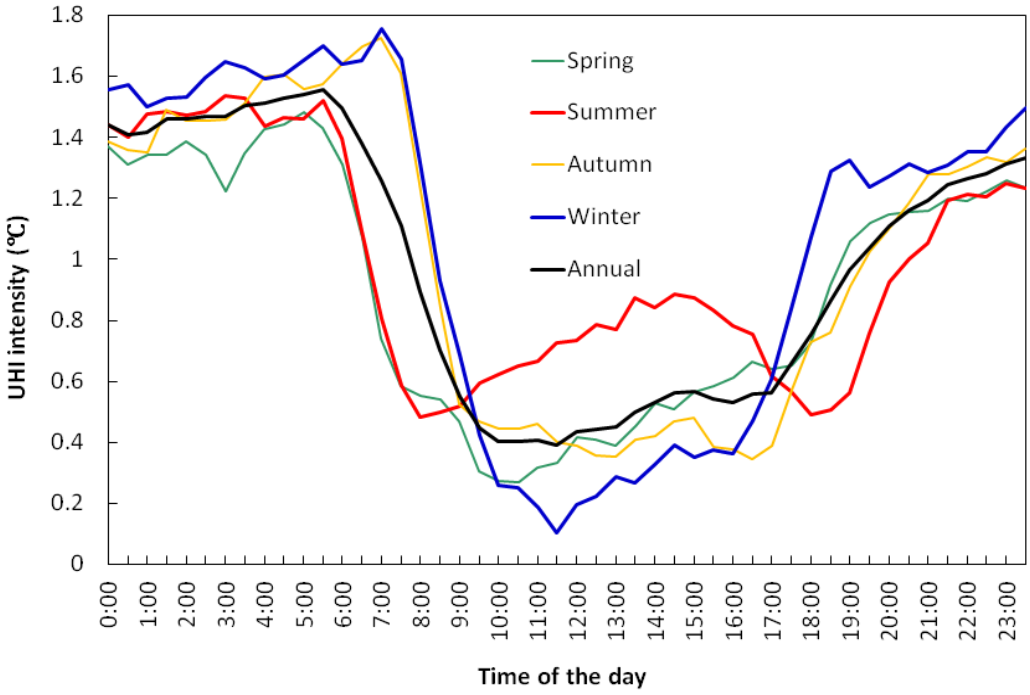

Figure 3.4 Seasonal and annual average hourly (local standard time) air temperature difference (measured at 4 m above ground) between the CBD and parkland-belt stations, for non-raining days only.

The average hourly temperature difference between the CBD stations and parkland-belt stations (i.e., UHII) was calculated for four seasons, excluding the raining days (Figure 3.4). Generally, the Adelaide UHII is larger at night, and smaller during the daytime, consistent with common knowledge of UHI phenomenon (*Oke*, 1982). The average UHII is around 1.4 ^{o}C at the night time, and 0.5^{o}C during the day time. From Figure 3.4, during the night time, the UHII in winter is larger than summer which contrasts with that mapped in Figure 3.2. This is because only non-raining days were used for Figure 3.4, while all days were used for the spatial mapping. (On raining days, the temperature difference between the CBD and the surrounding Park Lands becomes very small, thus, adding data of raining days decreases the calculated heat island intensity; and this impact is more obvious for the wet winter than the dry summer.) For all seasons, the maximum UHII occurs in the early morning before sunrise. This timing differs from other cities, where the maximum UHII often occurs around 10 PM (*Oke*, 1982). The mechanisms leading to such a different diurnal pattern of the UHII is worth further investigation.

The daytime UHII in summer looks quite different from that in other seasons, with a lower secondary peak around 2 PM, when the sea breeze is usually at its strongest stage in summer. Thus, this peak is probably related to greater cooling from that breeze in the Park Land than in the CBD (with its greater heat capacity and weaker sea-breeze). More discussion is given in Section 3.3. It is also under further investigation.

A thermal infrared image was collected by Airborne Research Australia for the CBD and the surrounding Park Lands at 0:30 – 2:30 AM CStdT, 7 March 2011. Figure 3.5 is the resulting map of surface brightness temperature (a quantity combining surface emissivity (assumed to be isotropic), and temperature effects on thermal radiation emitted and reflected by the surface (e.g. Siegel and Howell 2002)). The warmest surface temperatures occur in the northern part of King William Street, co-located with the urban air hot spots.

During the imaging flight time, a six-degree UHII was observed, with the warmest island centred at the northern part of the King William Street (see Figure 3.6 for the contoured air temperatures at mid-flight times), also consistent with the spatial pattern of the seasonal average UHII (Figure 3.2). The temperature contour in North Adelaide, however, differs from the seasonal average spatial pattern. This was probably owing to a warm air mass migrating to the CBD toward the end of the imaging flight (evidence for this is shown in Figure 3.10 later).

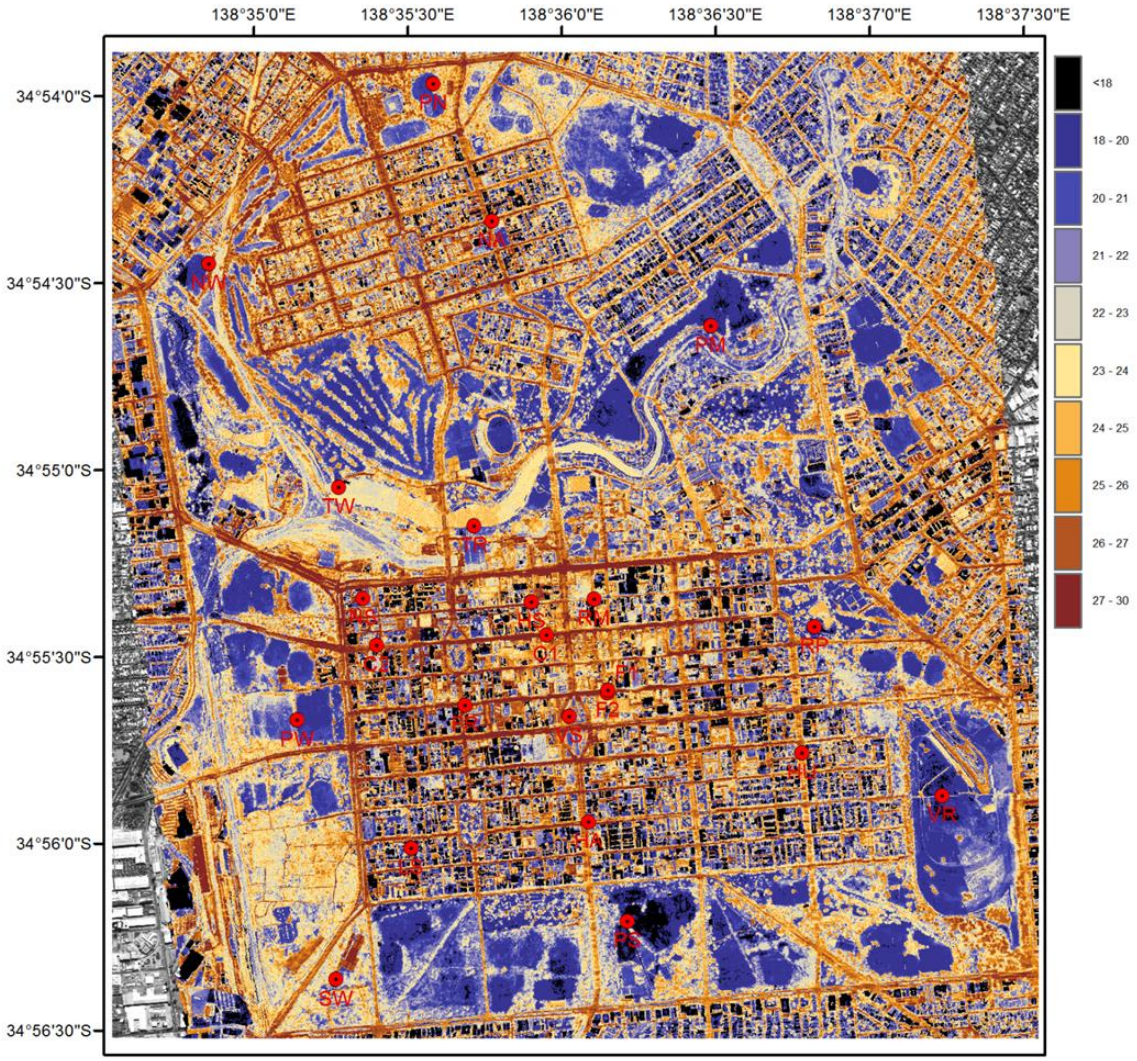

Figure 3.5 Surface brightness temperatures of the CBD and North Adelaide compiled from airborne one-metre resolution measurements made in the early hours (00:30 to 02:30 hrs) of 7 March 2011. The variation in temperature within the built-up regions is clearest along roads, while the Park Lands provide strong contrasts. The red dots indicate air temperature monitoring sites.

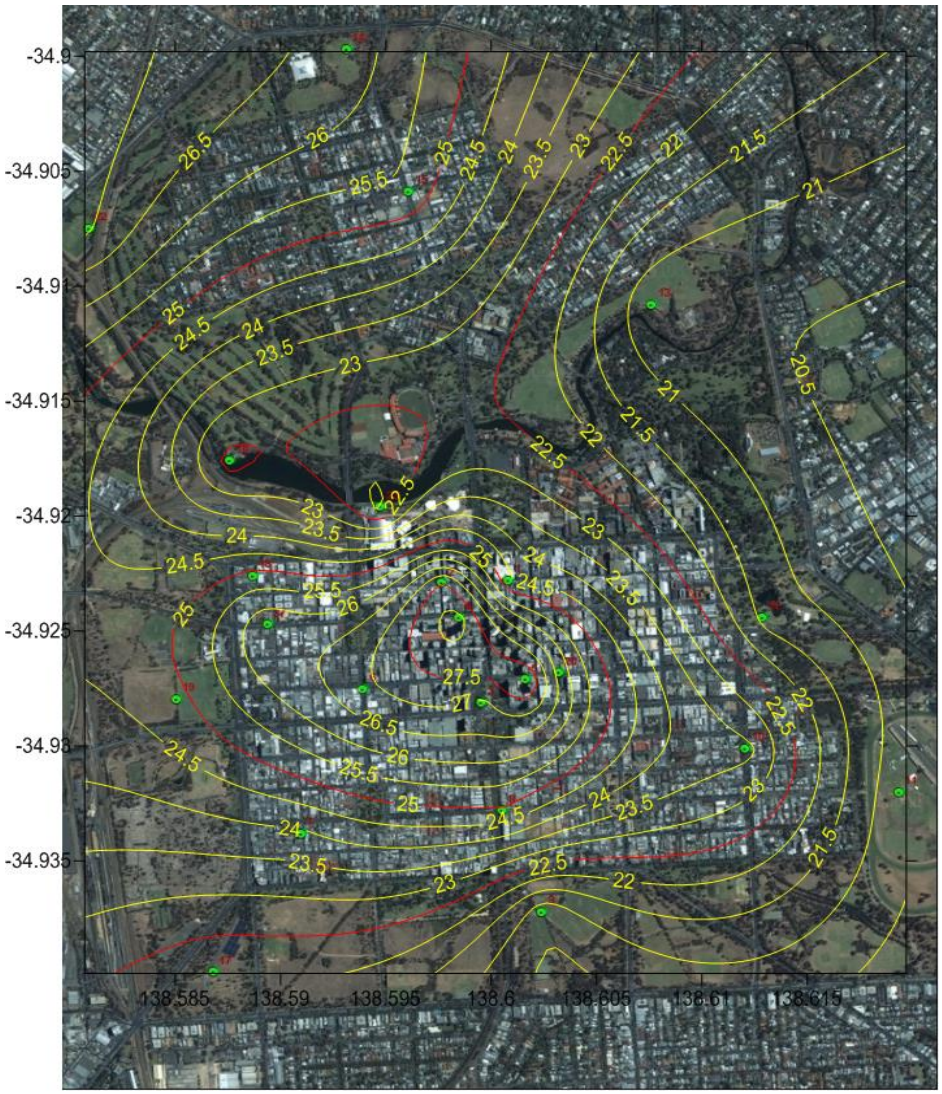

Figure 3.6 Air temperatures measured at 4 m above ground at 1:30 am local standard time on 7 March 2011, contoured to reveal patterns at the mid-time of the brightness temperatures shown in Figure 3.5.

3.3 Interpretation of CBD warm spots from urban forms.

The spatial patterns of the seasonally averaged UHI shown in section 3.2 can be interpreted by the three urban morphological factors: SVF (sky view factor), FAI (frontal area index), and ASE (absorbed solar exposure) defined in section 3.1. The night-time warm centre located in the north section of King William Street is associated with the concentration of tall buildings in the area. These tall buildings block the sky view for surface radiative cooling processes. This is clearly seen (Figure 3.7) in the calculated sky view factor map (refer to Zhu et al, 2013 for calculation details). A small sky view factor implies that the surface will be warmer during the night compared to areas with large sky view factors. That

variation is evident from the surface brightness temperature map (Figure 3.5). The warm surface maintains warmer air in that area compared with the much more open surroundings. A fair quantitative connection between the air temperature and surface brightness temperature for the CBD monitoring sites is shown in Figure 3.8, with air temperatures being about 3° warmer than surface temperatures. This difference typically begins after sunset, as both air and the surface start to cool down. The surface cools down faster as it radiates energy away (analogously to what happen during the daytime, when the surface heats up faster than the air once the sun strikes it).

The concentration of high buildings on both sides of the north section of King William Street may block or reduce wind speed, and consequently weaken advective cooling by night-time wind. The calculated FAI map (Figure 3.9) provides a spatial visualisation of how urban forms may influence advective cooling. On this FAI map, it is evident that the CBD has larger FAI values than those in the surrounding Park Lands. This difference in FAI values may contribute to an increasing daytime UHII in summer (Figure 3.4). During summer, sea breezes provide cool air to the Adelaide plain. In the CBD, this cool sea breeze is somewhat blocked by the buildings, thus its cooling effect on the CBD is smaller than the Park Lands. This difference in sea breeze cooling leads to an increase in UHII when the Park Land temperature is used as a reference in calculating the UHII (Figure 3.10). Additionally, it should be noted that during a sea breeze period, air temperatures in the CBD also decrease. Thus, in Adelaide, the sea breeze mitigates urban heat stress in summer (Guan et al., 2013).

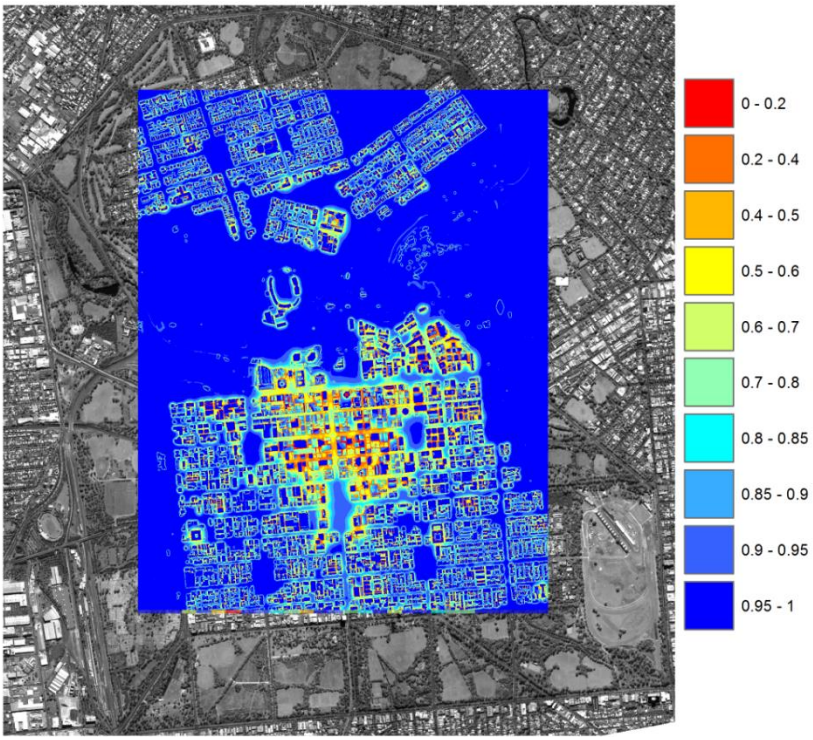

Figure 3.7 Variation of the sky-view factor for the Adelaide CBD and the surrounding area, calculated using data from the Adelaide CBD 3D model.

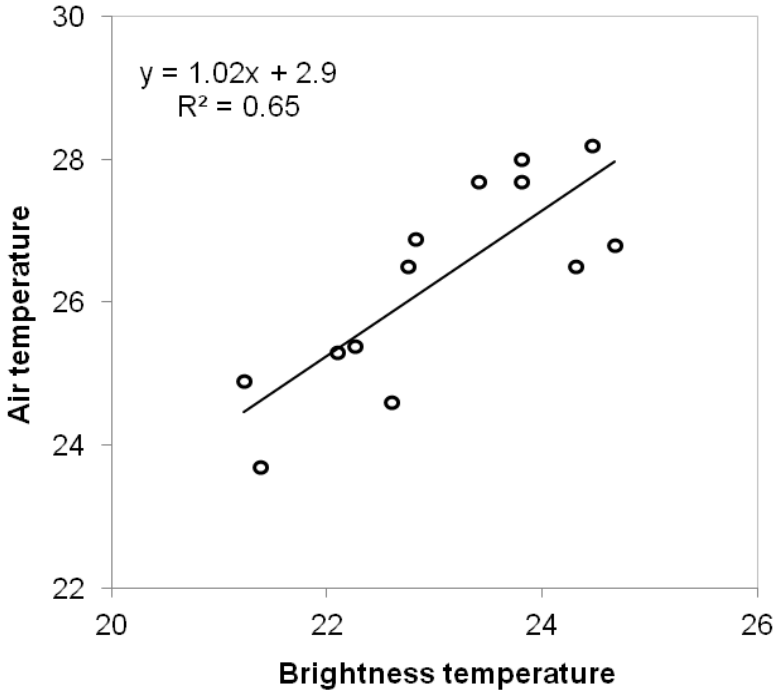

Figure 3.8 Scatter plot showing the increase in 4-m height air temperature at CBD sites with collocated surface brightness temperatures (averaged over 300m × 300 m blocks), together with the linear regression equation and its statistic of the fit to the line.

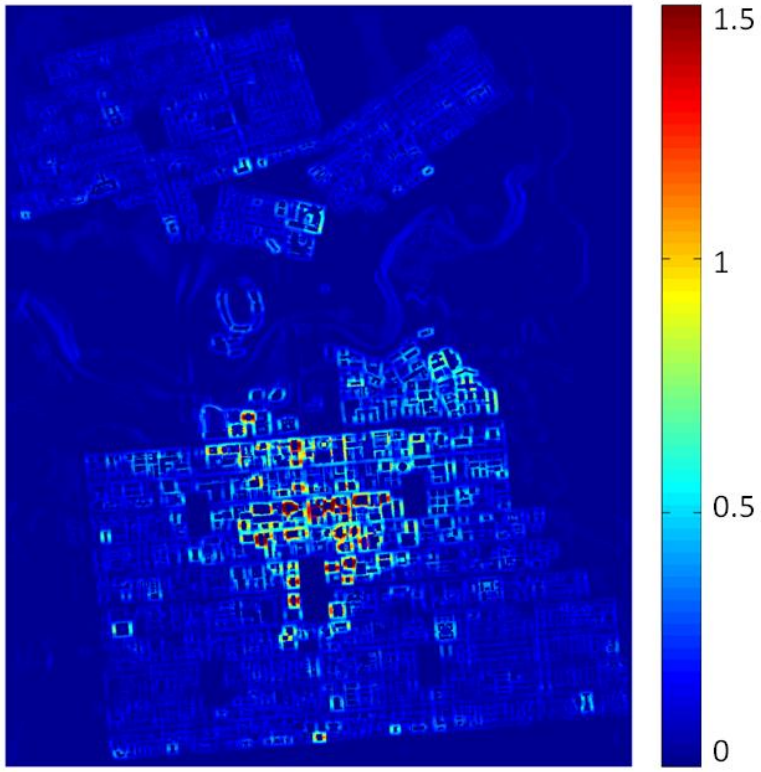

Figure 3.9 Variation of the frontal area index (dimensionless) (where large values reduce wind speeds), for E-W wind directions, for the Adelaide CBD and the surrounding area, calculated from data in the Adelaide CBD 3D model.

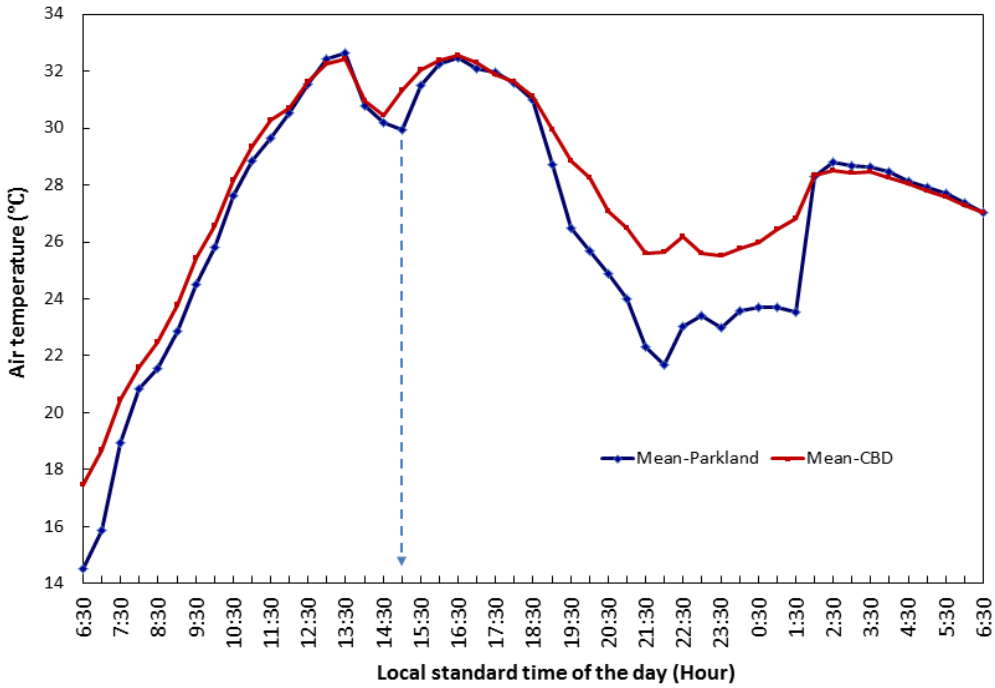

Figure 3.10 Spatial average half-hourly air temperatures (4 m above ground) of the CBD stations and the surrounding Park Lands stations, on 6-7 March 2011. Note that a warm air mass migrated to the area after 2:30 AM of 7 March 2011.

During daytime, a surface is heated by absorbed solar radiation. Surface albedo determines the fraction of down-welling solar radiation being reflected back to the sky. A surface albedo image was collected by Airborne Research Australia, Flinders University, on 17 April 2011 (Figure 3.11. In compiling this image, the reflectivity of a point on the surface is assumed to be isotropic, so albedoes are based on that assumption). Generally, green vegetation and water surfaces have a low albedo, while urban areas and bare ground have a relatively large albedo. Using the albedo map, absorbed solar exposure (ASE) was calculated for 6 March 2011 (Figure 3.12). The CBD absorbed less solar energy than the Park Lands due to it having a larger albedo. The smallest ASE occurs in the north section of King William Street. As a consequence, during daytime, this part of the CBD is expected to be relatively cooler than other parts -supported by the contour plot of Figure 3.3.

Although the parkland belt absorbs more solar energy during daytime (Figure 3.11), it is on average cooler than the CBD (Figure 3.3). Two mechanisms can be invoked to resolve this apparent conflict.

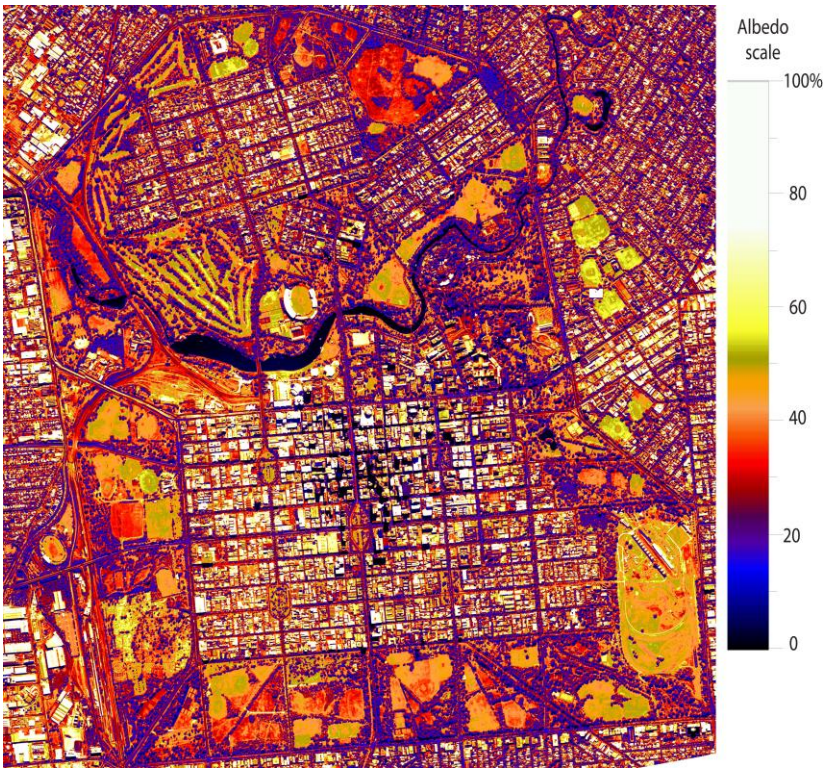

Figure 3.11 Albedo image taken by Airborne Research Australia at 12 PM local standard time of 17 April 2011, for Adelaide CBD and the surrounding area. (The black CBD points are shadow areas, the white patches are from rooftops with high reflectivity, and water in the Torrens Lake has an albedo of around 4-5%).

On the one hand, in the Park Lands, the processes of evaporation and vegetation transpiration use significant energy, making less available for surface heating from absorbed solar radiation. In contrast, anthropogenic heat released in the CBD adds heat to the urban environment, compensating for the reduced absorbed solar energy.

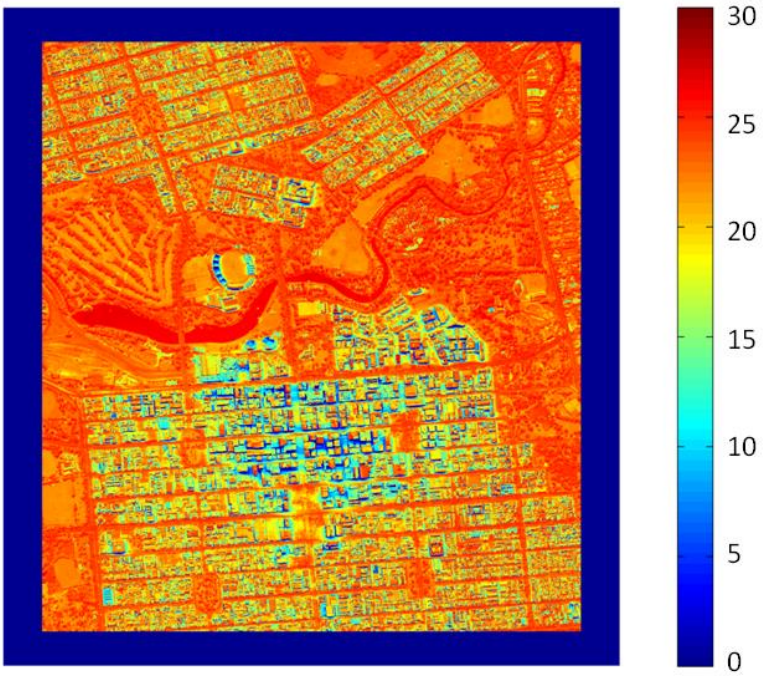

Figure 3.12 The spatial variation of absorbed solar exposure (MJ/m^2) of 6 March 2011, for the Adelaide CBD and the surrounding area, calculated from data in the Adelaide CBD 3D model and the albedo record above.

3.4 Estimation of the urban heat island intensity from urban morphology.

In the previous section, it has been shown that urban heat island intensity varies with three morphological parameters: SVF, FAI, and ASE. In the night time, the sky view factor is more important, while in the daytime the ASE effect is dominant. It is possible to estimate UHII from the urban morphology. Below we demonstrate how this works for the night-time UHII.

In the literature, one-way radiative cooling is considered in formulating the SVF (*Zhu et al.*, 2013). In reality, however, the radiative cooling of a surface results from the net out-going radiant energy flux. Particularly for cloudy and overcast skies, the down-welling thermal radiation can be significant. Thus, both in-coming and out-going energy flux densities should be considered in defining a sky-view factor. In this project, we do this via a

new parameter, an effective sky view factor (ESVF), to better quantify surface radiative cooling (*Zhu et al.*, 2013). This ESVF is useful for estimating night-time UHII values for all weather conditions. (Figure 3.13).

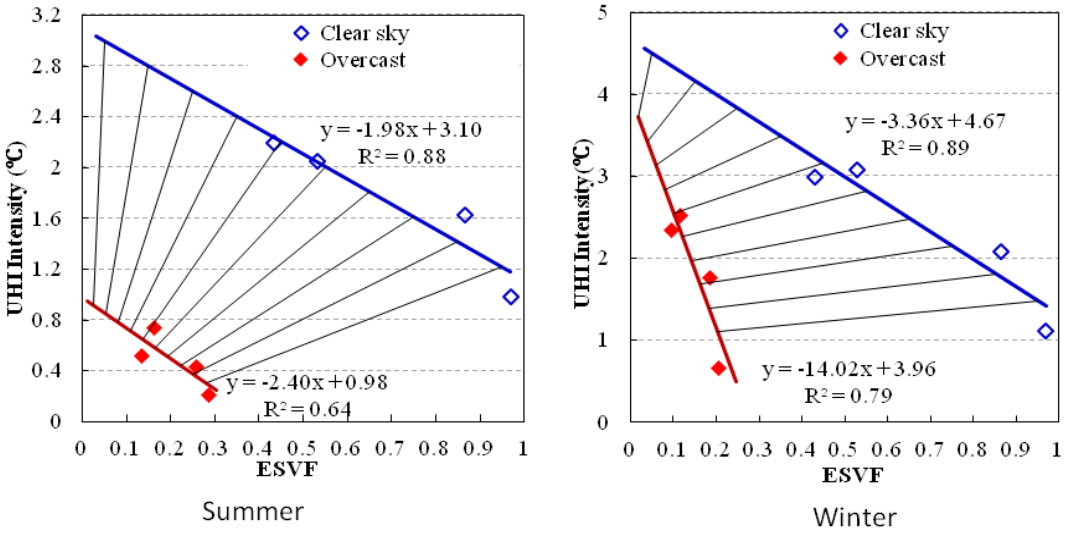

Figure 3.13 The UHI intensity (defined as the temperature difference between CBD sites and the average temperature in the Park Lands) and effective sky-view factor ESVF averaged over 100 m x 100 m squares for summer and winter. The blue line represents the relationship for clear sky conditions, the red line for overcast conditions, and the black lines each quantify how UHII varies with cloud cover fractions from zero (upper-right end) to 100% (lower-left end) for each point.

On average, from the statistics of the fitted data in Figure 3.13, the ESVF there accounts for nearly 90% of seasonal average urban heat island intensity (measured at 10 PM) in the Adelaide CBD for clear sky conditions, and about 65% for overcast sky conditions. With the aid of this diagram, the UHII can be estimated for any site in the CBD. Taking the summer diagram for example, for a site in the CBD with a clear-sky ESVF = 0.55 (we can calculate this from the CBD 3D model, e.g., Figure 3.7), on the clear-sky line we estimate that its average summer-time air temperature at 10 PM is two degrees warmer than the Park Lands. Under fully overcast conditions for this point, it would be about 0.6 degrees warmer than the Park Lands. The UHII for partly cloudy conditions lies between the clear-sky and overcast lines. If the site, however, has a measured UHII lower than the predicted value from the diagram, some other factors have contributed to mitigating the UHII at the site. Thus, the UHII-ESVF diagram can be used as a basis for testing the effectiveness of UHI

mitigation solutions. The diagram is also useful for predicting the effect of future urban buildings or changes of building heights on the UHII.

Air temperatures best correlate with sky view factors when the SVF is averaged over a certain source size. In the Adelaide CBD, this size is found to be around 100x100 meters. More details are given in Chapter 5. Thus, the equations given in Figure 3.13 can be used to estimate average 10 PM air temperatures averaged over 100 meter pixel size. The results are shown in Figure 3.14 for 10 PM UHII in summer, and in Figure 3.15 for 10 PM UHII in winter. Both show similar UHII spatial patterns, but with winter UHII slightly larger than the summer ones. With such maps, an average UHII can be estimated for any point in the CBD. Similar maps can be produced for overcast conditions.

If equations for estimating the UHII at other times of the day are developed, they can be used to estimate the spatial distribution of the UHII at those times.

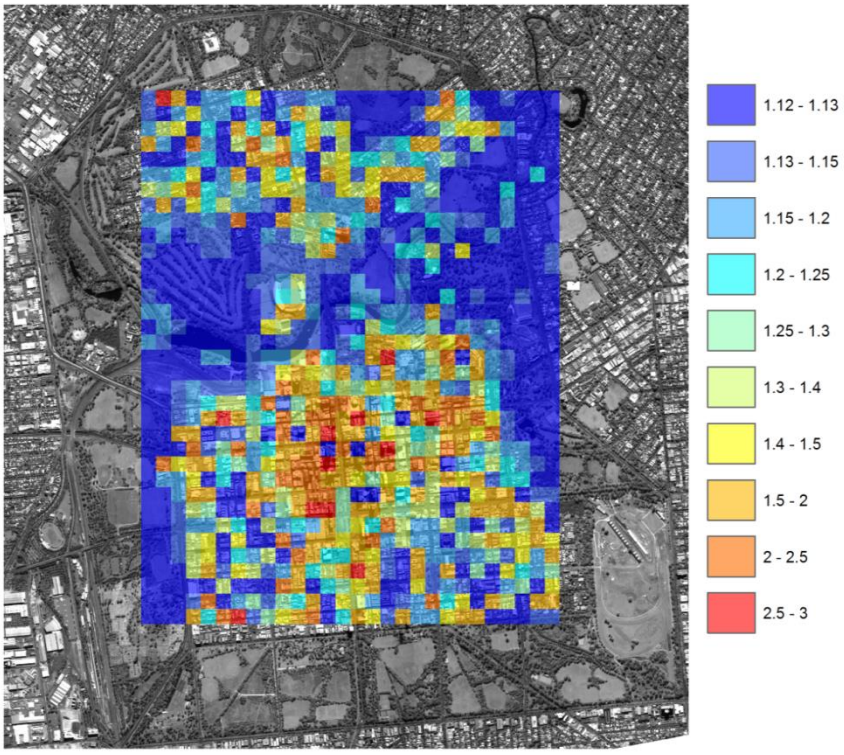

Figure 3.14 Estimated average summer 10 PM (CStdT) urban heat island intensity (^{o}C) for clear sky conditions, using the Park Lands average temperature as a reference. (Little reliance should be placed on Park Land UHII estimations as the equations were developed based on data from only the CBD stations).

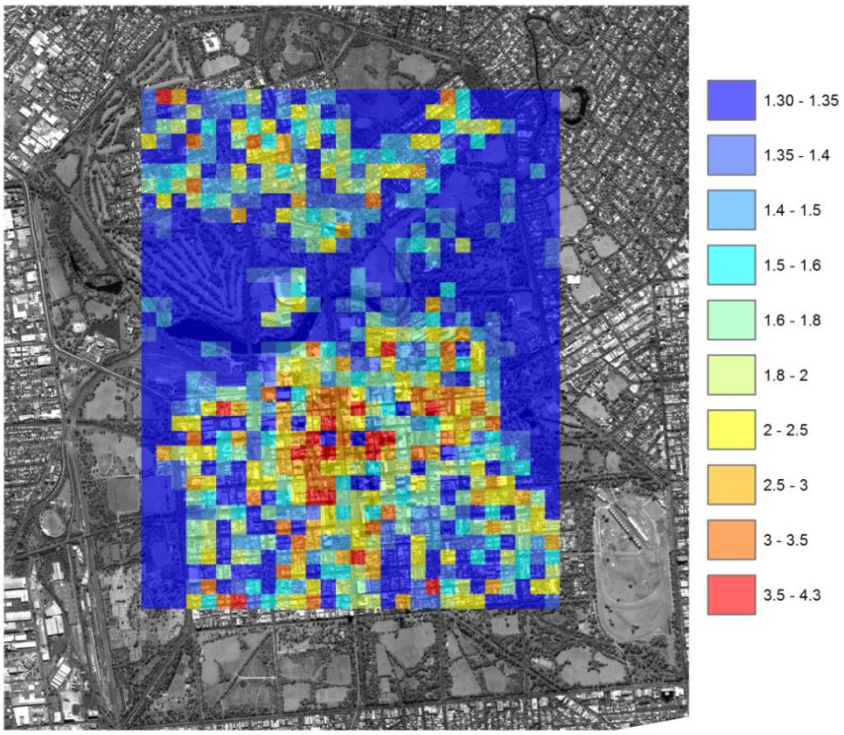

Figure 3.15 The estimated average winter 10 PM (CStdT) urban heat island intensity (^{o}C) for clear sky conditions, using the Park Lands average temperature as a reference. (The comment on the Park Land results in figure 3.14 caption applies here too).

It should be noted that the equations shown in Figure 3.13 were derived from the CBD data. They are not appropriate for estimating the UHII for the Park Lands where the surface is much more open. Thus, any interpretation of the portion of UHII maps over the Park Lands in Figures 3.14 and 3.15 should be avoided.

3.5 Predicted changes to the UHII from changed building regulations.

Recently, regulated maximum building heights in the Adelaide CBD were modified. Now a greater height is allowed for some zones in the CBD. The Adelaide City Council has projected an increase of future building heights (Figure 3.16). This increase will lead to a change in UHII. In the night time, taller buildings block more sky view and thus increase the UHII. The likely increase of 10 PM clear sky UHII is mapped for winter and summer in Figure 3.17 and Figure 3.18 respectively. The projected increase in building heights may increase night-time temperature by over 1^{o}C in winter and up to 1^{o}C in summer for clear sky conditions. In the daytime, taller buildings may block more solar radiation, thus reducing the UHII, which may reduce energy consumption of the office buildings now in shade (Chapters

7 & 8). However, based on the results of Figure 3.13, the effect of any changes to building heights can be estimated using form-dependent solar exposure and the frontal area index resulting from the changes. This is an aspect to be explored in the future.

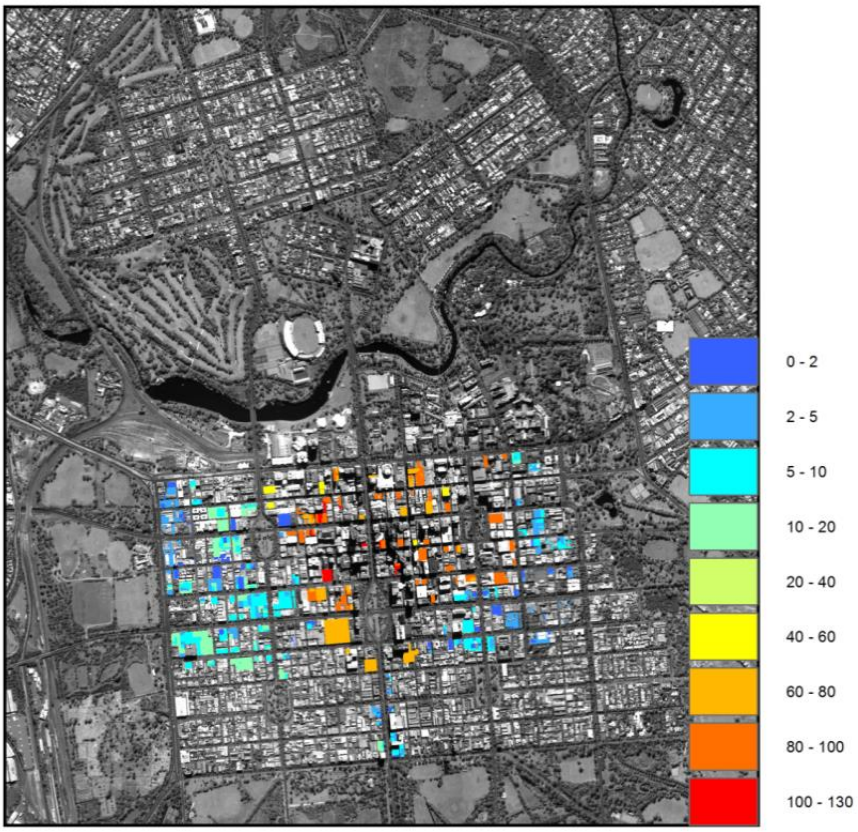

Figure 3.16 The Adelaide City Council projected increase (m) of building heights in the CBD.

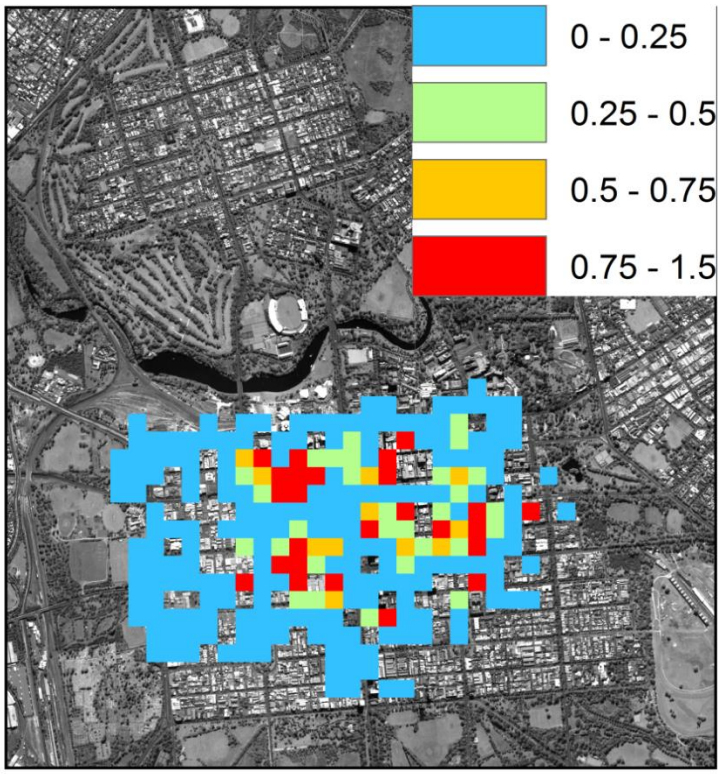

Figure 3.17 Patterns showing the estimated increase (°C) of winter clear-sky 10PM UHII resulting from the projected increase of building height.

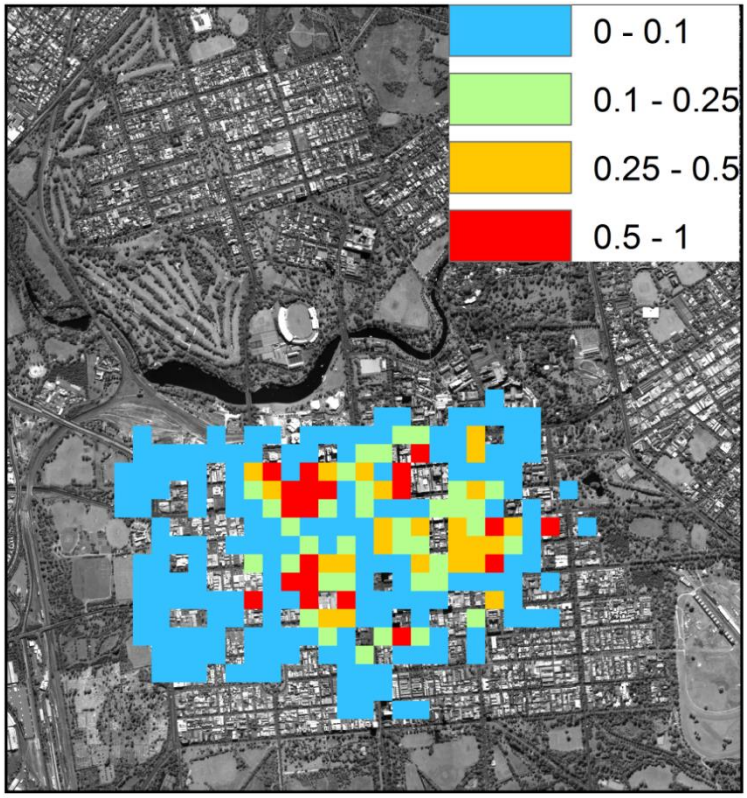

Figure 3.18 Patterns of the estimated increase (°C) of summer clear-sky 10PM UHII resulting from the projected increase of building height.

3.6 Conclusions.

In summary, the evidence here shows there is a significant urban heat island in the Adelaide CBD. On average, the CBD is 1.5°C warmer in the night time, and about 0.5°C warmer in the daytime, than the surrounding Park Lands, with some variations between seasons, and between weather conditions. The location of warm spots varies between day and night. During the night-time, a warm centre is located in the northern section of King William Street, while in the daytime, a warm spot appears in the northwestern corner of the CBD.

The night-time CBD urban heat island intensity can be largely accounted for by the sky view factor for any location. A new effective sky view factor has been developed which enables night-time urban heat island intensities to be predicted under various weather conditions.

The daytime CBD urban heat island intensity is more closely associated with absorbed solar exposure. Both sky view factor and solar exposure are highly dependent of urban morphology, such as building density and heights, and street orientation. In addition, evidence from other cities implies that buildings in the CBD reduce wind speeds, a factor which may contribute to an increased CBD urban heat island intensity as well. In Adelaide, the sea breeze can produce significant cooling during the summer daytime.

An increase of building heights in the CBD will change the urban heat island intensity. Generally, it will increase night-time UHII values, and may decrease daytime UHII.

We recommend that future work should focus on (1) daytime UHII estimation from urban morphology, (2) quantification of the anthropogenic heat release and its effect on the urban heat island in the CBD, (3) quantification of sea breeze daytime cooling effects during the summer, and (4) the UHII under the extreme weather conditions.

References for Chapter 3.

Ali-Toudert, F., and H. Mayer (2007), "Thermal comfort in an east-west oriented street canyon in Freiburg (Germany) under hot summer conditions", *Theor. Appl. Climatol.*, *87*(1-4), 223-237.

Gal, T., F. Lindberg, and J. Unger (2009), "Computing continuous sky view factors using 3D urban raster and vector databases: comparison and application to urban climate", *Theor. Appl. Climatol.*, *95*(1-2), 111-123.

Guan, H., X. Zhang, O. Makhnin, and Z. Sun(2013), "Mapping mean monthly temperatures over a coastal hilly area incorporating terrain aspect effects", *Journal of Hydrometeorology*, in press.

Oke, T. R. (1982), "The energetic basis of the urban heat island", *Q. J. R. Meteorol. Soc.*, *108*(455), 1-24.

Siegel, R. and Howell, J.R., (2002) "Thermal Radiation Heat Transfer", 4th edition, 868 pp..

Svensson, M. K. (2004), "Sky view factor analysis - implications for urban air temperature differences", *Meteorol. Appl.*, *11*(3), 201-211.

Unger, J. (2009), "Connection between urban heat island and sky view factor approximated by a software tool on a 3D urban database", *Int. J. Environ. Pollut.*, *36*(1-3), 59-80.

Whitelock, D. (1985), "Adelaide: From Colony to Jubilee, a Sense of Difference", 370 pp., Savvas Publishing, Adelaide, Australia.

Wong, M. S., J. E. Nichol, P. H. To, and J. Z. Wang (2010), "A simple method for designation of urban ventilation corridors and its application to urban heat island analysis", *Building and Environment*, *45*(8), 1880-1889.

Zhu, S., H. Guan, J. Bennett, R. Clay, C. Ewenz, S. Benger, A. Maghrabi, A. C. Millington (2013), "Influence of sky temperature distribution on sky view factor and its applications in urban heat island", *International Journal of Climatology*, DOI: 10.1002/joc.3660.

Chapter 4 Influence of the Park Lands on the Adelaide CBD Thermal Environment

Vinodkumar, Huade Guan, John Bennett, Caecilia Ewenz, Chris Kent, Craig Simmons

4.1 Introduction.

Local climate change effects due to urbanization have prompted a growing demand for the use of well-vegetated urban parks to create more comfortable, healthy, and sustainable urban environments. The research of this chapter has been undertaken to understand the current benefits of the Adelaide Park Lands on the city area it encompasses. In addition to quantifying the built-up and greened area temperature differences at different time scales, the chapter aims to investigate broad scale cooling effects, induced by Adelaide's unique Park Lands, on the CBD temperatures.

The study utilizes temperature data from the dense network of sensors strategically deployed both in the city and adjacent Park Lands (Fig. 2.1). To increase understanding of meteorological processes and effects associated with the unique urban-parkland structure, the state-of-art WRF / Noah Land Surface Model / Urban Canopy Model numerical system (Chen *et al.,* 2011) was used in conjunction with the temperature observations. The urban canopy model (UCM) in the WRF modelling system can include more realistic geometry of the urban region than the commonly used slab models in other meteorological models. The advanced numerical and physical schemes in WRF modelling suite makes it one of the best available to study the urban heat island and related phenomenon.

4.2 Field data analysis.

The urban-parkland temperature difference is calculated in this chapter as the difference between the half hourly mean urban (T_u) and the park (T_p) temperatures, i.e.:

$$\Delta T_{u\text{-}p} = T_u - T_p$$

The diurnal variations of this $\Delta T_{u\text{-}p}$ in Adelaide were analysed using its mean and standard deviations over the observational period from June 2010 to May 2011. Figure 4.1

depicts the results from the above analysis and show that the urban built-up area is consistently warmer than surrounding parks by 0.6 – 1.45 ^{o}C, with the magnitude being usually higher at night compared to the day time. (This figure can be compared with Figure 3.4 (and 3.10 for one day's variation), and shows a similar overall pattern in the annual means). Although not shown here, appreciable differences in $\Delta T_{u\text{-}p}$ exist in the data between the four seasons. Interestingly, the magnitudes of $\Delta T_{u\text{-}p}$ values at night time from winter and summer season are quite similar, but the day time values show the parks tend to be relatively cooler than the CBD on summer days than on winter ones. The increase in incoming solar radiation into a summer season is an important influence in determining the magnitude of $\Delta T_{u\text{-}p}$ during the day time (see chapter 3). Under the normally clear sky conditions in spring and summer, the urban built-up surface becomes a massive heat reservoir, whereas the parklands impart thermal moderation in the form of evaporative cooling and low thermal mass. This could be more pronounced in day-time when radiation loads on the surface are higher. But into the winter months, net radiation into the surface decreases, while the usual northward component of propagating synoptic scale frontal systems advect cool air from higher latitudes. The decrease in net radiation limits the magnitude of surface heating and, combined with cooler air, restricts energy available for free convection, evaporation and transpiration.

From the standard deviation of data from the annual half-hourly means (Fig. 4.1), it is observed that the dispersion in $\Delta T_{u\text{-}p}$ is significantly higher at night time compared to day time. This was also observed in the seasonal values of standard deviation. Since standard deviation is less resistant to outliers, it is possible that the odd extreme weather conditions resulted in high standard deviation. This will be more prominent at night since the temperature difference between the city and a park are mainly due to differences in radiative cooling, which latter is less significant during day time.

Figure 4.2 depicts a scatter plot of $\Delta T_{u\text{-}p}$ against ambient air temperature records in the CBD in day time (Fig. 4.2a) and night time (Fig. 4.2b) hours. The results indicate that day-time urban-park temperature differences sharply decrease at temperatures above about 17°C, giving average temperature differences of about 0.5°C on days warmer than about 30°C. At night, even in cases with ambient air temperature more than about 27°C, the parks were cooler by about 2°C on average.

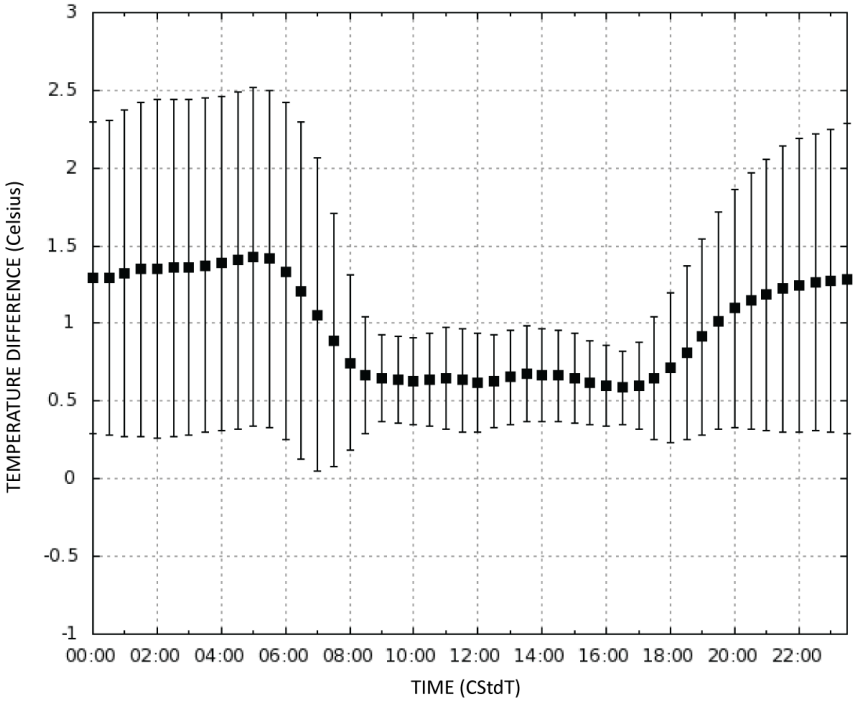

Figure 4.1 Half hourly variation of urban-park temperature difference. The filled squares represent the annual mean and the bars represent the standard deviation variation about the mean values.

Such a thermal contrast can impart a cool divergent outflow at lower levels from parks to the surrounding urban built-up area (*Oke et al, 1989*). Results from earlier studies (e.g. *Upmanis et al., 1998*) indicated that this cooling effect can extend beyond 1 km from a park boundary, extending less for smaller parks, and vanishing for areas less than 2.5 ha (See also *Spronken-Smith and Oke 1998*). Any extension would be welcome relief to residents from hot days, especially to high-risk groups such as the elderly (*Clarke & Bach I971*).

The association of observed urban-park temperature differences with synoptic wind speeds are shown in figure 4.3. The upper frame (a) is for data obtained under clear sky conditions (0 Okta), while the lower (b) is for completely overcast conditions (8 oktas). These results show that the urban – park temperature contrast effectively vanishes when wind speeds exceed 8 m s^{-1} for both clear and cloudy conditions. But the figures also make clear that the contrast decreases quite rapidly as speeds increase above roughly 3-4 m/s (perhaps slightly lower for cloudy conditions), indicating that mixing of air at these speeds and higher, rapidly removes the majority of contrasts between the two areas.

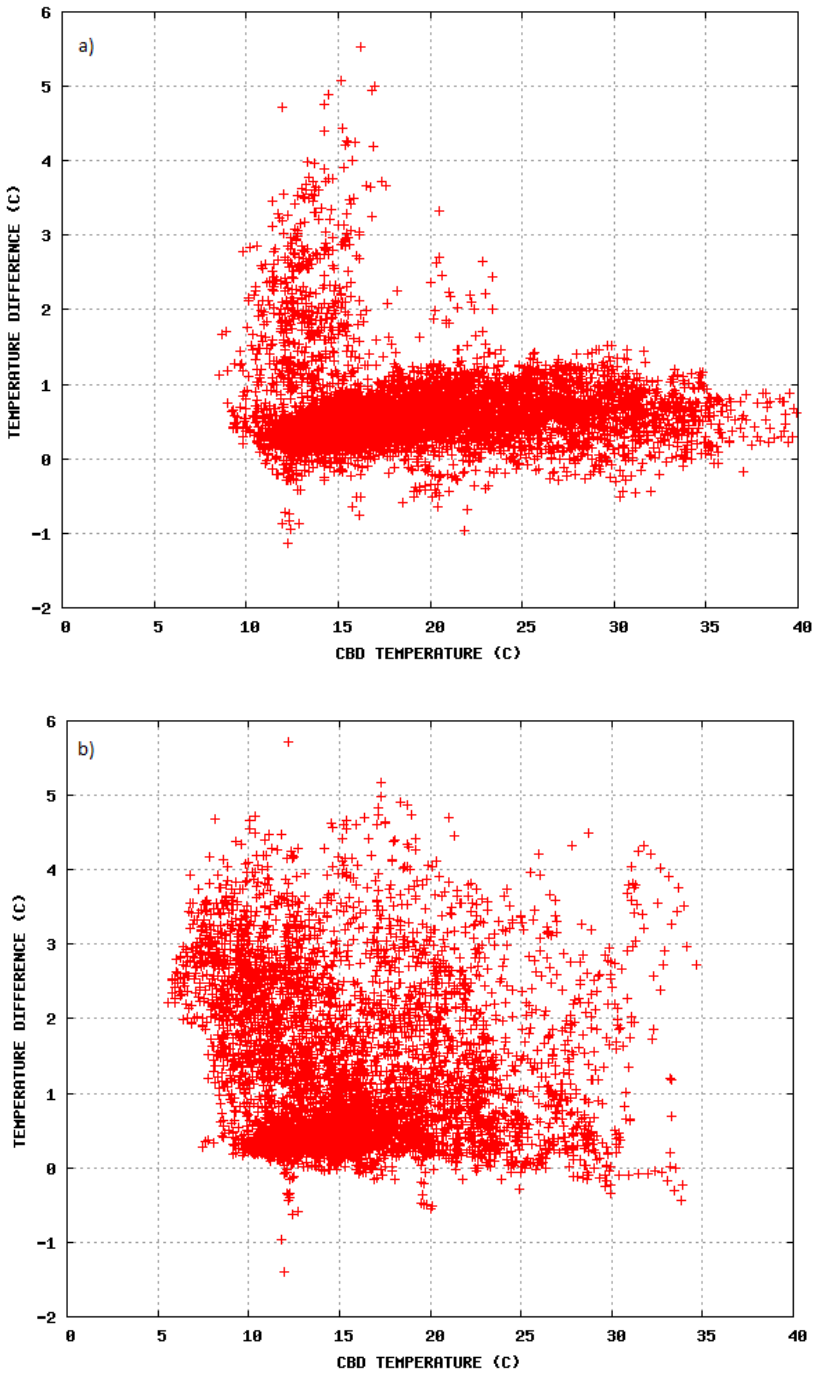

Figure 4.2 Scatter plots of urban-park temperature difference (°C) vs. ambient air temperature observed in Adelaide CBD during (a) Day time (sunrise to sunset), and (b) Night time.

The smaller contrast between urban and park temperatures in figure 4.3 for cloudy conditions at the low wind speeds arises from the reduction in radiative losses from the parklands relative to the buildings with their larger thermal mass, by clouds.

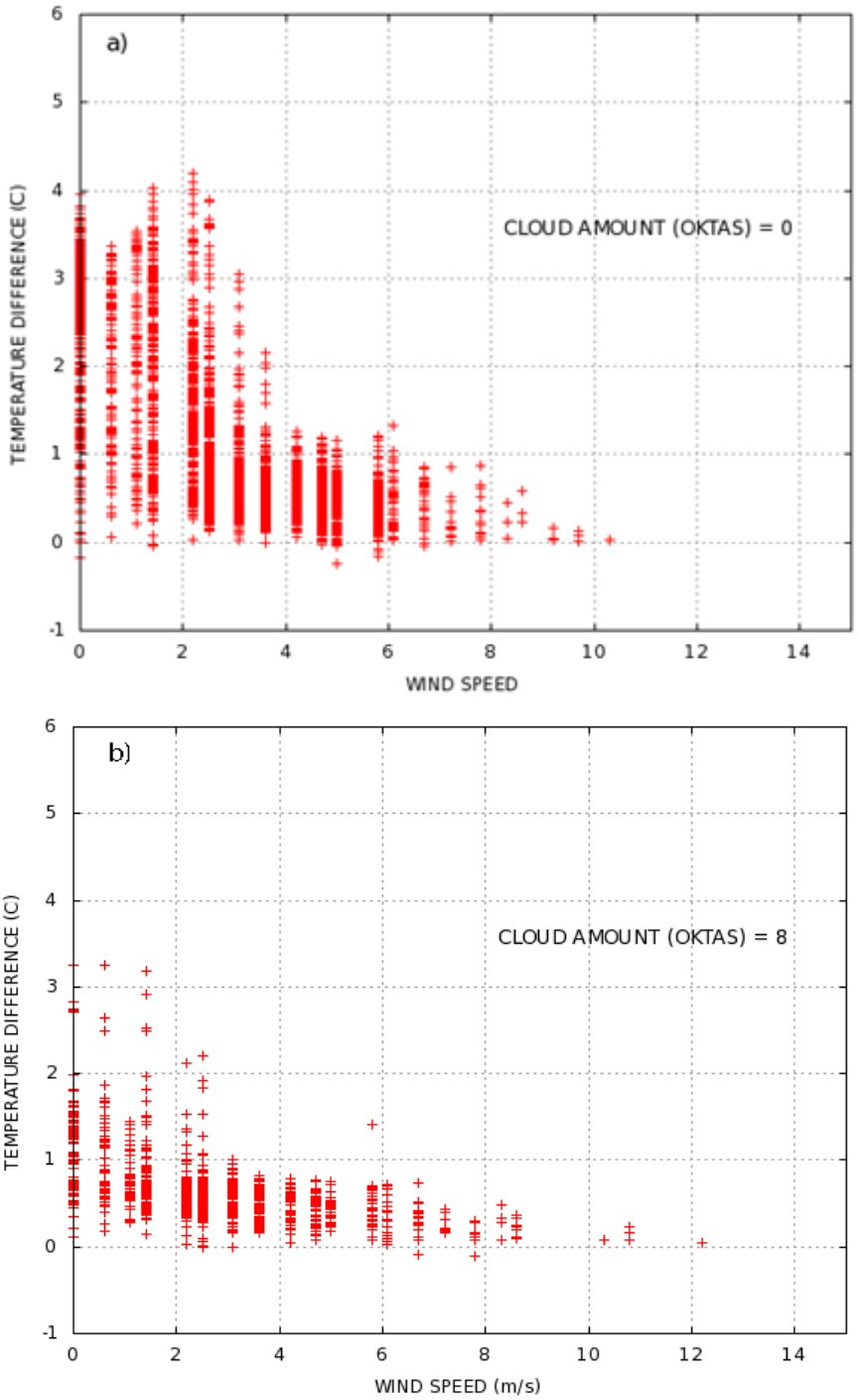

Figure 4.3 Scatter plot showing the dependence on wind speed of measured urban-park temperature differences under clear (a) and completely cloudy (b) skies. There is a rapid decrease in contrast around 3-4 m/s speeds for both conditions, and effectively no contrast above 8 m/s.

4.3 Numerical experiments - setup.

Numerical modelling experiments were devised to examine the effect, if any, that the parklands might have on the CBD air temperatures. The WRF modelling suite was

configured to run in six nested domains with the finer one having a spatial resolution of 125 m and 41 vertical levels. The urban parameters used in the study are given in table 4.1. The vegetation fractions of the three urban classes are assigned to 5%, 25%, and 50% based on the visual analysis of aerial photographs of the Adelaide region, while the albedo values for the three urban classes were specified based on an earlier study (*Coppin, 1977*). Most of the parameters used by the urban canopy model (UCM) in this study are default values since there was no prior information for the study region.

Table 4.1 Urban morphological, thermal, and radiative parameters used in the UCM simulation. The columns ULUC1, ULUC2, and ULUC3 denote the properties of the commercial/industrial area, the high-density residential area, and the low-density residential area, respectively.

Parameter	**ULUC1**	**ULUC2**	**ULUC3**
Artificial surface fraction (%)	95	80	60
Mean building height (m)	10.0	7.5	5.0
Roof width (m)	10.0	9.4	8.3
Road width (m)	10.0	9.4	8.3
Heat capacity for roof and wall (MJ m^{-3} K^{-1})	1.0	1.0	1.0
Heat capacity of road (MJ m^{-3} K^{-1})	1.4	1.4	1.4
Thermal conductivity for roof and wall (W m^{-1} K^{-1})	0.67	0.67	0.67
Thermal conductivity of road (W m^{-1} K^{-1})	0.4	0.4	0.4
Albedo for roof and wall of buildings	0.2	0.2	0.2
Albedo of road	0.2	0.2	0.2
Emissivity for roof and wall	0.9	0.9	0.9
Emissivity of road	0.95	0.95	0.95
Thickness for roof and wall (m)	0.05	0.05	0.05
Number of layers for roof, wall, and road	4	4	4

The time period chosen for the study (centred on 12 June 2010) corresponds to weak synoptic forcing and associated clear and calm weather. The isobaric gradient was weak with a high pressure region situated above the study area for most of the simulation time, giving low cloud amounts (mostly clear skies, or no more than 1 okta), and low windspeeds (less than about 2.5 m/s, weakening later). Earlier studies (*Velazquez-Lozada et al., 2006*) have shown that the weather, particularly wind and cloud, affects the strength of heat islands and that the intensity is greater under calm and clear weather conditions (Chapter 3 of this report addresses aspects in some detail). The model was integrated from 12:00 UTC (9:30 PM LST) 11 June 2010 up to 13 June 2010 00:00 UTC (09:30 AM LST), with the total simulation time of 36 hours for each experiment.

Two numerical experiments were designed to understand the effects of parkland on the city it encloses. The numerical experiments were to examine what impact the current parklands have on the CBD air temperature, and covered the following two cases:

1. CTRL experiment with the current parklands geometry.

2. NOPL experiment with the existing parklands replaced with the urban surface type, to compare with the current surface state.

Results from the finest domain (125 m resolution) are used in the following discussion, unless otherwise specified.

4.4 Model results for the sensitivity of CBD temperatures to altered land-use.

What is reported here are the results of comparing current with modified parkland surfaces, in order to assess the sensitivity of CBD temperatures and meteorology to such changes. The changes involved the existing parkland geometry being replaced with the 'Commercial/Industrial' land-use (NOPL experiment). This numerical experiment was integrated over the same time as the CTRL experiment, i.e., from 12:00 UTC of 11 June 2010 to 00:00 UTC of 13 June 2010.

In the following sections, we use the term "park cool island index" (PCI) (*Spronken-Smith & Oke, 1998*) instead of UHII, to emphasise that the spatial scale which is being considered is smaller than the one often used by others for the UHII (in describing the CBD to rural temperature differences).

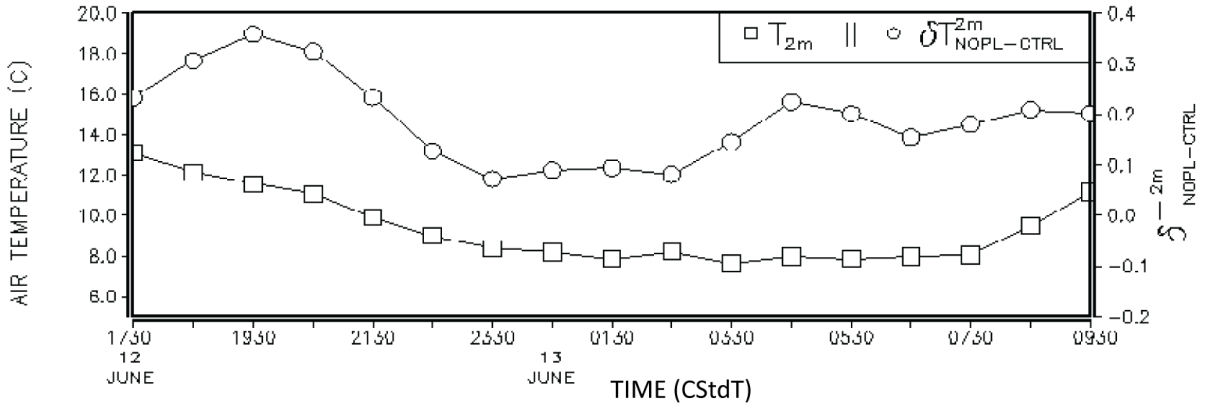

Figure 4.4 shows the modelled nocturnal time series of CBD-averaged 2 m air temperature difference between the NOPL and CTRL (open circles), and the 2m air temperature from the CTRL experiment (open squares).

The time sequence of average 2 m air temperature differences in the CBD between the NOPL and CTRL cases (Figure 4.4) shows that removing the Park Lands would warm the CBD area by an average 0.21°C at night time. This value of course would vary with different weather conditions than those modelled here. Such a small change in average CBD temperature indicates that for the light and slackening wind conditions used in the modelling, cool air in the Park Lands was not advected far into the CBD to affect a large fraction of the entire CBD area, over which the averaging has been done.

Figure 4.5 depicts the magnitude of this average park cool island index calculated from 2 m air temperatures simulated by both CTRL and NOPL experiments. For the average park cool island index (PCI_a), the spatially averaged temperatures are used, both for the urban park T_{pa} and the surrounding urban areas T_{ua}.

i.e., $PCI_a = T_{ua} - T_{pa}$

Previous research employing observational methods revealed that the park influence extends to a distance equivalent to its diameter into the surrounding urban region (*Spronken-Smith & Oke, 1998*). Hence for the calculation of T_{ua} we consider five urban grid

points (~725 m) on the CBD side of the parklands (downwind of the CBD, for a south-easterly simulated air flow). In order to study how the PCI_a index would change on removing the parkland, a similar index (called $sPCI_a$ or sensitivity PCI_a) is calculated over the same location for NOPL experiment. The PCI_a and $sPCI_a$ indices are compared in Fig. 4.5. During night time, the open parkland radiates thermal energy to the sky, cools further due to its low thermal inertia and so causes significant nocturnal cooling of 2 m ambient air temperatures. The simulated park cooling reaches 3°C before sunrise. The predicted cool island effect is present over most parts of the day and it increases as the two surfaces (built-up and vegetated) cool at different rates. By contrast, the $sPCI_a$ values lie within a range of +0.2°C to -0.3°C, indicating the whole park cool island effect is attenuated with the replacement of parklands with urban fabric. Further, this form of surface cover would block cold air intruding into the CBD, keeping it warmer.

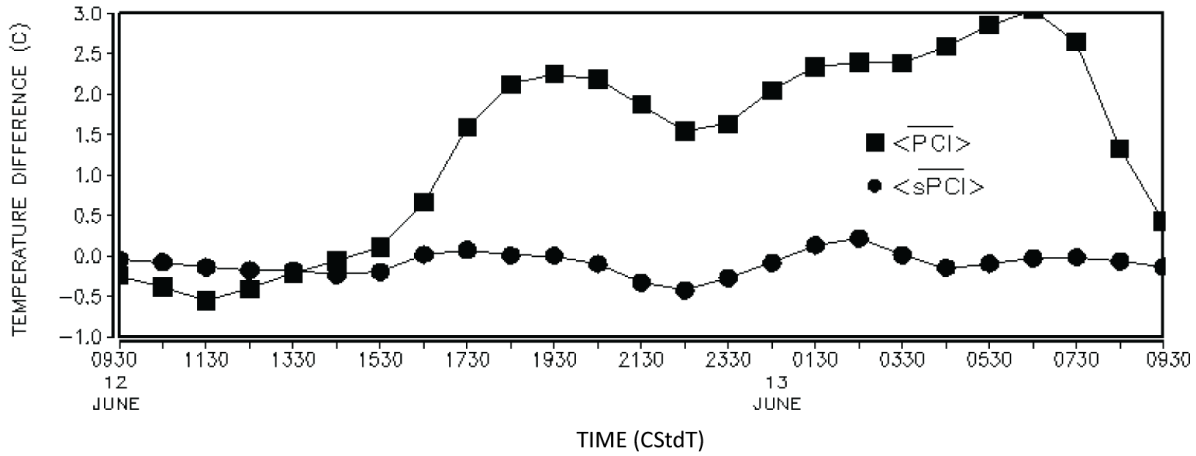

Figure 4.5 Diurnal variation of the calculated "area averaged" park cool island indices for CTRL (PCI, filled square) and NOPL (sPCI, filled circle).

4.5 Conclusions.

The present study establishes baseline knowledge on the environmental function of the central Adelaide parklands. The effect of the parks are analysed in this chapter using 11 months of half hourly data obtained from the temperature monitoring network established in the CBD and parklands. The parks are found to be cooler by about 0.64°C in day times and 1.32°C in night times, when averaged annually. The results indicate that the variation of

night time urban-park temperature difference differs little from winter to summer, though the day-time values show that the parks tend to be relatively cooler on summer days than on the winter ones. The parklands were cooler most of the time and of the year, with the reverse occurring only on less than 0.5% of the observations. The urban-park thermal contrasts were influenced by cloud cover and wind speeds, with overcast conditions and high wind speeds limiting the growth of differential urban-park cooling. The wind speed, for which the thermal effects were nullified, was found to be about 8 m s^{-1}, but the differences decreased rapidly with increasing wind speeds above 3-4 m/s. The parks were substantially cooler (~ 2 °C) than the urban built-up areas on warmer nights, and hence it is assumed that in calm or near-calm conditions, adjacent and downstream urban areas would benefit by movement of cooler air from the parklands.

The 'cooling effect' on the Central Business District (CBD) of Adelaide due to the unique parklands surrounding it was also studied using the WRF model. Modelling sensitivity studies indicate that replacing the parkland with urban surfaces would increase the ambient temperature over the entire CBD on an average by ~0.2°C, and presumably much larger close to the urban-park boundary. It is important to note that this predicted increase will vary for different weather conditions and seasons, as implied by the figure 4.4 results. The simulated average park cool island has the highest magnitude of 3°C, underlying the importance of parklands in Adelaide's thermal environment.

Although the model could simulate the base state temperature and flow fields reasonably well, biases still existed in the simulation. Recent modelling studies (e.g. Wang *et al*., 2011) show that critical heat exchanges and surface temperatures are sensitive to the urban geometry and the thermal properties of surfaces, but that vegetated grounds have lower impact on them. This could be a possible reason for the relatively small magnitudes of differences between the parks and the urban built-up area as simulated by the model. Further validation and fine-tuning of the coupled modelling system is required to understand better the model behaviour and dependence on those parameters. This is because the coupled mesoscale-land surface model is sensitive to various surface characteristics like soil moisture availability which is an important controlling parameter on the flow pattern and on surface energy fluxes. Ambiguities in accurate specification of such fields will have some influence on model biases. Nevertheless, the model does capture the

observed trend in urban canopy temperature and hence has the potential to simulate the urban environment more realistically at such higher resolutions. The greater focus on urban observational studies and modelling in recent times should lead to improved agreement in future between modelling and observations over a wider set of circumstances than was able to be addressed here.

References to Chapter 4.

Clarke, J.F., and Bach, W., 1971. "Comparison of the comfort conditions in different urban and suburban microenvironments", *International Journal of Biometeorology*, **15**, 41 – 54.

Chen, F., Kusaka, H., Bornstein, R., Ching, J., Grimmond, C. S. B., Grossman-Clarke, S., Loridan, T., Manning, K.W., Martilli, A., Miao, S., Sailor, D., Salamanca, F.P., Taha, H., Tewari, M., Wang, X., Wyszogrodzki, A.A., and Zhang, C., 2011, "The integrated WRF/urban modelling system.development, evaluation, and applications to urban environmental problems", *International Journal of Climatology*, **31**, 278 – 288.

Coppin, P.A., 1977. "The albedo of natural surfaces", Flinders University Research Report, **28**.

Oke, T.R., Crowther, J.M., McNaughton, K.G., Monteith, J.L., and Gardiner, B., 1989, "The micro-meteorology of the urban forest". *Philosophical Transactions of the Royal Society of London, Series B,* **324**, 335 – 349.

Spronken-Smith, R.A., and Oke, T.R., 1998, "The thermal regime of urban parks in two cities with different summer climates", *International Journal of Remote Sensing,***19**, 2085 – 2104.

Upmanis, H., Eliasson, I., Lindqvist, S., 1998, "The influence of green areas on nocturnal temperatures in a high latitude city (Göteborg, Sweden)", *International Journal of Climatology,***18,**681 – 700.

Velazquez-Lozada, A., Gonzalez, J.E., Winter, A., 2006, "Urban heat island effect analysis for San Juan, Puerto Rico", *Atmospheric Environment,***40**, 1731 – 1741.

Wang., Z.H., Bou-Zeid, E., Au., S.K., Smith, J.A., 2011, "Analyzing the sensitivity of WRF's single-layer urban canopy model to parameter uncertainty using advanced Monte Carlo simulations", *Journal of Applied Meteorology and Climatology*, doi. 10.1175/2011JAMC2685.1).

Chapter 5 - Micro-climate modelling of the Adelaide Urban Heat Island

Cäcilia M. Ewenz

5.1 Introduction.

The Adelaide Urban Heat Island was first studied in the early 1970s, when Flinders University undertook an enhanced observation program throughout the CBD and suburban Adelaide (Lyons, 1974).

A new observational study, the basis of this report, covering the CBD, the parkland and suburban Adelaide was established, with a main focus to understand the effect of the parklands on mitigation of the Adelaide UHI. *Kent's (2010)* analysis, using observations for winter 2010, showed an average UHI of about 3°C difference between the Adelaide CBD and the "rural" area (the latter defined in this chapter as the Bureau of Meteorology (BoM) station at Edinburgh Airport, about 25 km from the CBD). A maximum UHI strength of 9°C was encountered in winter 2010. *Vinodkumar et al. (2012)* modelled the UHI and Park Lands interaction using the meso-scale limited area model WRF. That high resolution study with a horizontal grid resolution of approximately 150 m showed a clear impact of the Adelaide Park Lands on the development of the UHI, and was reported upon in the preceding chapter.

This chapter describes the results of applying a high resolution micro-scale numerical model to parts of the CBD to investigate street level atmospheric conditions, such as temperature gradients across streets due to variation in shade, ventilation effect of street layout and effect of green areas on the surrounding, with a horizontal resolution of up to 5m. The urban model used is Envi-Met (*Bruse, 1999; Bruse & Team, 2012; Bruse and Fleer, 1998*) and is freely available.

Modelling the urban micro-climate provides two major insights into processes associated with an urban heat island. Firstly, several aspects can be addressed which are difficult to treat observationally. A much finer spatial and temporal resolution of temperature variations can be examined compared to the established iButton network. As

well as temperature, the distribution of other atmospheric variables such as wind speed and direction, radiation, sensible and latent heat fluxes (all of which impinge on the UHII), can be obtained. The urban micro-climate model allows detailed horizontal and vertical profiles of parameters to be extracted. Secondly, such a model can be used to explore the effects of changed building configurations and surface treatments on urban climate, for example to test the effect of different building height distributions, and street layouts (e.g. street widths, and surface characteristics of footpaths). This second approach is also helpful for investigating the effect of climate change, in order to inform planning decisions.

5.2 Model and Sites.

5.2.1 The Envi-Met model.

The three-dimensional micro-climate model ENVI-met (http://www.envi-met.com/) is designed to simulate the surface-plant-air interactions in urban environments. The typical resolution of the model ranges from 0.5 m to 10 m in space with a maximum time step of 10 seconds. The total simulation time is up to 1 to 2 days. The resolution allows the analysis of small-scale interactions between individual buildings, surfaces and plants. The model is based on the thermo-hydrodynamic set of equations. Calculations include long and short wave radiative fluxes accommodating shading and reflection from buildings and vegetation, sensible and latent heat fluxes from vegetation and photosynthetic energy exchange, surface and wall temperature on a grid point and wall basis, water and heat exchange into the soil as well as bio-meteorological parameter and inert gas and particle dispersion at leaves and surfaces (*Bruse, 1999; Bruse & Team, 2012; Bruse and Fleer, 1998*). For a detailed program description please see http://www.envi-met.com/, the official Envi-Met website.

A model domain was defined as an x,y,z-grid with 99, 96 and 25 grid points respectively. The horizontal resolution was set to 5m (for reasons set out below, thus giving a model horizontal area of approximately 500 m x 500 m), and the vertical resolution was set to 4 m in the lowest 30 m of the atmosphere, then increased by 15% each level up to the top of the model which was at 471.08 m height. For each simulation a nesting grid of 10 grid points was defined around the model area to minimise boundary effects on the area of interest.

In a model domain, it was necessary to specify each exposed surface as to type and properties (albedo, emissivity, thermal conductivity, specific heat, density etc., with more detail than the broadly applicable values given in Table 4.1 of the previous chapter), because the thermal behaviour of a site and its surroundings depends upon the physical characteristics of the surface and what underlies it. Soil data were estimated from a summary of a comprehensive soil survey made in the 1970's (*Sheard, 1996*). That survey states that the soil in Adelaide is predominantly of clay and sandy clay types. These types define soil thermal properties. Soil profiles were established from the surface characteristics data set. Sandy clay as well as clay, was set below the surface types of asphalt, various pavements and grassed areas.

Bruse & Team (2012) state that the buildings in the model are active elements. Although the same settings apply for each building in the simulations here, the exchange of heat between indoors and outdoors can be specified. The system is defined by the temperature in the building, which is kept constant throughout the simulation and the thermal exchange through walls and roofs. Storage of heat in the walls is not yet implemented in the current model version. The heat exchange between inner and outer wall and roof only depends on the temperature gradient between both sides. This does not provide realistic roof and wall temperatures yet; sunny sides will overestimate the temperatures, while shady sides display a quick decline in temperature. A storage of heat and a slow release of this heat during the night, which is major urban heat island characteristic, is therefore not part of this model setup. The urban heat island effect mainly results from the surface energy balance for the various urban materials, e.g. bitumen roads and concrete footpaths.

5.2.2 City locations.

Models were run for three zones including particular buildings in the Adelaide CBD. The areas were chosen to encompass the studies on some building aspects reported in Chapters 6 & 8.

The shape, height, and position of each building and surrounding area in the selected zones was evaluated from the Adelaide 3D digital data set, provided by the Adelaide City Council (ACC). Information on vegetation or surface type for each grid cell, e.g. tree, road

surface or pavement was also derived from data sets provided by the ACC. Missing data was filled with information taken from Google imagery (some inconsistencies may still occur), so in the following figures, not all buildings and spaces are precisely defined. A 1m by 1m raster data set for each surface parameter was evaluated and provided by S. Benger (Flinders University) from the original GIS data sets. The resolution used in all model simulations was reduced to 5m by 5m, where each 5 m by 5 m square was set to the centre point value gained from the $1m^2$ resolution data set.

The position of all three city zones in Adelaide was set to a latitude of 34.93°S and a longitude of 138.60°E. The differences in latitude and longitude of the three sites from these particular values has negligible effect on the solar radiation input, lying well within the margins of error arising from uncertainties in temperature, humidity and wind observations used to drive or check the model.

The contexts of the three zones are as follows.

5.2.2.1 Victoria Square.

Victoria Square is an open and green space intersected and surrounded by roads and footpaths.. To the east of Victoria Square, the buildings are typical for a medium height city centre district. The grassed area of the Square would possibly mitigate any urban warming effect on temperatures in the environment surrounding the buildings. Figure 5.1 shows the modelled area for this zone.

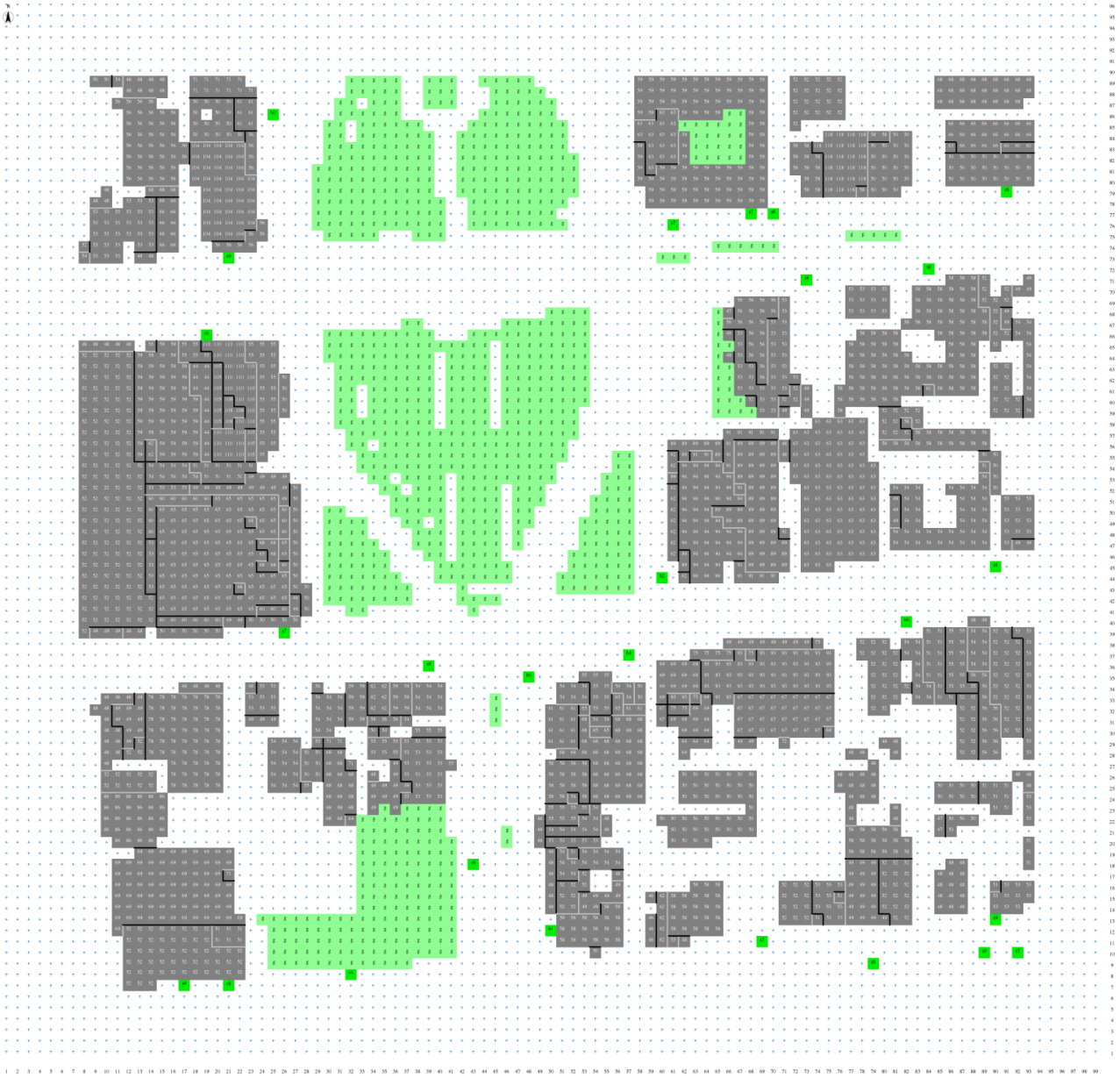

Figure 5.1 Built up area around Victoria Square. The grid orientation is to the cardinal points with north at the top. The green areas define vegetation of either trees or grass. The height of the buildings, the surface characteristics and the major trees are defined by the 3D building, roads, paths and trees data sets provided by the ACC (Benger, 2012).

5.2.2.2 CBD city centre.

The second zone of interest was centred approximately on the intersection of Pirie and King William streets. This is close to the CBD's highest building, hence a strong heating effect around this area would be expected. Figure 5.2 shows the modelled domain, with the northern tip of Victoria Square at the bottom centre, Franklin-Flinders Streets running left to right just north of that point.

Figure 5.2 Built up area near the CBD centre, King William St/Pirie St intersection. Other details as in Figure 5.1

5.2.2.3 Northern CBD, King William St.

The third zone is in King William St near North Terrace, amongst other Adelaide CBD high rise buildings, the corner of King William St and Currie/Grenfell Sts (near to and across the southern boundary) especially displaying the lowest sky view factor values in the CBD. Observations show highest temperatures in this region. The zone is shown in figure 5.3, with the green area corresponding to the edge of lawns in Government House adjacent to North Terrace.

Figure 5.3 The northern CBD built-up area, King-William St/North Terrace. Other details as in Figure 5.1.

5.2.3 The initial atmospheric model conditions.

The 19th of January 2011 was chosen for the model evaluation, because on that date, a comprehensive city traverse data set was acquired (Figure 5.5), complementing the fixed IButton data from the UHI project.

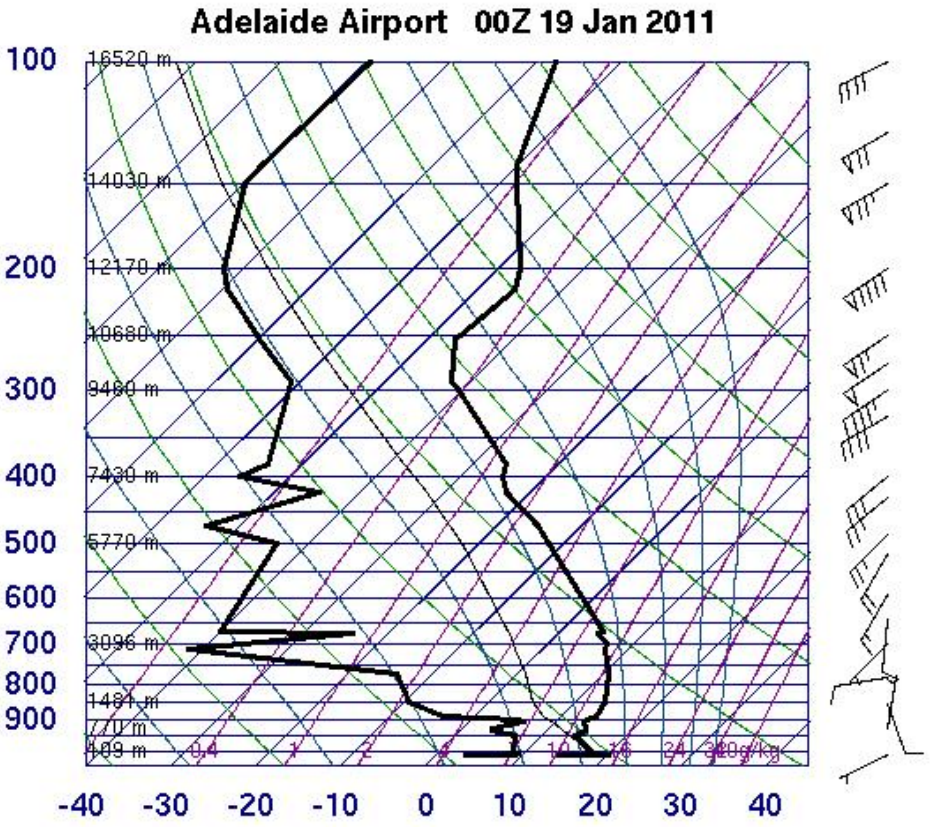

Figure 5.4 Skew T-log P diagram showing the variation of temperature (right hand heavy line), humidity as dew-point (and mixing ratio) (left hand heavy line), and winds (arrows on the right), with height above Adelaide on the 19th January 2011, 9:30 am CStdT. The model used data from the lower levels of this sounding. (Bureau of Meteorology Adelaide Airport radiosonde data, from UWYO 2011).

Envi-Met was initialised at 4 am CStdT (UTC+9.5hrs) on the 19th of January 2011. A night-time start of the model is generally preferred so that the simulated atmosphere can slowly adjust to the applied conditions. Strong convection which is often found in day–time hinders this process.

The simulation was run for 48 hours and hence included the period of the traverse observations. The initial atmospheric data were 0.5m/s wind at 10 m above ground from a south westerly direction (225°). The initial air temperature at 2 m above ground was set to 18.8°C. The relative humidity at 2 m was set to 55% and specific humidity for the model's one-dimensional initialisation at 2500m height was 0.86 g/kg. These surface and higher level atmospheric values were set according to radiosonde data from Adelaide airport from 19 January 2011, 9:30 am, CStdT (Figure 5.4).

An initial soil temperature for the top layer was 19.85°C. The atmospheric turbulence closure was chosen to be prognostic in three-dimensions. The lateral boundary conditions for temperature and humidity were set open and for turbulence kinetic energy (TKE), the lateral boundaries were forced.

5.3 Results from the traverse measurements.

Chapter 2, Figure 2.4, shows the vehicle setup for the measurements on this traverse. The temperature data measured in 1.8 m above the ground were combined with GPS data in order to quantify the location of the individual measurement. In Figure 5.5 the corrected temperature data from the traverse is shown as coloured dots, each colour specifying a temperature range around the displayed isolines' temperature from the iButton data field.

Figure 5.5 shows the greater variation of the temperature at street level (1.8m above the surface) compared to the fixed iButton network (at 4m above the surface). However, the differences here do not result from the measurement height difference alone. The traverse data set has a much finer resolution and hence exhibits a larger variation of heat exchange (urban energy balance due to surface conditions and heat exchange properties) in the urban area than the coarse iButton network can display. While some of the traverse data perfectly agrees with the iButton field (e.g. southern Adelaide CBD around South Terrace), there are higher temperatures than in the iButton field, especially to the west of the city along West Terrace.

These variations on a smaller scale can be explained by fine resolution micro-scale modeling, here employing the "urban-scale" model Envi-Met.

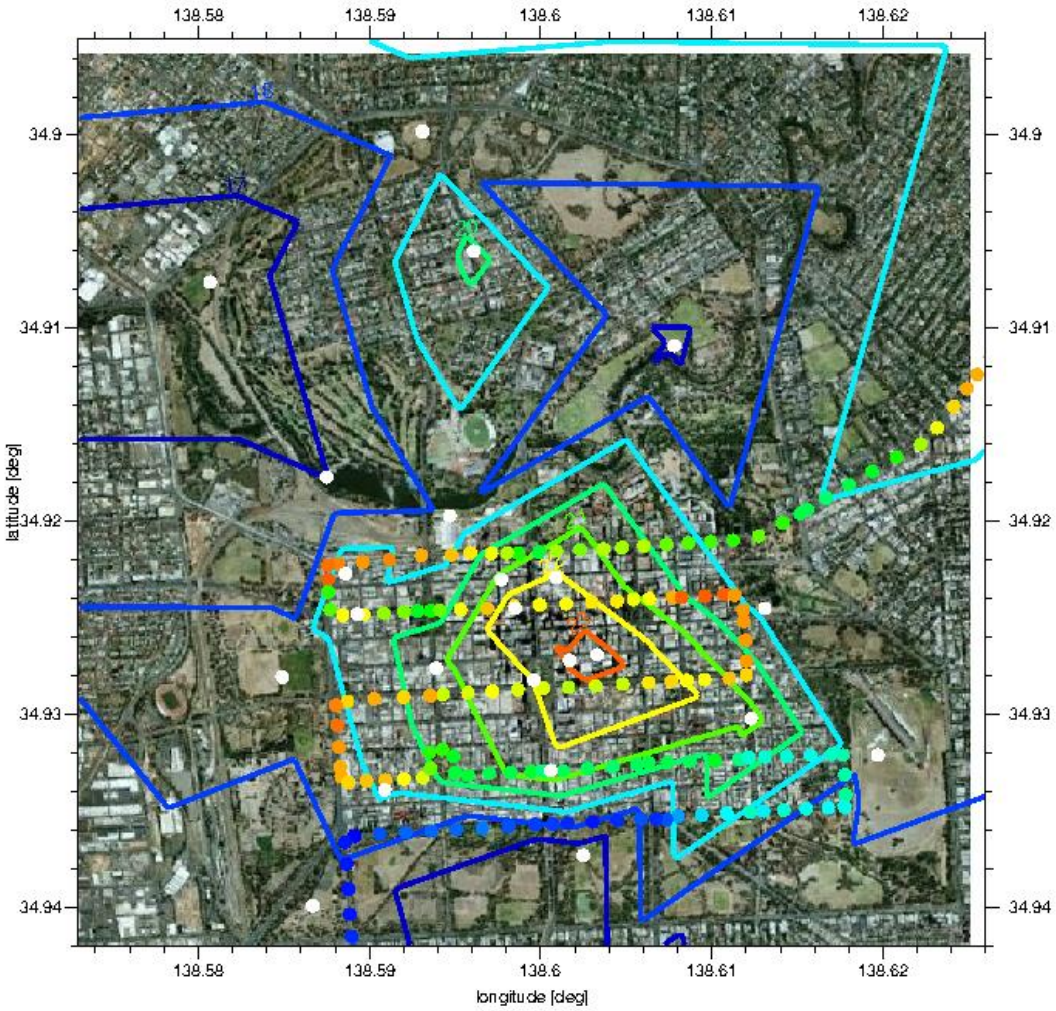

Figure 5.5: iButton data for 20 April 2011, 3am (indicated by coloured isolines, temperature difference between the lines is 1 °C, light blue represents 19 °C and light green is 20 °C) and vehicle traverse temperatures (coloured dots) for 2.30am to 3.30am, 20 April 2011. The colours of the isolines and dots are equivalent. The isolines show the distribution of the iButton field, while the dots represent a temperature range around the equivalent isoline colour. The wind at Netley (EPA) displayed a weak wind of 0.4 m/s from a direction of 298° at 3am.

5.4 Results from modelling.

Simulations of the flow fields and temperature patterns for the three defined city areas were run for 48 simulation hours each. The first six hours are used as spin up time for the model to adjust the atmospheric fields to the model equations and approximations of the model environment. The simulations were initialised during the model night during weak or absent turbulence conditions. This minimises any numerical error and noise in the results.

Results are shown for one simulation for all three locations in the Adelaide CBD, initialised with the same meteorological conditions as defined earlier. For the SA Water House case, additional simulations were run, pointing out variations in the overlying wind direction and the resulting changes to the meteorological fields.

5.4.1 Victoria Square.

For this location, the model results clearly show that the green space of Victoria Square reduces environmental temperatures, especially overnight, hence reducing the urban heat-island effect on the surrounding buildings. Temperatures near Victoria Square are generally lower overnight, exhibiting a larger cooling over the grass surface (from larger outgoing long-wave radiation fluxes). The concrete and stone of the buildings and the bitumen surfaces of paths and roadways store daytime heat longer due to their higher heat capacity.

A 3-dimensional view of the study area with the temperature distribution in 1 m above ground at midnight, 20 April 2011 is shown in Figure 5.6, Buildings are embedded in the approximate field of open space around Victoria Square and the street channels through and adjacent to the square. Here the temperature distribution is similar to the 2 am distribution below, indicating that over these two hours, there has been little evolution of the modelled temperature distribution.

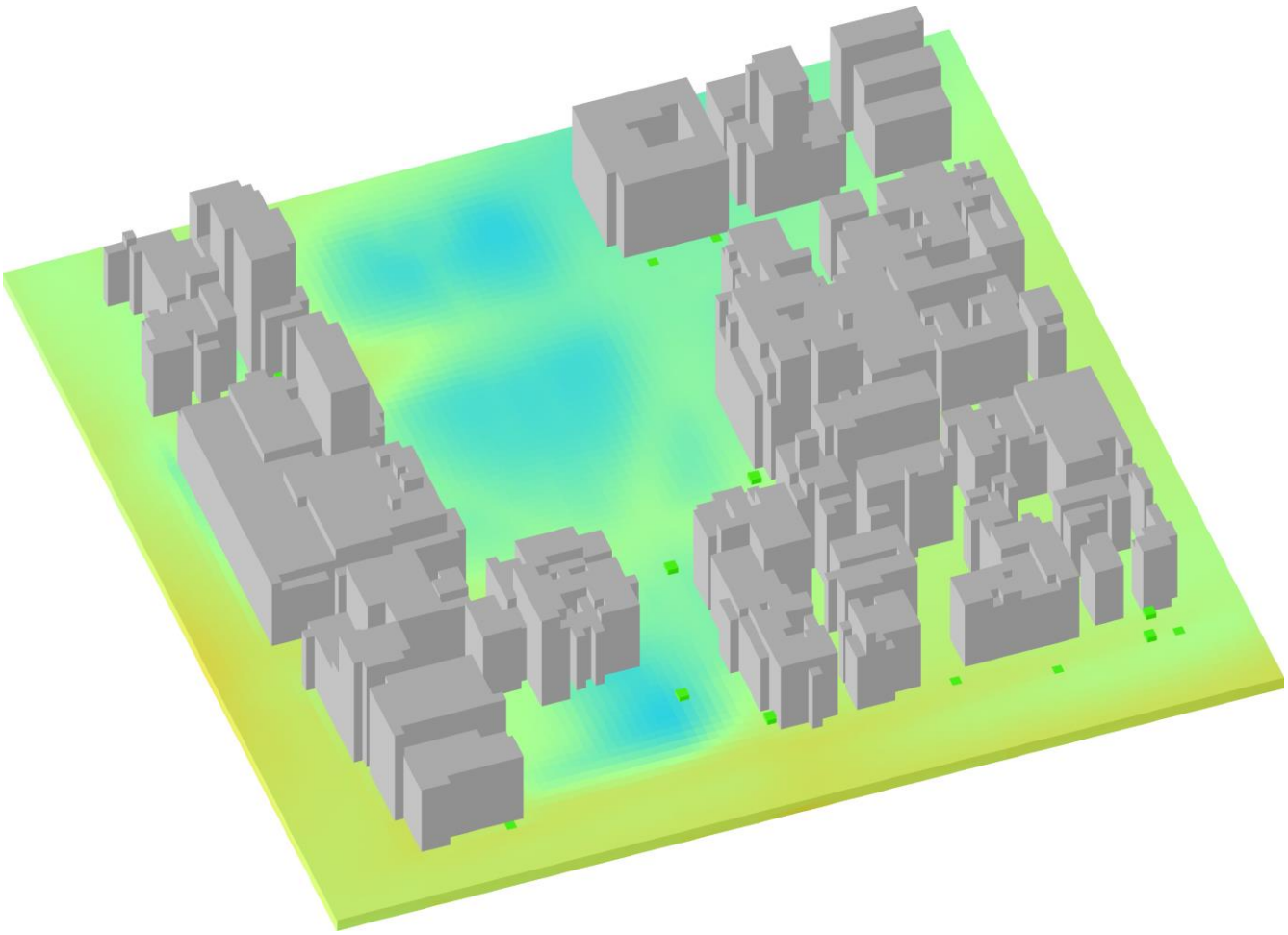

Figure 5.6 The temperature variations at 1 m height at 00:00 CStdT, for 20 January 2011, set within a 3-dimensional view around Victoria Square and surroundings. The colour range displays an approximately 0.3°C potential temperature deviation from the domain average. Buildings are marked in grey, while the major trees are visible as small green cubes.

Figure 5.7 displays the 2 am modelled temperature at 4 m height. The temperature is lowest over the grass surface of Victoria Square. The fields of lower temperature are elongated to the north-east, from the light breeze at 2 am from the south-west.

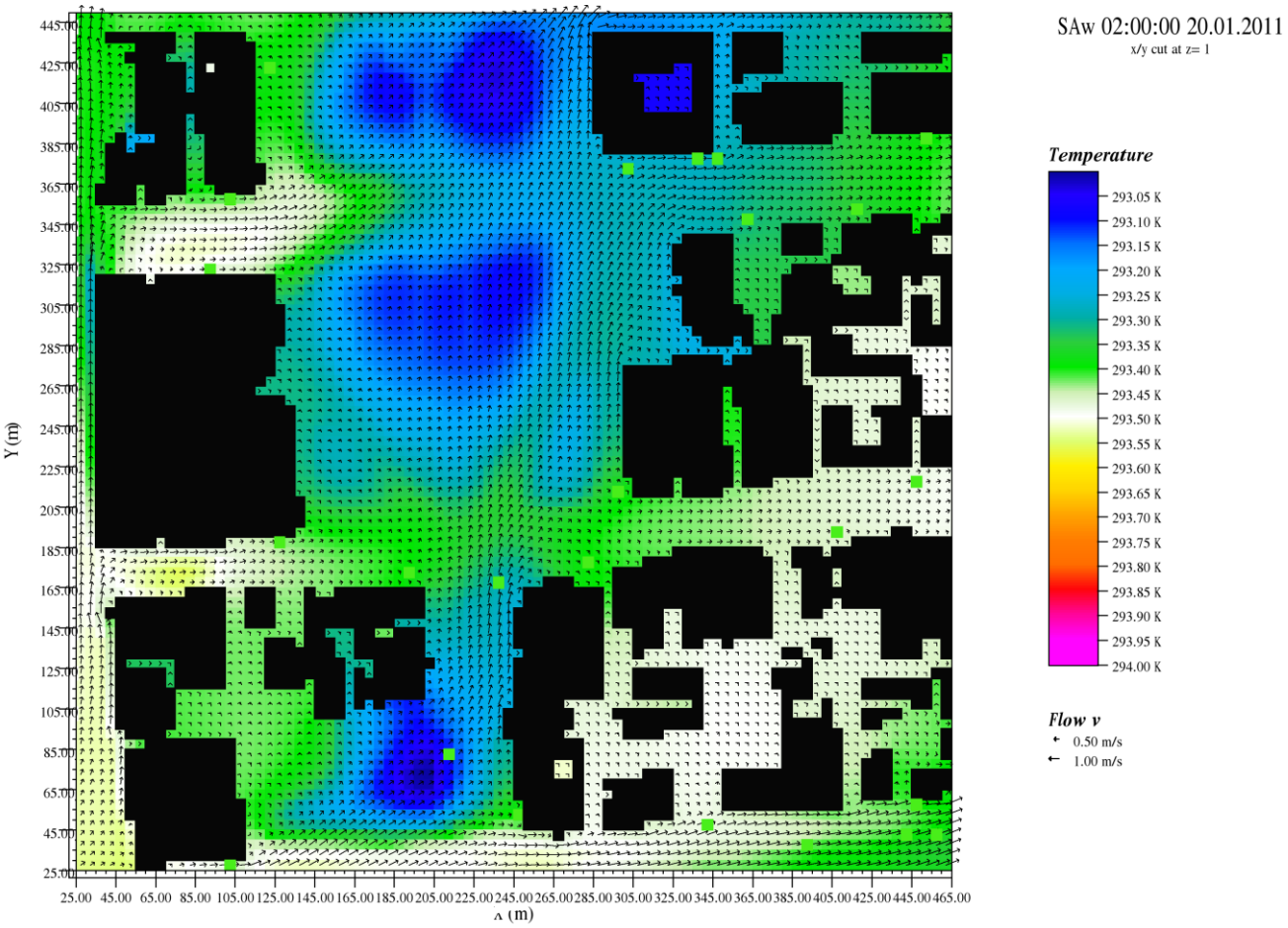

Figure 5.7 Victoria Square zone 1: 20th January 2011, 2 am view of the temperature and wind fields at 4 m height (temperatures in Kelvin, subtract 273.15 to convert to Celsius). The colour coding is for a temperature range of almost 1°C (1 K), blue (cooler) to pink (warmer). The near surface wind field is displayed by arrows, the length of each arrow represents the wind speed (scale shown below the temperature panel on the right) and the arrow's direction displays the wind direction.

The temperature over the grass surface is approximately 0.3°C cooler than the surrounding open roads. In street channels the temperature is higher and the difference is positive up to 0.15°C.

During the daylight hours, the modelled patterns are significantly different from the night-time ones. The effect of the circulation through the street channels as well as the shading of areas due to buildings is evident in the 12:00 pm temperature deviation, Figure 5.8. The southern (shaded) sides of the buildings exhibit generally lower temperature. Eastern and northern sides display a temperature elevation from exposure to the sun to that time. Although the grassed area of Victoria Square does mitigate the temperature

increase, warmer as well as cooler air is transported with the wind through the different street channels and leads to changes in temperature across Victoria Square.

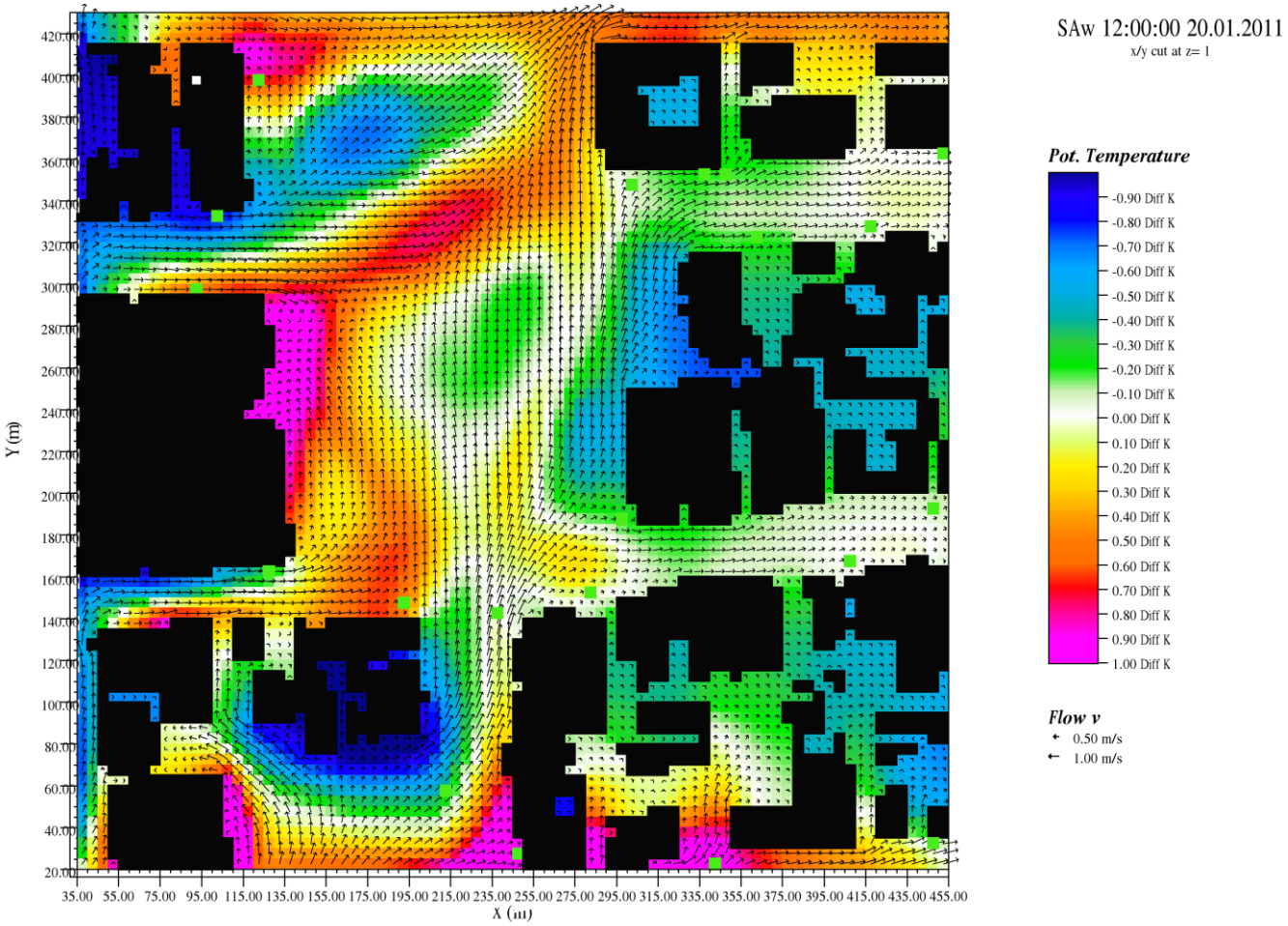

Figure 5.8: Temperature and wind patterns around Victoria Square, on 20 January 2011, at 12:00 CStdT. Details as in Figure 5.7, but with a temperature range of 2°C here.

5.4.2 CBD city centre zone.

This zone has some of the highest buildings and hence one of the lowest sky view factors in Adelaide. In the street channels heat can be trapped, so the night-time temperatures can be significantly higher than around Victoria Square (see section 5.1).

Figure 5.9 displays the temperature observations for two locations at Flinders St (north and south, see chapter 2 for details of the observational network) and for the same two locations of the simulated CBD city centre case at the surface and 4 m height level, the latter being the level from which the observations were made. While the two iButton data sets are very similar in their diurnal variation (a pattern that also persists over longer records with only minor deviations), the modelled air temperatures at 4 m height show the

daily variation with a peak around the same time as observed, but with a significantly smaller variation and a slightly lower mean value –and the modelled results for the two site are effectively indistinguishable. By contrast, the modelled surface temperature for the Flinders St north site follows the 4 m observations quite closely, peaking at the same time and having a similar amplitude, whereas Flinders St south exhibits a larger modelled diurnal variation than observed, with an earlier peak. Some of that difference between the two modelled surface results arises from the longer solar exposure on the southern side of the street compared to the northern side (and is qualitatively realistic), some arises from comparison of a point value from the site with the modelled result from a 25 m^2 average, but the quantitative differences between the observations and the model can only arise from modelled surface temperatures and resulting convective heat fluxes being too low, at least up to the 4 m level.

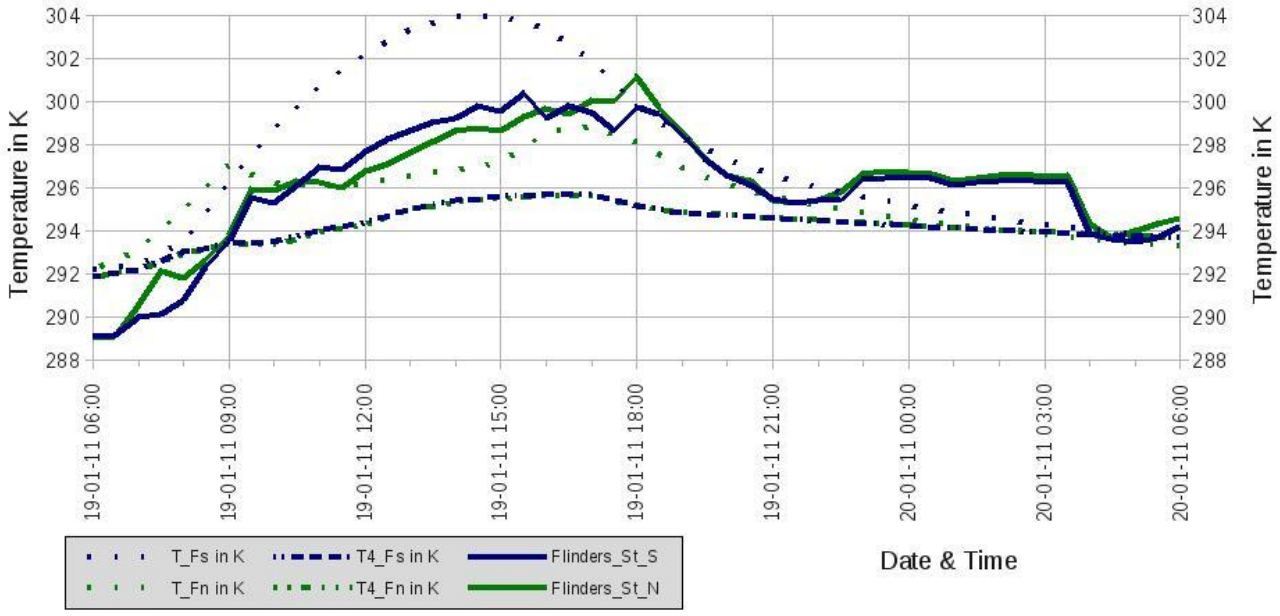

Figure 5.9 Diurnal temperature variations for two locations on opposite sides of Flinders St. Shown are the model data at the surface (dotted lines), the model data at 4 m height (dash-dotted lines) and the iButton network observation (solid line) for Flinders St south (in blue) and Flinders St north (in green).

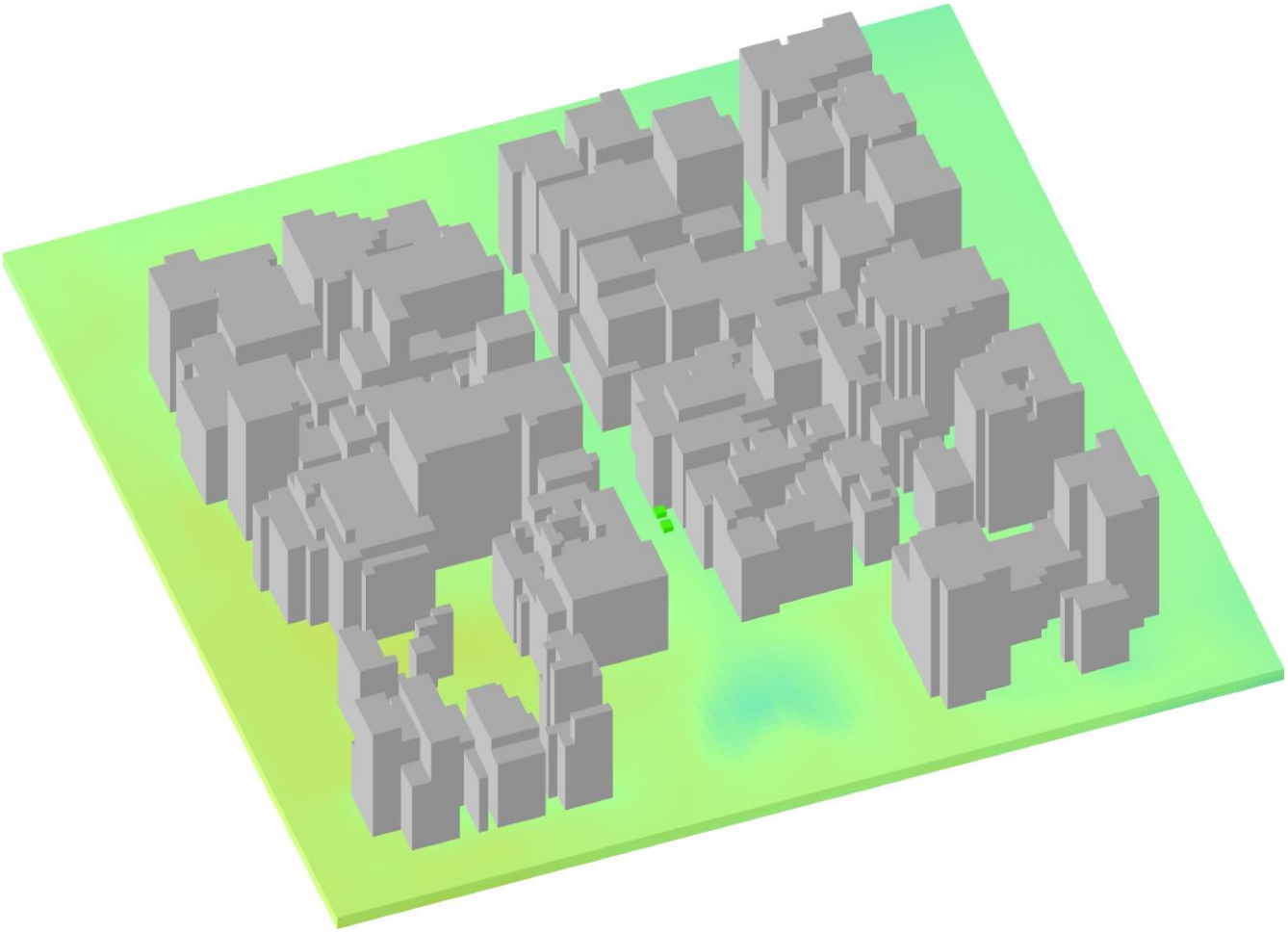

Figure 5.10 The modelled temperature distribution at 1 m height in the central CBD zone, for the 20 January 2011 00:00 CStdT. Details as in Figure 5.6.

The view shown in Figure 5.10 at 00:00 CStdT, exhibits a cool patch in the northern part of the Victoria Square, consistent with the modelled result for the Victoria Square zone alone, shown in figure 5.7. Temperatures in the narrow street channels show little variation with position. Some very narrow streets appear cooler (see Figure 5.11 below) which may be an artifice of the fact that every surface that was unspecified in the base data was set to a bare surface or that the narrow streets did not receive any sunlight at the surface directly. More work has to be done to clarify these details.

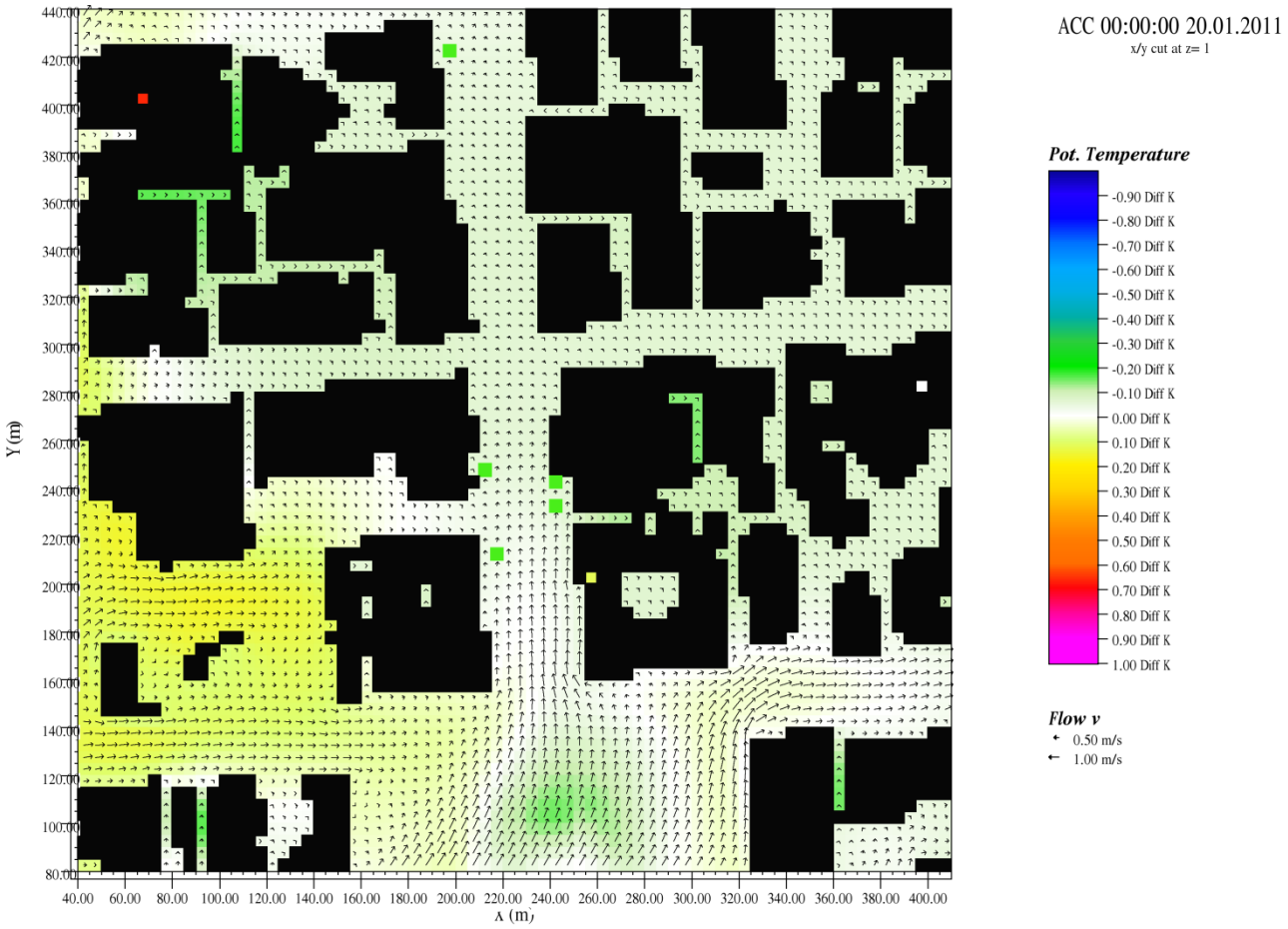

Figure 5.11 Temperature and wind variations at 4 m height in the CBD central zone on 20 January 2011 at 00:00 CStdT Details as in figure 5.7, but with a temperature range shown of 2°C here.

5.4.3 Northern CBD zone.

This zone includes several high rise buildings. However, north of North Terrace, there are parklands and the grounds of Government House, providing some green space. This has resulted in lower modelled air temperatures in the area. Figure 5.12 show the modelled results on the same date and time, and at 1 m height, as for the other buildings.

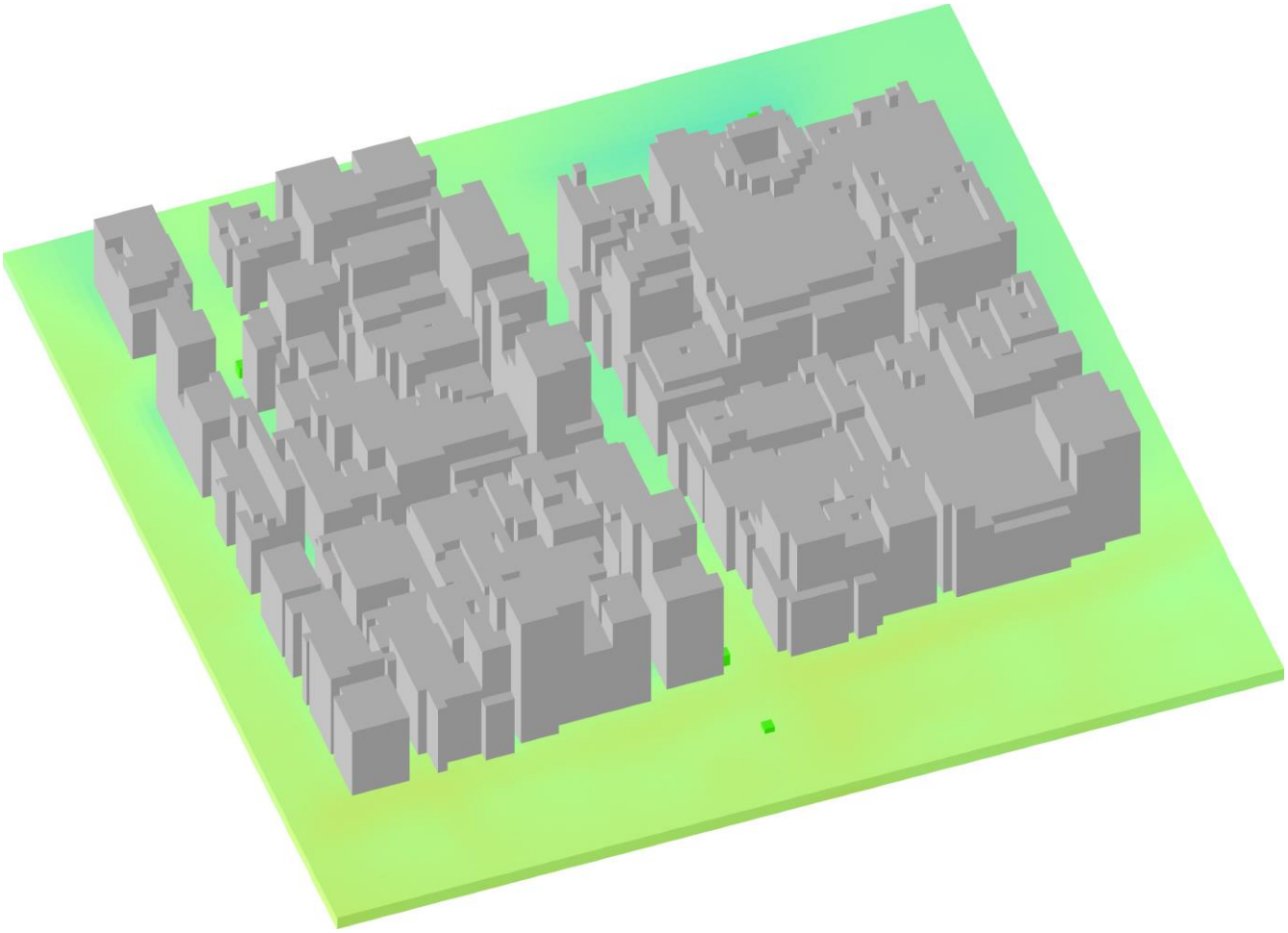

Figure 5.12 3D view of the northern CBD zone, and the modelled temperature distribution, at 1 m height at 00:00 CStdT, for 20 January 2011. King William road runs through the centre. Details as in Figure 5.6.

5.5 Conclusions.

The Envi-Met urban scale atmosphere-vegetation-surface model has provided broadly realistic flow and temperature patterns for the three areas investigated in the Adelaide CBD. However, it has shown limited capability to simulate the detailed urban environment of the three chosen locations. It is believed that currently, the model generally underestimates the sensible and latent heat flux (Nice, personnel communication), which then would result in an underestimation of the diurnal air temperature changes and moisture fluxes. While nothing yet can be said about the moisture changes, comparisons of modelled diurnal temperature changes with observations from nearby UHI network monitoring sites support the view that temperature variations are indeed underestimated.

Overall, the three CBD zones display the UHI effect of concrete and asphalt structures on the urban temperature field, while grass surfaces show lower temperatures. Wind-driven atmospheric mixing is able to mitigate the UHI effect on nearby built up areas.

The central zone, which includes the city's highest buildings and has the least green area is clearly warmer during the night than the Victoria Square zone, or the northern CBD zone with green space of Government House to its north.

References for Chapter 5.

Benger, S., (personal communication) 2012: x,y data set in 1x1 m2 resolution from the ACC: 3D, roads and path and trees data sets, personal communication. Flinders University, School of the Environment.

Bruse, M., 1999, "Die AuswirkungkleinskaligerUmweltgestaltung auf das Mikroklima. Entwicklung des prognostischennumerischenModellsEnviMetzur Simulation der Wind, Temperatur und Feuchteverteilung in städtischenStrukturen", *PhD thesis Ruhr University, Bochum, Germany, 217pp.*

Bruse, M. And Fleer, H., 1998, "Simulating surface-plant-air interactions inside urban environments with three dimensional numerical model", *Environmental Modelling & Software 13, 373-374.*

Bruse, M. and Team, 2012: ENVI-met 3. http://www.envi-met.com/ [accessed 2 July 2012]

Kent, C., 2010: "The Adelaide Urban Heat Island", *Honours thesis Flinders University. 74pp.*

Lyons, T.J. 1974. "Adelaide's urban climate", *Research paper no. 12, The Flinders Institute for Atmospheric and Marine Sciences, 31 pp.*

Sheard, M.J., 1996: "Soils, stratigraphy and engineering geology of near surface materials of the Adelaide Plains", *Regional Geology Branch, MESA and GM Bowman, Division of Soils, CSIRO, Report Book 94/9, July 1996*

Taylor, J.K., Thomson, BP and Shepherd, RG, 1974, "The Soils and Geology of the Adelaide Area", *Bulletin 46.Department of Mines, Geological Survey of South Australia, Adelaide, South Australia.*

UWYO, 2011 Refer to http://weather.uwyo.edu/upperair/sounding.html.

Vinodkumar, H. Guan, C.T. Simmons J.M. Bennett, C.M. Ewenz, C. Kent, *submitted, "*Influence of parks on urban environment: Observational and numerical study over Adelaide, Australia".

Chapter 6 - Infrared Thermographic Analysis of the Urban Environment and its Individual Components

Simon Benger, Roger Clay, Alex Waldron

6.1 Introduction.

This chapter seeks to characterise UHI effects through both ground based and aerial measurements of thermal infrared radiation from the CBD and its individual components. This includes examining how the city structure, individual buildings and their surroundings in Adelaide's CBD contribute to the UHI effect. Spatial distribution of surface temperatures, canyon effects, the mean façade temperature of individual buildings and ground level surfaces such as roads and footpaths were investigated. This extends the work of chapter 3 into the radiometric aspects of warming and cooling of the urban landscape.

6.2 Thermal characteristics of the Adelaide CBD.

Aerial thermal imaging of the CBD was carried out on 7 March 2011, at approximately 1.30 am, by Airborne Research Australia (ARA), utilising a thermal infrared camera. The maximum temperature at Kent Town weather station (2 km from Adelaide CBD) for the preceding 24 hours until 9 am of this date was 34.9°C with a minimum temperature of 21.6°C (BOM, 2011). The thermal image was taken in early autumn as the UHI effect is strongest then (and in winter), and at night, when the UHII is growing -as surrounding areas are losing heat that is trapped by the urban landscape (EPA, 2008).

A large number of individual images were compiled to generate the thermal image of the CBD shown in Figure 6.1. This shows a range of surface temperatures across the CBD, ranging from -4.0 to 32.3 °C, despite the night time imaging. The low temperatures result from reflective materials on the roofs of some city buildings that reflect sky temperatures (low under cloud-free conditions), while the higher temperatures come from high thermal mass structures and surfaces which have retained heat from daytime heating by the sun.

These higher temperatures are particularly evident in the CBD road network.

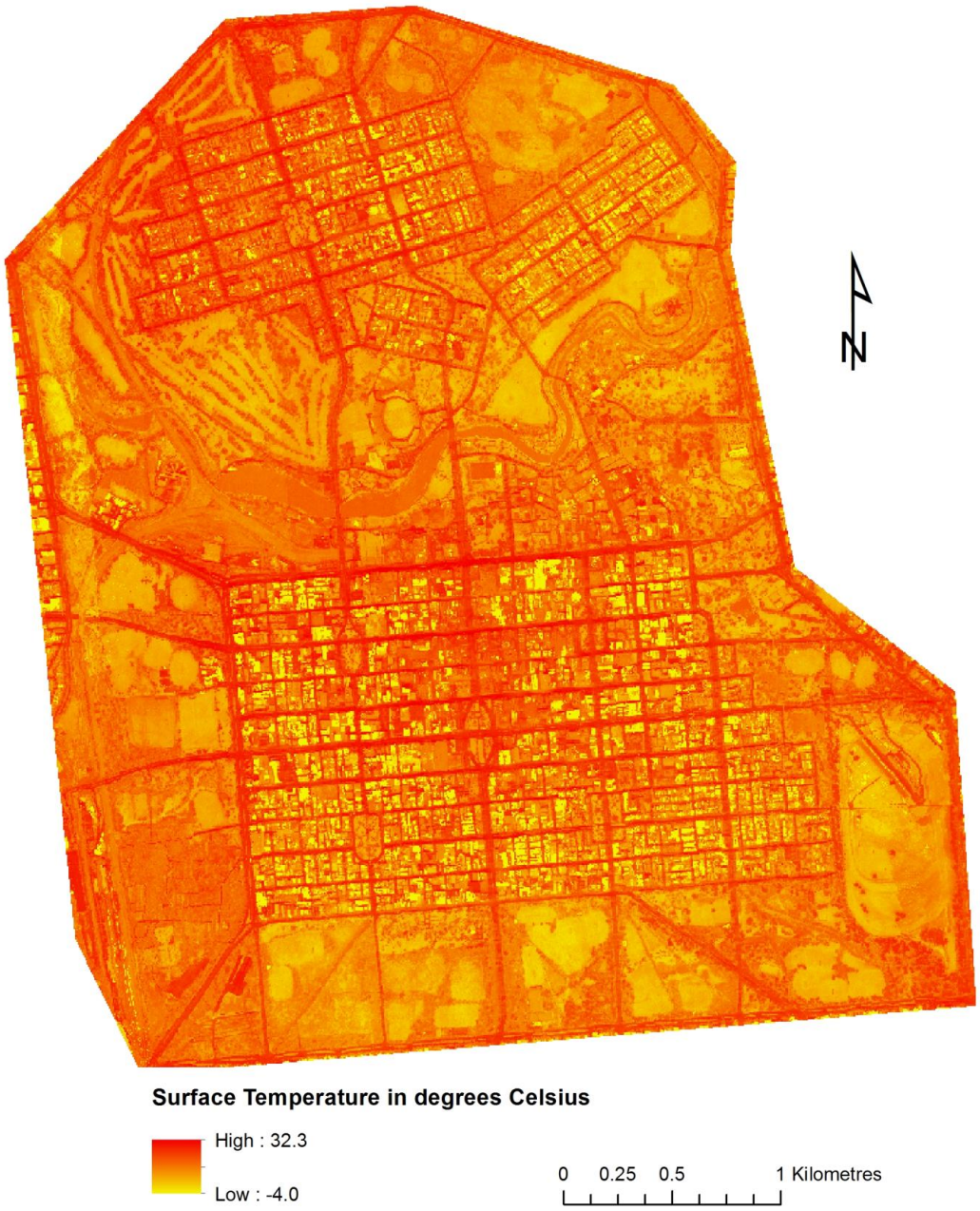

Figure 6.1 Thermal image of Adelaide CBD, 0130 hrs 7 March 2011 (cf figure 3.5).

Ambient air temperatures in the city were measured as described in Chapter 2. At the time of imaging the CBD, air temperatures indicate the UHI hotspot maximum of 27.5°C was centred just to the north of Victoria Square. Utilising this hotspot centre, Figure 6.2 shows the variation in mean surface temperatures in the thermal image with distance from

the centre. It shows a general pattern of decreasing temperature with increasing distance, with variation caused by the changing composition of the CBD, including building heights, impervious surface coverage and surface composition. (Refer to chapter 3 for some aspects, and later in this chapter). Figure 6.3, constructed from ACC data, clearly shows a greater density of taller buildings around the CBD hotspot, with building heights generally decreasing towards the parklands.

Figure 6.2 shows results that are consistent with a UHI effect. Higher surface temperatures are located around the centre of the CBD, with temperatures gradually dropping until the parklands area. Contributing factors such as low-albedo surfaces, enclosed urban geometry, and more impervious surfaces are all present in the high temperature areas in the city centre.

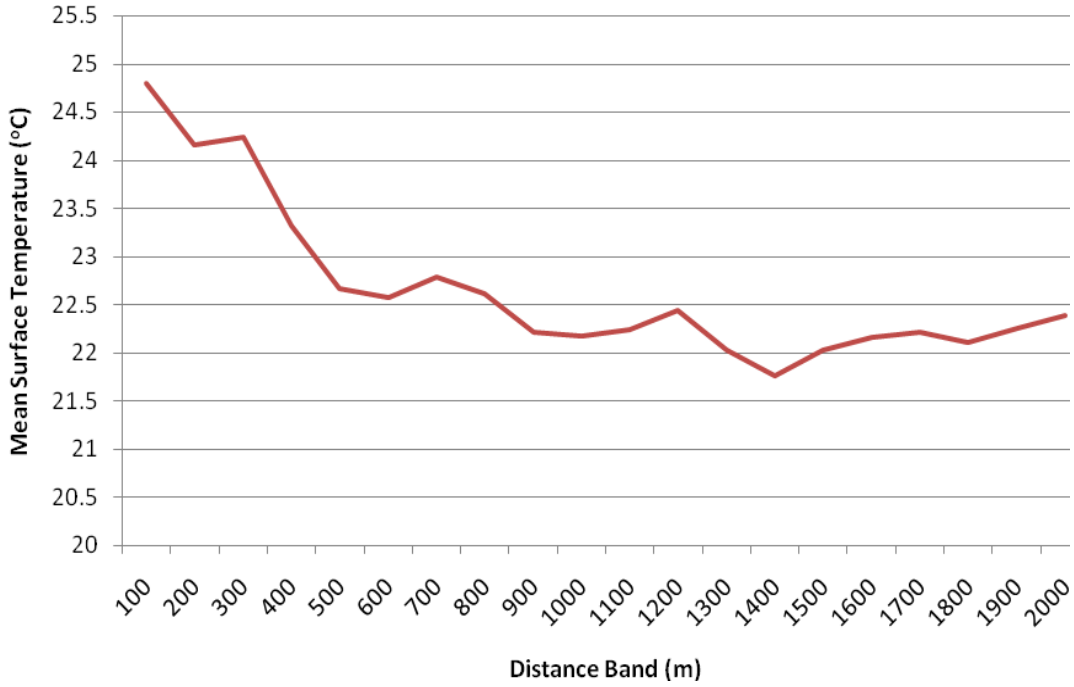

Figure 6.2 Surface Temperature Distribution across Adelaide CBD, 0130 hrs 7 March 2011

As the temperature drops there are more vegetated areas, fewer low-albedo surfaces, and the urban geometry is more favourable for heat loss as urban canyons are not present. The parklands have the lowest temperature as vegetation is the predominant land cover, their heat capacity is low, and they are open to the sky.

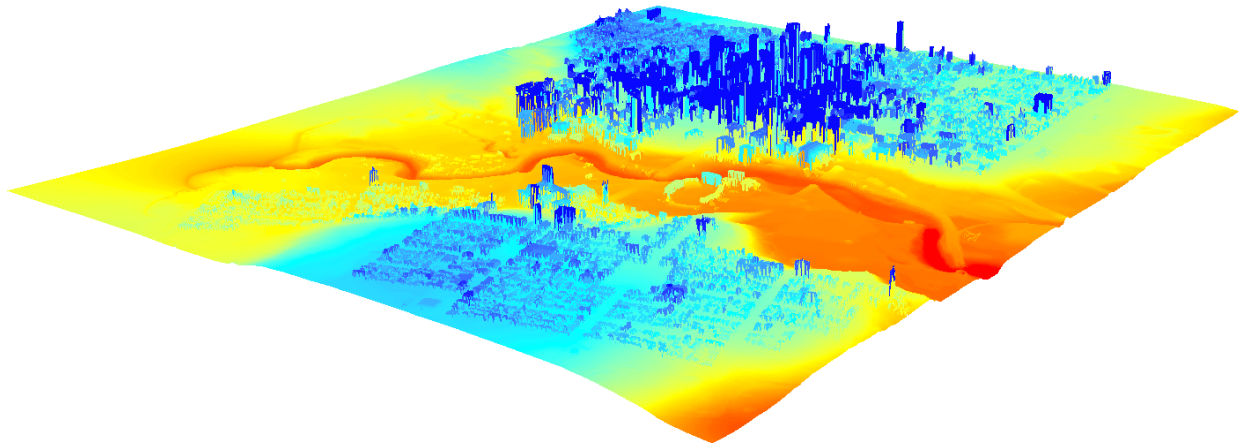

Figure 6.3 3D city representation, viewed from the north looking southeast, shown at 3x vertical exaggeration. Modelled from ACC data.

6.3 Infrared sky temperatures.

In the daytime, buildings receive solar energy on sunlit surfaces predominantly at visible and infrared wavelengths. On a sunny summer midday, this energy reaches unobscured ground level at a rate of about one kilowatt per square metre. Buildings lose energy in part by it being radiated away at wavelengths which are related to the temperature of surfaces, in the mid-infrared part of the spectrum, with wavelengths centred around 10 micrometres. So, night-time infrared studies can tell us about where buildings lose radiated energy, to cool overnight. The building cooling rate is affected by how much energy is returned by our atmosphere to the ground, because our atmosphere itself has warmth. That warmth is usually interpreted as an equivalent infrared sky temperature, and the process by which it occurs is sometimes called the greenhouse effect. For instance, it is commonly noticed that cloudy nights are warm and this is because the clouds return thermal radiation back to the ground, thus reducing its rate of cooling. Invisible greenhouse gases (predominantly water vapour) have a similar effect to clouds but at a less extreme level. Studies of the infrared sky temperature in the CBD can thus tell us about the ability of any surface to cool by radiating to the sky.

Figure 6.4 shows infrared 'sky' and air temperatures measured whilst driving through the city at about 5:00 am (a time when the cooling processes are likely to have an appreciable effect). Changes in the horizontal lines in the figure mark various locations along the route (including the start and end). There are ten of these locations which are: corner of Greenhill and Unley Roads (far left), South Terrace and Pulteney St, Hurtle Square, Britannia Roundabout, Victoria Square, West terrace and Grote Street, West parklands, (returning) West Terrace and Grote Street, Victoria Square, King William street and South Terrace.

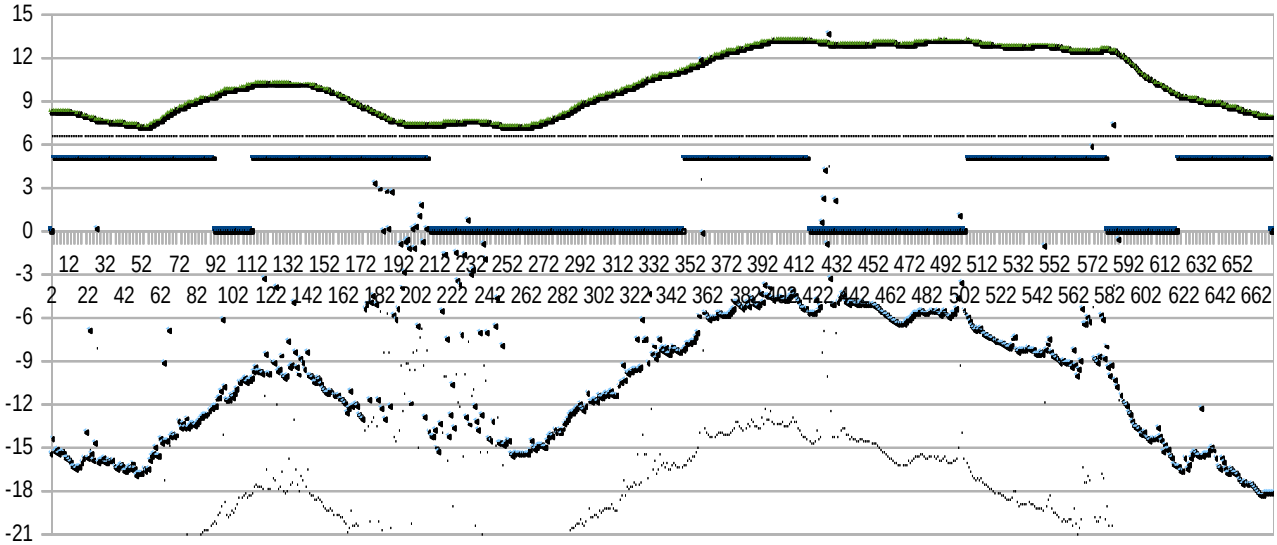

Figure 6.4 Air temperature (top) and infrared sky temperature (bottom) in °C, measured in an early morning transit of the city, 2 June 2011. See text for route locations.

In figure 6.4, the upper graph shows the air temperature (between 6 and 14 degrees Celsius) and the lower graph shows the infrared sky temperature. The infrared sky is at much lower temperatures because a clear sky is very cold (by contrast, the 'random' hot points are where the sensor was below trees –which are much warmer than the clear sky).

The air temperature clearly shows the urban heat island effect (UHI) for the CBD with a 6 degree difference in temperature between the parklands and the more central CBD areas. Although the infrared sky is at much lower temperatures, its variation is important and remarkable. The CBD sky temperature varied up to 10 degrees higher than outside the CBD. Since the sky temperature controls the city's ability to cool at night by radiation, this

effect is a serious issue and suggests that there are greenhouse processes in the CBD which are still to be understood.

This effect is not found to be measurable under cloudy skies but is often seen on clear mornings. Figure 6.5 shows a westward transit between the Britannia Roundabout and West Terrace/Grote Street on another clear morning.

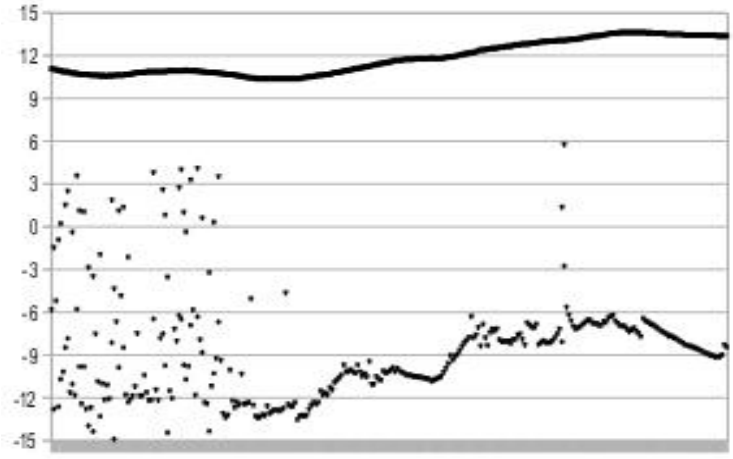

Figure 6.5 A transit on the early morning of 25 April 2011 during clear skies from Britannia roundabout to West Terrace. Air and infrared sky temperatures are shown in °C, as in figure 6.4.

6.4 Building surface temperatures at night in the city.

If one is in the open on a clear and calm night, one feels cold because one's body heat is rapidly radiated into the cold clear sky. In a city, building walls are warmer than the clear sky, and only a fraction of the cold sky is visible from ground level. As a result, building surfaces have surroundings which are, on average, much warmer than the cold clear sky. Their ability to cool overnight is thus reduced. The average surrounding temperature thus depends on the fraction of view of the sky which is unobstructed, the temperature of building walls, and the temperature of the ground. With James Lau of the University of Adelaide, we have investigated by radiative modelling how that 'average surrounding temperature' depends on properties of the physical structure of an idealised city street with adjacent buildings – its street width and building heights. Some results are shown in figures

6.6, 6.7 and 6.8 for a road with all adjacent buildings reaching 25 m height. Figure 6.6 shows that, for an air temperature of 25°C, there is a temperature reduction of two degrees when a street width of 20-30 m is reached, roughly the height of the surrounding buildings. The important factor in this work is the extent of sky which is viewed from a particular point, so roads should be wider if the buildings are higher, in order to have the same cooling. This reinforces the findings of chapter 3 that were based on street temperature observations.

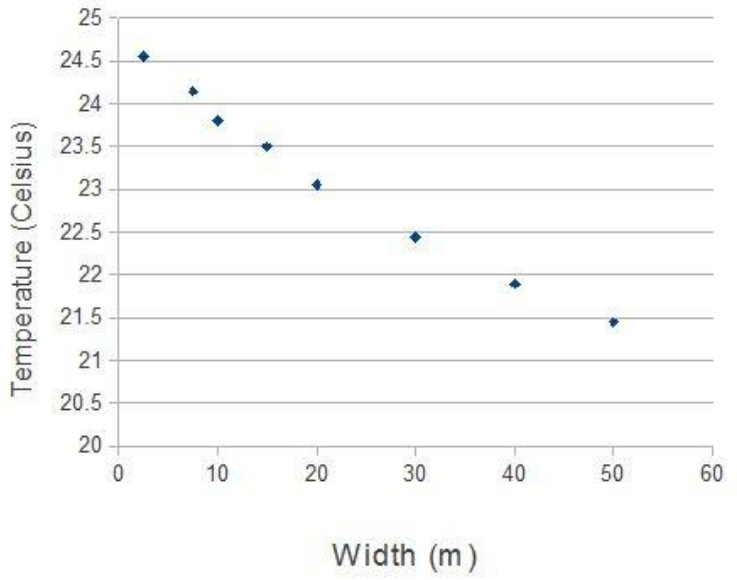

Figure 6.6 The predicted effect on the night-time air temperature, at a point in the middle of a road, of changing the width (in metres) of a roadway between buildings which rise to a height of 25 m (8 floors) on both sides.

Figures 6.7 and 6.8 illustrate further properties of the resulting radiation effects in an 'urban canyon'. Figure 6.7 shows that temperatures above a street surface only reduce when the view of the sky increases appreciably. In this case, a 10 m wide street with adjacent 25 m high buildings does not show substantial radiative cooling until a height of 15 m above street level is reached. Figure 6.8 reminds us that greenhouse gases (in this case water vapour) inhibit radiative cooling and a typical range of values found in an urban environment can result in a substantial variation in surface temperatures.

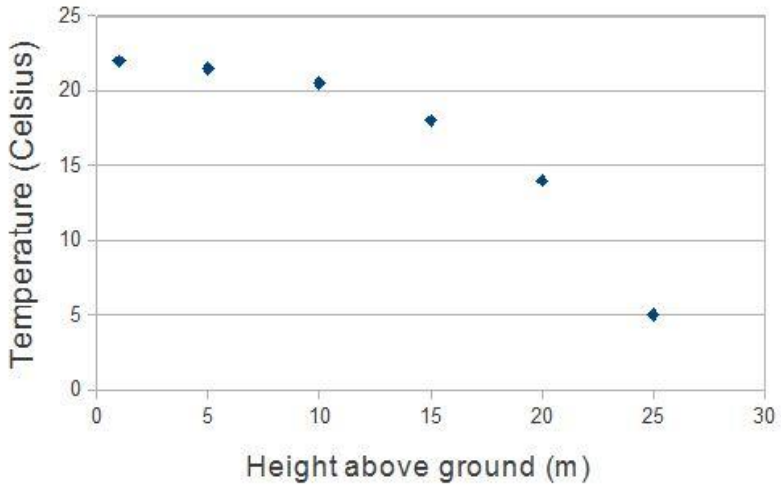

Figure 6.7 The variation of night time air temperature with height above the centre of a 10 m wide roadway between buildings with heights of 25 m (8 floors). Warm temperatures are found below a height of 15 m, above which cooling to the clear sky becomes effective.

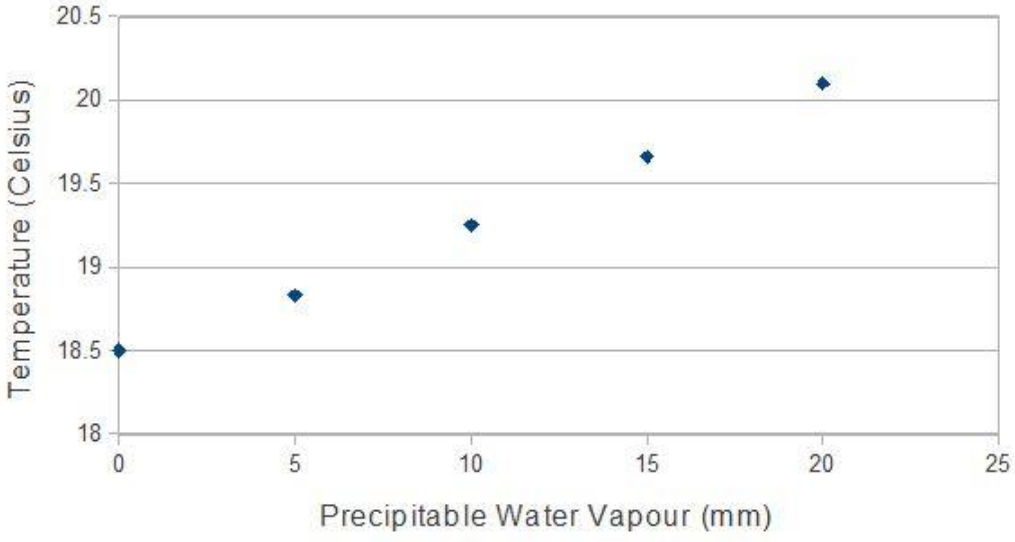

Figure 6.8 The effect of the atmospheric water vapour content (precipitable water vapour – PWV, in mm), on the night-time temperature at a height of 15m in the same street geometry ('urban canyon') as for figure 6.7.

6.5 Urban landscape component analysis.

While aspects of the effects of buildings on air temperature were modelled in Chapters 3, 4, 5 and in the last section above, this section examines the role of landscape components to radiative heating and cooling, based on the image in figure 6.1. The contributions of individual buildings and urban landscape components to the thermal signatures recorded in the image were assessed through a GIS-based analysis. A buildings layer that contains building footprints and other individual information (such as a unique building number (UBN), the number of floors, the building height and floor area), which covered the study area was provided by the Adelaide City Council. Similarly, a layer for footpaths and roads were supplied by the Adelaide City Council. These layers included polygons of segments of footpaths and roads as well as the type of material that made up the surface. A layer that contained points identifying the location of most trees was also provided.

Buildings with twelve floors or greater were selected at random to make up the *tall* buildings group. The closest one or two story building to its associated *tall* building was selected to compare small and tall buildings. Roads were selected to include three wide roads and three narrow roads. All selected roads run east-west to ensure some consistency in the amount of solar radiation received. However, this also depends on building proximity and height. Footpaths were used if they were neighbouring the building in question. Where footpaths were interrupted by other features in the urban landscape such as buildings, verandas, balconies, and trees, these elements were excluded.

The buildings layer was used to identify the boundary of each building selected for the study. The polygons for each individual building were used as zones when calculating zonal statistics in ArcGIS (ESRI, 2011). Before this could be done the issue of topographic displacement was addressed. The thermal image (Figure 6.1) of Adelaide's CBD displays some topographic displacement, and is this is greater for higher buildings far from each image nadir. Topographic displacement is caused by the perspective geometry of the camera relative to a surface with varying elevations (Paine & Kisler, 2003). By contrast, the buildings layer supplied by the Adelaide City Council contains the building footprint of each building in the CBD. Therefore, in the image, the roof of a building will be displayed in a

different position to its footprint by an amount depending upon the height of the building and the distance the building is from the image nadir. Since the building layer is used to calculate zonal statistics of the thermal image, it is important for the building layer to be aligned with the correct pixels of the thermal image. To correct for this difference, the building footprint for each individual building was moved and altered to correspond with the roof of the building.)

An important effect of the observed topographic displacement is that many taller buildings have their façade visible in the thermal image, allowing their temperatures, as viewed from above, to be measured.

Roads are a major component of the urban area, which, in Adelaide's CBD, are made from bitumen. These roads have surface characteristics that are known to enhance the UHI effect, being dark coloured, and rough, and hence with a low albedo (Akbari et al, 2001). Six different roads throughout the study area were used. Each initially was comprised of many road segments containing different unique identification numbers. The roads segments were merged together to form one polygon for the whole road area, which was then used in applying zonal statistics to determine the mean road temperature.

Footpaths surrounding the associated building were used, with any obstructions of the footpath removed with Editor in ArcMap (ESRI, 2011).

Zonal statistics were used to calculate the mean temperature for each building, façade, footpath and road. Using the zonal statistics tool, the mean temperature for each polygon from the building, façade, footpath and road layers based on the temperature data in the thermal image, were calculated. Where the building layer included several polygons for one individual building, the unique building number (UBN) was used to identify separate buildings.

Vegetation cools an area through evapotranspiration and shading of the ground during the day (Akbari, 2001). Therefore, trees were excluded when obtaining the mean temperature for footpath areas as they would reduce the mean temperature for a footpath segment. A five meter buffer around each tree point was created and excluded from the analysis as well. Also, some trees that were not represented in the layer, but were identified through aerial imagery, were manually excluded.

Table 6.1 shows the mean temperature of roofs, facades and footpaths for 25 selected buildings in the CBD. Buildings that were not tall enough or were obstructed by other buildings, have no temperature recorded for the façade. There is no clear relationship between building roof temperature and façade temperature, indicating the highly varied nature of construction materials used on buildings and different levels of exposure to the sun. Façade temperatures are obviously best observed from ground level (presented later in this chapter), but they are included here as part of the analysis of the city thermal image.

Table 6.1 Building location, building height (m), and mean temperature (°C) for roof of building, façade and associated footpath area. (N/A: data not available)

Location	Building height (m)	Mean Temperature (°C)		
		Troof	Tfacade	Tpath
91 King William Street	130.36	25.3	26.4	28.7
19 Grenfell St	70.14	25.9	24.3	25.1
33 King William St	69.34	23.9	23	N/A
1 King William St	68.02	24.8	25	27.6
67-79 Waymouth St	67.95	24.1	25.9	27.9
8 Grote St	63	25.8	22.4	20.7
22 King William Street	60.23	24	24	24.9
431 King William St	58.38	22.7	24.5	25.8
250 Victoria Square	54.4	12.3	N/A	18.8
25 Pirie St	51.46	24.5	N/A	24.9
136 North Terrace	50.74	25.1	24.5	25.8
81 Flinders St	50.24	24.4	24.9	27
60 Waymouth St	48.89	23.2	21.4	24.9
11 Hindmarsh Square	45.53	23.1	16.8	N/A
144 North Terrace	45.12	23.2	27.3	N/A
215 South Terrace	42.1	23.3	23.3	24.1
100 Pirie St	40.38	22.2	19.8	21.3
51 Pirie St	33.37	22.7	N/A	24.9
169 Pirie St	28.26	19.9	18	23.8
84 Flinders St	15.23	20.6	N/A	21.5
10 Waymouth St	14.89	24	N/A	24.8
76 Light Square	13.49	15.2	N/A	21.2
18 Grote St	12.66	10.8	N/A	20.7
142 South Terrace	10.03	19.1	N/A	N/A
213 South Terrace	9.65	14.3	N/A	N/A

Using the data in Table 6.1, correlations between the various parameters were examined. Footpath temperatures show a weak correlation (R^2=0.49) with building roof temperatures. The correlation is slightly higher against facade temperatures (R^2=0.55). The scatter could come from a number of sources. Some footpath temperatures could not be obtained for some locations due to obstructions from trees and buildings. The orientation of

the footpaths and their position relative to surrounding urban geometry would have a significant effect on these results. However, it is evident that 85% of footpath areas had a greater mean temperature than the associated building roof, which is consistent with the canyon effect of higher temperatures at ground level posited in section 6.3.

The relationship between roof temperatures and building height is shown in Figure 6.9. This shows a weak positive relationship between this temperature and building height. However, building radiative roof temperature, as recorded from above, is highly dependent on the roofing materials used in any individual building and their reflective properties, especially in relation to night time sky temperatures. This, together with proximity to open space, may explain the weak correlation observed.

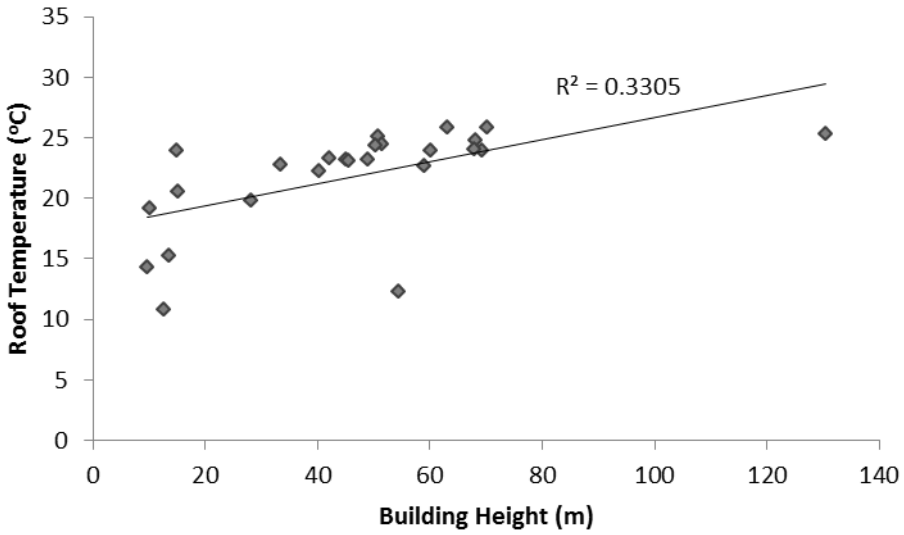

Figure 6.9 Relatonship between roof temperature (°C) and building height (m)

From air temperatures measured in the CBD network (described in chapter 2) at the time of aerial thermal imaging, air temperature contours were obtained. These contours were used to define zones, with half degree Celsius ranges, within which data on the associated mean height and number of buildings, and buildings per ha were extracted. Table 6.2 shows the results. The temperature zone above 28°C has the highest average building height of 40.0 meters. The average temperature decreases as height decreases; by an average building height of 12.1 meters the temperature has dropped to the 26 – 26.5°C

range. The average building height remains stable between 12 and 11 meters until the last temperature zone of 23.5 - 24°C.

The number of buildings per ha is highest in the 23.5 – 24°C temperature zone, which is the outermost zone in the CBD. The higher temperature zones in the city centre have a lower ratio of buildings to area, with the temperature zone 27.5 - 28°C having 6 buildings per ha, which is indicative of the larger buildings in these areas of the CBD. These results show that higher average building heights are associated with higher ambient air temperatures.

Table 6.2 Temperature zones and areas, number of buildings, average building height and buildings per ha

Zone Temperature (°C)	Zone Area (ha)	No. of Buildings	Avg Bldg Height (m)	Buildings / ha
Above 28	1.22	13	40.0	11
27.5 - 28	13.67	87	23.0	6
27 – 27.5	18.11	170	17.0	9
26.5 - 27	25.31	193	14.5	8
26 – 26.5	37.65	599	12.1	16
25.5 - 26	39.81	480	11.1	12
25 – 25.5	40.05	526	11.1	13
24.5 - 25	41.93	584	11.0	14
24 – 24.5	42.96	656	12.2	15
23.5 - 24	54.81	1022	11.1	19

6.6 External infrared building temperatures.

Infrared measurements at street level on different occasions were also used to obtain surface temperatures of buildings in the current study. Such surface measurements are very difficult using any other technique but care has to be taken when making them. This is because infrared radiation from a surface has two components, one the emitted radiation, the other reflected. The reflected component does not reflect from surfaces in the same way as light. Street level measurements of infrared radiation coming from the upper levels of buildings will thus include a component of reflection from the cold sky and so will underestimate the true surface temperature. Some surfaces (such as unpainted metals) have a very low infrared emissivity and will not give correct temperature readings from IR measurements. However, careful infrared surface measurements (usually expressed

crudely as a 'temperature') can show surface temperatures which are characteristic of various locations and can show where buildings are radiating substantial energy (often through older style windows which, though opaque to infrared radiation, readily conduct heat energy. Newer windows may be more insulative.)

Infrared measurements of city buildings such as those shown in figures 6.10-6.15 were made from November 2011 to June 2012. (Some buildings are located in the zones of the preceding chapter. Such buildings are labelled X, Y and Z for anonymity. Building X is in the Victoria Square zone, building Y in the northern CBD zone, and building Z in the central CBD zone). The surface temperatures of buildings which are not surrounded by other constructions can be contrasted with those from more closely packed buildings. Figures 6.10 to 6.15 show some false colour infrared images of city locations. These images each contain a dotted straight line, along which the infrared 'temperature' variation is shown in the accompanying graph. The horizontal scale of the graph is in terms of pixels along the line in the image.

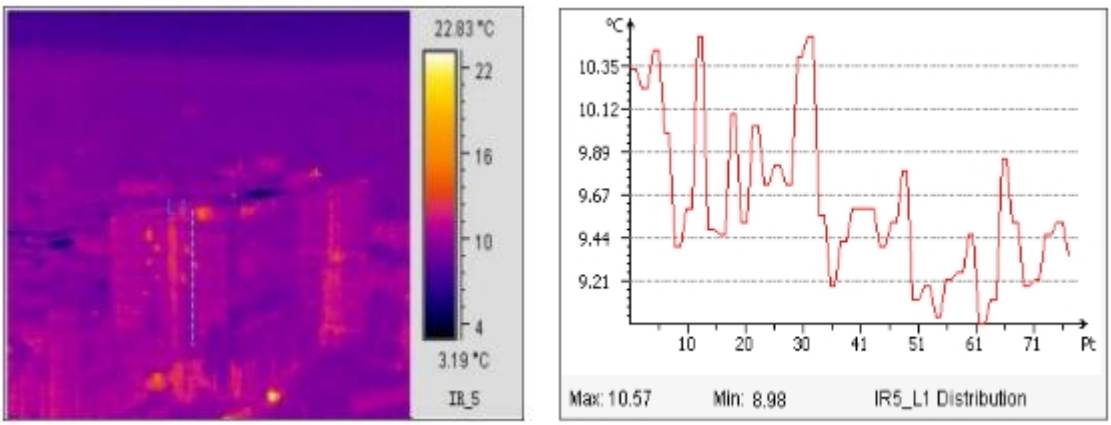

Figure 6.10 False colour infrared temperature image of building X (left) taken about sunrise on a clear day. This is a building which is in a rather open environment and most of its levels can radiate freely to the cold sky. The temperature distribution shown on the right (along the dotted line – bottom to top) exhibits only about a one degree variation.

Figure 6.10 shows an image of building X taken with an infrared camera, and figure 6.11 shows results for a less open environment – Grenfell Street, an urban 'canyon'. The infrared images were taken at times between 07:00 and 08:00 before solar heating was significant.

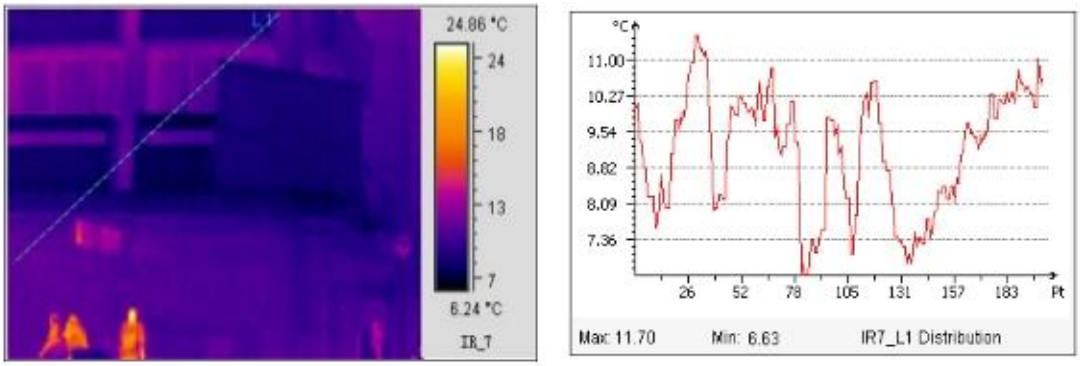

Figure 6.11 Infrared image of the ground floors of a building in Grenfell Street. The temperatures depend on the shading and construction materials of the walls.

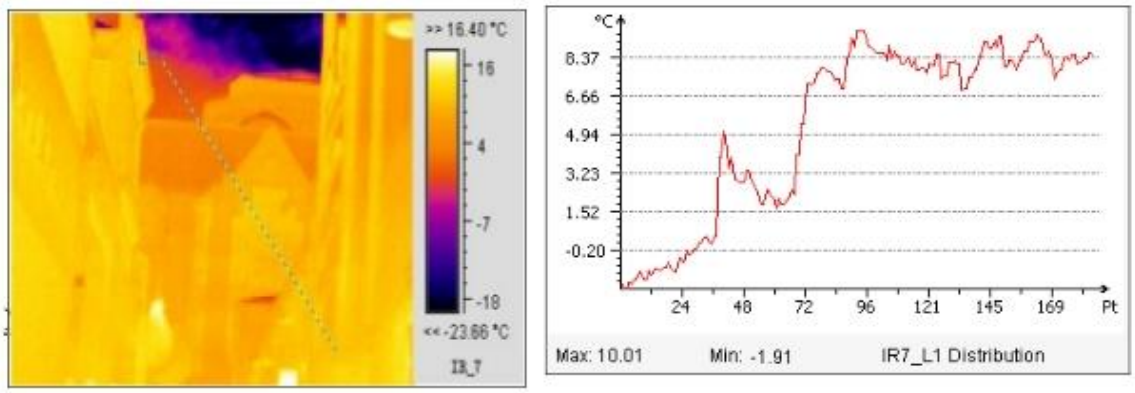

Figure 6.12 Infrared image of James Place, an extreme example of a canyon. The temperature data past pixel 96 correspond to temperatures within the canyon, where the uniformity of the temperature is clear. Temperatures before pixel 96 follow the line in the figure from the very cold sky through exposed areas of the left hand building.

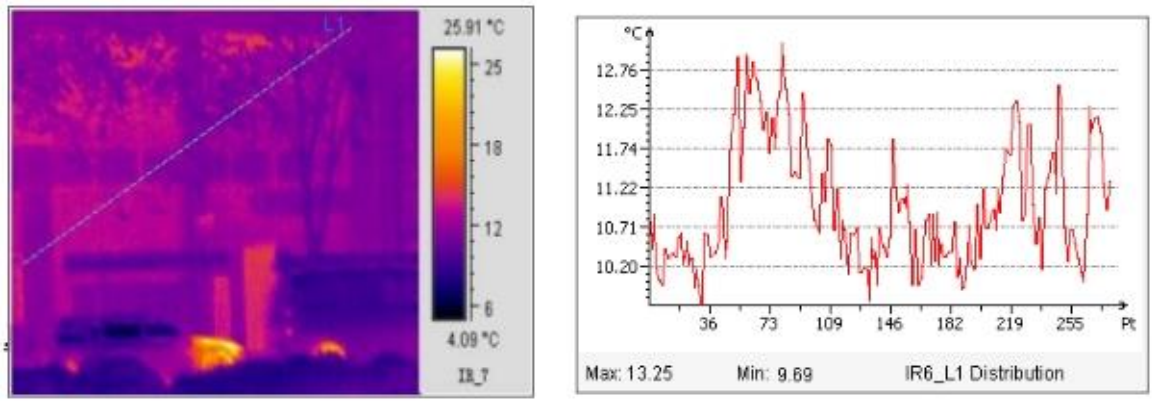

Figure 6.13 Building Y in King William Street is within a wide canyon but is also protected by tree plantings which reduce the heat loss to the sky. Its higher levels are much more exposed than street level.

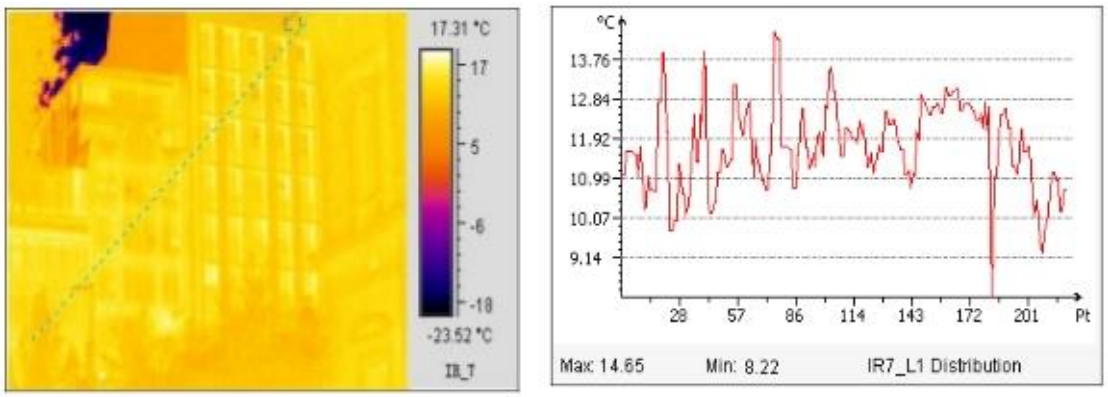

Figure 6.14 Buildings on the CBD side of North Terrace are not in a canyon and can have cold surfaces after a clear night.

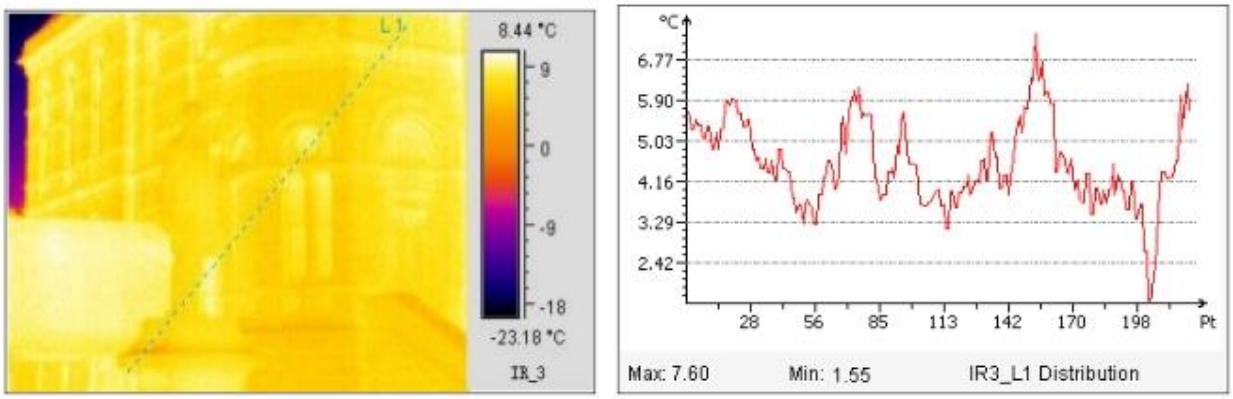

Figure 6.15 An infrared image of the facade of the State Library. Tree planting in a partially enclosed area such as outside the State Library can make the area into an almost enclosed canyon with a very uniform temperature. The exception here is the upper surface of the statue's pedestal which has cooled due to exposure to the cold overnight clear sky.

Figure 6.16 shows that wall temperatures in Grenfell Street and in James Place correlate very well with each other. The locations are separated by about 50 m and both are in canyons. James Place is narrower than Grenfell Street but the buildings are not as high.

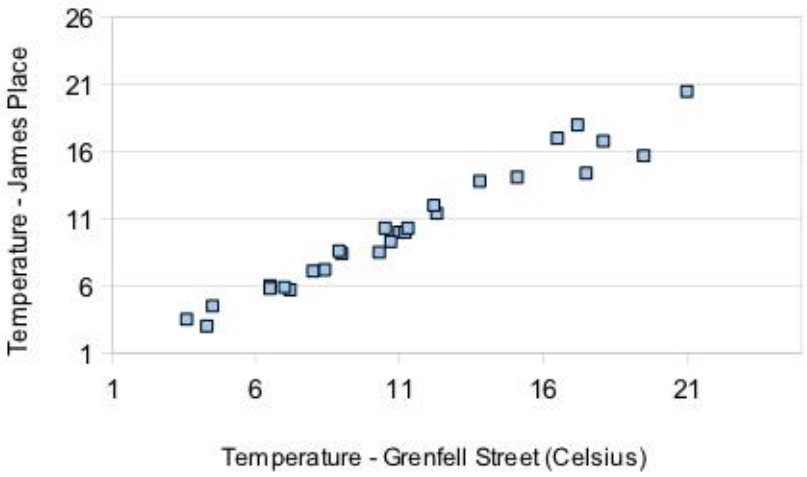

Figure 6.16 A comparison of infrared wall temperatures (°C) in Grenfell Street and James Place. Each point is for a different day with each measurement in a pair being taken at close to the same time, all between 07:00 and 08:00. The temperature agreements are very close.

Figure 6.17 compares the temperatures of the building in Grenfell Street with building X in Victoria Square. The temperatures correlate but there is appreciable scatter. The Grenfell Street temperatures are generally higher than in Victoria Square which is a more exposed environment.

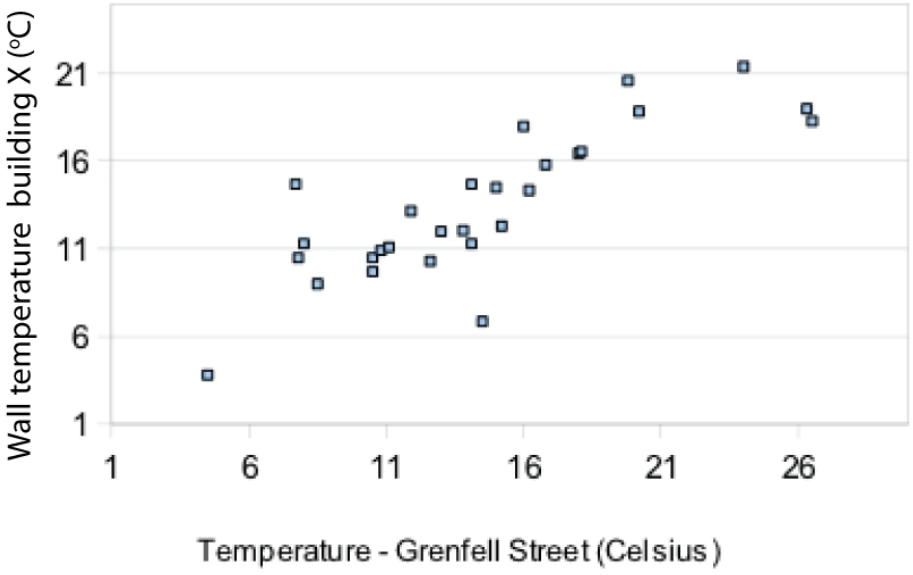

Figure 6.17 Infrared wall temperatures in Grenfell Street (horizontal axis) compared to wall temperatures (^{o}C) for building X (vertical axis). The more exposed location of the latter building results in lower building surface temperatures around sunrise.

In some circumstances, wall temperatures can vary over quite small distances if the environment varies. Figure 6.18 compares temperatures in Gawler Place with temperatures along North Terrace just around the corner. In this case, the averages of the temperatures are very similar but the scatter is high. The buildings are of similar construction but North Terrace is more exposed. It is possible that the scatter is associated with the different effects of wind, surface materials, and/or thermal mass effects between North Terrace and the Gawler Place 'canyon'.

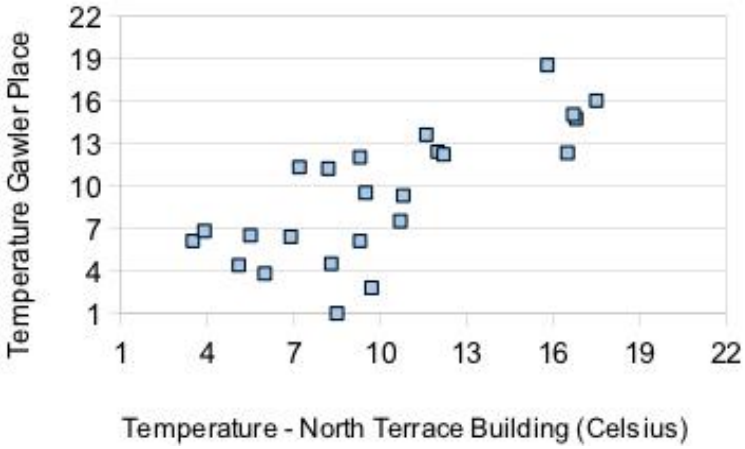

Figure 6.18 Infrared surface temperatures (^{o}C) on North terrace buildings (horizontal axis) compared to a building just inside Gawler Place (vertical axis).

It is notable that wall temperatures within the CBD vary from place to place. They can also differ appreciably from the Kent Town Bureau of Meteorology air temperature measured at 1.5m above a grassed surface. Figure 6.19 relates the infrared surface temperature for building Y, 1.5 m above street level to Kent Town air temperature measurements.

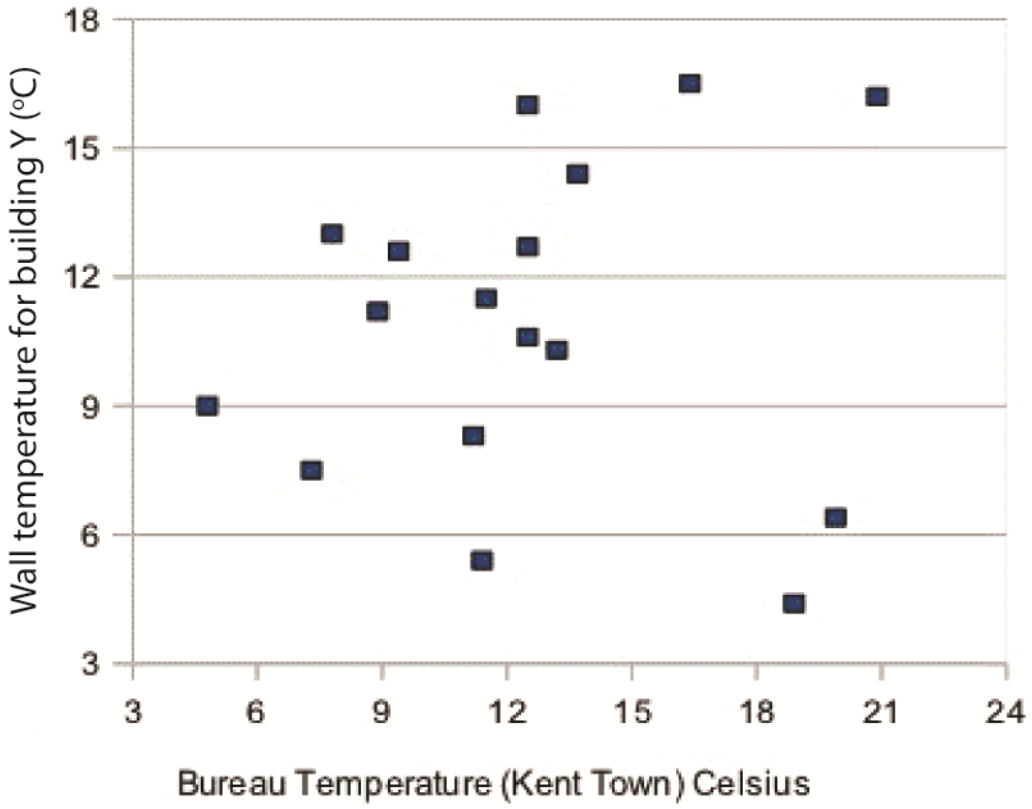

Figure 6.19 Temperatures (^{o}C) measured in air at Kent Town (BoM) (horizontal axis) compared to the infrared surface temperature of building Y in King William Street (vertical axis).

6.7 Diurnal surface temperature variation of buildings.

Three city buildings X, Y, and Z, were imaged from street level with a handheld thermal camera on 8 March, 2012, at approximately 30 minute intervals to examine the changes in façade temperatures over the course of the day. In the results here, vertical temperature profiles are averaged across ten horizontal pixels. Figure 6.20 shows the heating of the western façade of building X between 0955 and 1613 hrs. Façade temperatures increase slowly as the external air temperature increases in the morning. After midday, temperatures increase by 2-5^{o}C each hour as the façade surface receives direct solar irradiation. Generally, temperatures are slightly higher closer to ground level and decrease towards the top of the building as the influence of surrounding street surfaces decreases. The high frequency variation is caused by the different materials separating each level of the building, and this variation becomes less pronounced as the building heats up.

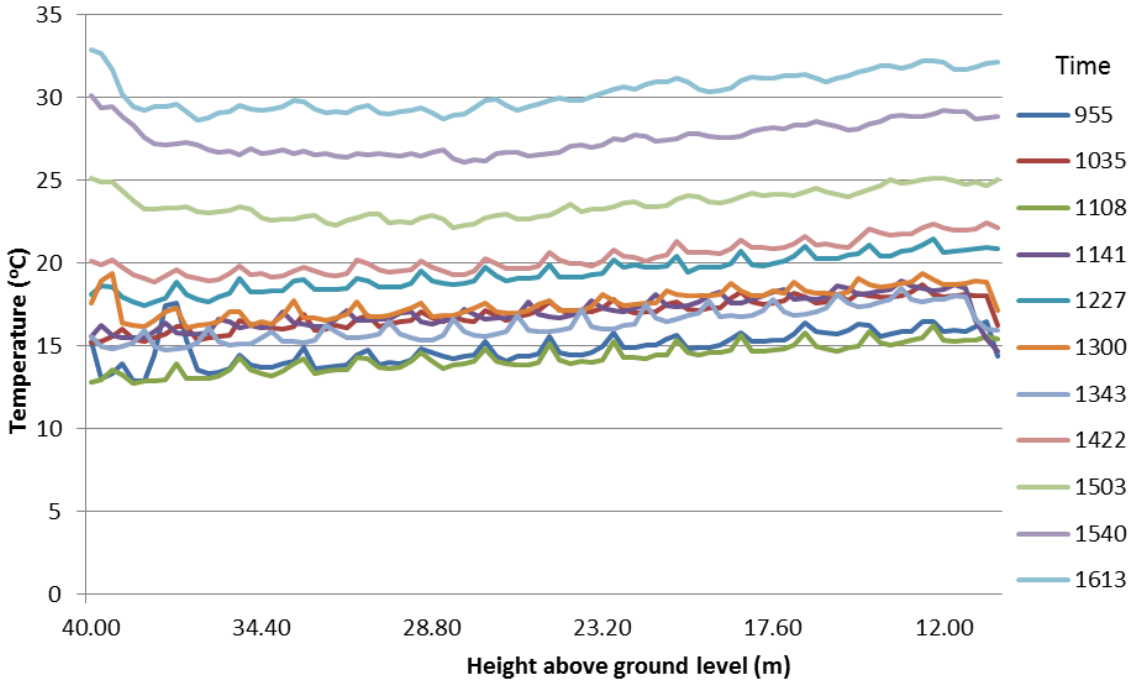

Figure 6.20 Daytime temperature change (°C) with height above ground level on the west façade of building X, 8 March, 2012

For contrast, Figure 6.21 shows the heating of the southern façade of the same building X between 0955 and 1659 hrs. Once again, the façade heats up progressively throughout the day. However, as the southern façade receives little direct sunlight, the rate of temperature increase throughout the day is much smaller. The non-uniform distribution of the surface materials which make up this façade results in greater high frequency spatial variation, with the reflective glass surfaces appearing considerably cooler. The temperature gradient (7-10°C) between the top and the bottom of the building is greater than that observed for the western façade (2-3°C), which is most likely due to the canyon effect on the southern side of the building. These results indicate that the orientation of the facades of a building has a substantial impact on their thermal behaviour including maximum temperature and rate of heating, as does the surrounding city geometry. Buildings also radiate more heat closer to ground level.

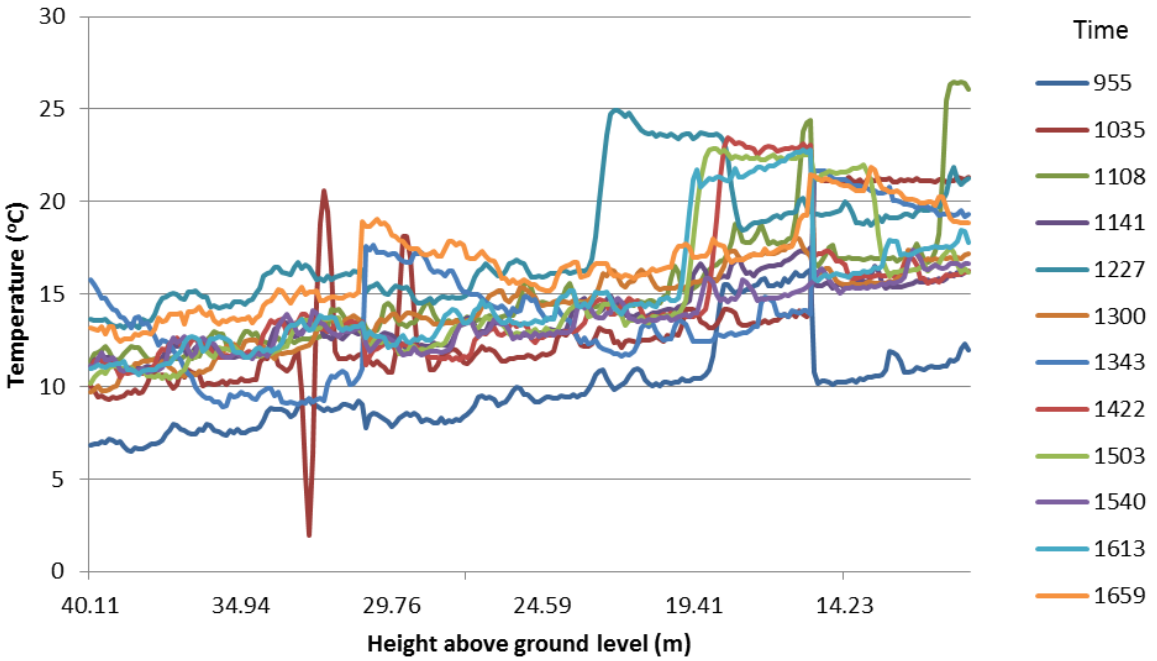

Figure 6.21 Daytime temperature change (^{o}C) on the south façade of building X, 8 March, 2012

6.8 Strategies to reduce UHI effects in relation to buildings.

An effective, cheap and simple way of reducing UHI effect is to use high-albedo materials on urban surfaces such as roofs, roads, car parks and footpaths (Taha et al, 1992). The terms cool roofs and cool pavements are popular terms used to describe the implementation of high albedo materials on these surfaces. Cool surfaces have become an increasingly popular method of cooling due to its low-cost, efficiency, and ease of use (Rosenfeld et al, 1995). The two major factors that contribute to heating a surface are its level of solar reflectance (its albedo) and its infrared emittance. Increasing solar reflectance and infrared emittance will decrease the surface temperature of the surface and in turn reduce ambient air temperature as the intensity of heat convection (sensible heat flux density) from a cooler surface is lower (Synnefa et al, 2008). Implementing cool surfaces can be an easy process: by simply painting a surface white, the solar reflectance is increased dramatically. Taha et al (1992) measured the albedo and surface temperatures of a variety of surfaces in the field and found that white coatings with an albedo of 0.72 were 45°C cooler than black coatings (with an albedo of 0.08). Painted building surfaces are generally painted every 10 years; in the next painting cycle, they can be painted with high solar

reflectance and high emittance paint as part of the normal upkeep of the building. Incorporating cool surfaces into building codes is an easy way to ensure that new buildings or any new works use high-albedo materials (Taha et al, 1992). Using high albedo surfaces is an especially effective way of mitigating the UHI in locations where weather conditions or water availability restrict the ability for vegetation to act as a climate moderator (Taha et al, 1992). Building X was designed to be a cool building and uses high-albedo surfaces and efficient cooling systems. It is an example of how a large building can have a low mean temperature (roof temperature 12.3°C, table 6.1) by incorporating cool surfaces in its construction.

There is significant potential for using high-albedo surfaces in urban areas. For example, Berdahl and Bretz et al (1997) found that Sacramento (USA) had surface components which were 28% rooftop, 16% streets, and 14% other impervious surfaces, of the city area. High-albedo surfaces could be applied to many of these surfaces to reduce urban temperatures. However, there are some issues that are associated with implementing high-albedo surfaces. Most notably, glare problems could arise from the highly reflective surfaces, which may lead to hazards, discomfort and radiation to surrounding surfaces. Also, colour preference could limit the selection of colour/hue being used on homes and buildings; white or other high albedo colours may not suit a particular design of a building (Taha et al, 1992). Another issue is the dirt attracting qualities of the surfaces treated with these colours. Albedos change over time as the surface weathers and wears. Building surfaces are exposed to solar radiation, dust, rain and humidity for instance; other urban surfaces like roads and footpaths are exposed to vehicle and pedestrian traffic (Taha et al, 1992).

The Government of South Australia released a discussion paper on cool roofs regulation in South Australia in December 2010. Public comment was sought on the proposal for a cool roof requirement for certain categories of commercial building. Specifically sought were views relating to the additional costs of supplying the specialist coating required in order to reflect heat. Public consultation closed on 11 February 2011 followed by a review of the responses. The review concluded that introducing cool roofs in commercial buildings was justified and as a result, a South Australian state variation was

included in the Building Code of Australia for air-conditioned commercial buildings from 1 May 2012.

An alternative to a high albedo roof (cool roof) is a green roof, a roof that has a vegetation layer on it. Green roofs offer a unique opportunity to introduce vegetation into a dense, urban area where ground vegetation is often not an option. The surface of a green roof can be cooler than ambient air temperatures, but by contrast, conventional rooftop surfaces can exceed ambient air temperatures by up to 50˚C (EPA, 2008). High moisture levels in vegetation play a role in reducing daytime surface temperatures through evaporation and plant transpiration, because the conversion from liquid water to vapour in these processes consume large amounts of latent heat, leaving less for heating (Rosenzweig et al, 2006). Green roofs also reduce temperatures from shading by vegetation. The greater the foliage density of plants, the more the conductive heat flux through a roof decreases and the more that surface temperatures drop (Clark et al, 2008). A lower surface temperature reduces the amount of heat transmitted into the building and re-emitted into the atmosphere. Surface temperatures have been recorded at being 11-25˚C less due to the shading of trees (Akbari et al, 1997). Green roofs may offer benefits in savings of energy used for heating and cooling. Reducing surface and ambient air temperatures reduces the amount of cooling needed, while in winter the green roofs act as insulation to reduce heating and associated costs (EPA, 2008).

Trees and vegetation also help in mitigating the effects of UHIs. Shading from trees reduces the amount of solar radiation that reaches the canopy below a tree or plant (Akbari, 2001). The shade from the tree can cover buildings or other urban surfaces, reducing the amount of heat that is transferred into the building or transmitted back into the atmosphere. Also, trees cool the air through evapotranspiration. Ideally, a scheme to combat the effects of UHIs would include the incorporation of cool surfaces and urban vegetation. But the emphasis should be on cool surfaces first, because they are more effective than trees, and cost little if high-albedo surfaces are incorporated into routine maintenance programmes. Also, the results from cool surfaces are seen immediately, whereas trees may require many years to grow large enough to produce significant energy savings (Rosenfeld et al, 1995).

6.9 Conclusions.

Thermal infrared measurements support results from static temperature sensors, that the Adelaide CBD shows an appreciable urban heat island effect. The narrow streets surrounded by high buildings have their own micro-climates which can vary appreciably from place to place. As a result, these areas have cooling and heating rates which are strongly affected by their specific environments. Additionally, their infrared facade temperatures can vary greatly from the Bureau of Meteorology Kent Town air temperature measurements.

Individual buildings have a variable temperature contribution to the UHI effect, some higher and some lower than the air temperature. The surroundings of buildings (footpaths and roads) contribute to the UHI effect with generally higher infrared temperatures than the neighbouring building. Methods to mitigate UHI effects should be employed when constructing new buildings and when maintenance of existing buildings takes place.

References for Chapter 6.

Akbari, H., M. Pomerantz, and H. Taha. 2001. "Cool surfaces and shade trees to reduce energy use and improve air quality in urban areas", Solar Energy, 70(3):295-310.

Akbari, H. 2001. “Energy Saving Potentials and Air Quality Benefits of Urban Heat Island Mitigation” Lawrence Berkeley National Laboratory Report No.LBNL-486-4287, Berkeley, CA.

Akbari, H., D. Kurn, S. Bretz, and J. Hanford. 1997. “Peak power and cooling energy savings of shade trees”, Energy and Buildings, 25:139-148.

Akbari H., W. Bos, S. Bretz, J. Hanford, A. Rosenfeld, D. Sailor, and H. Taha. 1992. “Monitoring Peak Power and Cooling Energy Savings of Shade Trees and White Surfaces in the Sacramento Municipal Utility District (SMUD) Service Area: Project Design and Preliminary Results”, Lawrence Berkeley National Laboratory Report No. LBL-33342, Berkeley, CA.

Berdahl P. and S. Bretz. 1997. “Preliminary survey of the solar reflectance of cool roofing materials”, Energy and Buildings, 25:149-158.

Bureau of Meteorology, 2011. Climate Data Online, available: http://www.bom.gov.au/climate/data/ (accessed 27/10/11)

Clark, C., P. Adriaens, and F.B. Talbot. 2008. “Green roof valuation: a probabilistic economic analysis of environmental benefits”, Environmental Science and Technology 42(6):2155–2161.

EPA 2008: Environmental Protection Agency (U.S) 2008, Reducing Urban Heat Islands:

Compendium of Strategies, Washington DC, USA.

NOAA. 1995. Natural Disaster Survey Report: July 1995 Heat Wave. Retrieved 10 August 2011 from <http://www.nws.noaa.gov/om/assessments/pdfs/heat95.pdf>.

Paine, D. and P. Kisler 2003, Aerial photography and image interpretation, John Wiley and Sons, New Jeresy.

Oke.T.R. 1987.Boundary Layer Climates. New York, Routledge.

Oke, T.R. 1982. "The Energetic Basis of the Urban Heat Island", Quarterly Journal of the Royal Meteorological Society. 108:1-24.

Oke, T.R. 1997. Urban Climates and Global Environmental Change. In: Thompson, R.D. and A. Perry (eds.) Applied Climatology: Principles & Practices. New York, NY: Routledge. pp. 273-287.

Rosenfeld A., H. Akbari, S. Bretz, B. Fishman, D. Kurn, D, Sailor, and H. Taha. 1995. "Mitigation of Urban Heat Islands: Material, Utility Programs, Updates", Energy and Buildings, 22;255–265.

Rosenzweig, C., Solecki, W., Parshall, L., Gaffin, S., Lynn, B., Goldberg, R., Cox, J., Hodges, S., 2006. Mitigating New York City's heat island with urban forestry, living roofs, and light surfaces. In: Proceedings of Sixth Symposium on the Urban Environment, January 30–Feburary 2,

Synnefa, A., A. Dandou, M. Santamouris, and M. Tombrou (2008), "On the use of cool materials as a heat island mitigation strategy", J. Appl. Meteorol. Climatol., 47, 2846–2856.

Taha H. 1997. "Urban Climates and Heat Islands: Albedo, Evapotranspiration, and Anthropogenic Heat", Energy & Buildings - Special Issue on Urban Heat Islands, Volume 25, Number 2 (1997), pp. 99-103.

Taha, H., D. Sailor, and H. Akbari. 1992. "High-Albedo Materials for Reducing Building Cooling Energy Use", Presented at the 1st CIEE R&D Conference, August 27–29, 1991, University of California at San Diego. Also Report No. LBL-31721, Lawrence Berkeley National Laboratory, Berkeley, CA.

Chapter 7 - Response of Office Building Electricity Consumption to Urban Weather and its Implications

Huade Guan

7.1 Introduction.

This chapter explores the relationship between electricity consumption of selected office buildings and urban weather in the Adelaide Central Business District. This work contributes to improving understanding of the impacts of climate change and urban development on local energy consumption and associated carbon emissions. It provides information useful for devising adaptation solutions to problems associated with these changes.

According to the IPCC (IPCC, 2007), in the last three decades, the average global land temperature has increased by 0.24^{o}C per decade. In Australia, the average temperature has increased by 0.9^{o}C since 1950. Increasing greenhouse gases (GHG) are considered to be the most likely factor contributing to this observed global warming. In 2005, CO_2 concentration in the atmosphere was 379 ppm, contributing to 63% GHG radiative forcing for global temperatures. Australia has set an unconditional goal of 5% reduction of GHG emissions from the 2000-year level by 2020, and up to 15% and 25% reduction depending on international agreements (DCCEE, 2012).

It is estimated that the building sector contributes 23% of the total GHG emission in Australia (CIE, 2007). Electricity consumption is sensitive to weather conditions, primarily in its use for air conditioning (cooling on hot days, and heating on cold days). Thus, electricity consumption often varies with air temperature (Psiloglou et al., 2009; Valor et al., 2001). In addition, humidity is also found to influence energy consumption (Ihara et al., 2008). If this weather-dependent electricity consumption is quantified, it can be used to predict climate change impacts on electricity load demand (Eskeland and Mideksa, 2010; Franco and Sanstad, 2008; Mirasgedis et al., 2007; Ruth and Lin, 2006; Thatcher, 2007) and associated carbon emissions, and consequent economic activities. Such quantification would also be useful for forecasting electricity demand for urban areas a few days in advance (Cancelo et

al., 2008), and planning for electricity allocation during heat waves, in periods when reliable weather forecasts are available.

Around 85% of Australians live in urban areas with 64% in the eight capital cities (DSEWPaC, 2011). As explained in the preceding chapters, the urban microclimate is controlled by urban morphology, surface properties, micrometeorological and hydrological conditions, and anthropogenic heat release, leading to a warmer urban area than surrounding rural areas. Such heating will be increased by expansion of urban areas and population. For example, a study in Phoenix, Arizona, suggested a 1.4 °C increase in the June (summer) monthly minimum temperature per 1000 home completions in the vicinity of a weather station (Brazel et al. 2007).

The subjects discussed in this chapter will be of considerable interest to governmental and industrial partners such as departments of planning and climate change adaptation, to city councils, energy companies, water supply companies, and emergency service organisations.

7.2 Temperature-dependent building electricity consumption.

The level of energy use within buildings, and its variation with environmental temperature, is clearly important for energy efficiency and from environmental perspectives. The level of energy use depends in part on how thermally effective the building's external walls are in isolating the building from that environment. It also depends on the requirements for cooling and heating by the occupants of the building, and on energy management protocols for the building.

During the working week's daytime hours, heating or cooling energy demand can be high when there are large differences between the outside and inside temperature, and comfort levels are to be maintained. The building energy use is thus dependent on outside temperature when the temperature is beyond a "human comfort level", or threshold temperature range. It is expected to rise when outside temperatures increase above that level, or decrease when outside temperatures falls below the comfort range/level. This temperature dependence will vary between climates and buildings as outlined in other chapters of this report. Some conceptualized types are illustrated in Type-2, -3 and -4 energy consumption- outdoor temperature curves in Figure 7.1

At night, when office building occupancy is often low or absent, energy use may be reduced to a minimum. At that time, no requirement exists for cooling or heating, so outside temperatures can range widely and have very little effect on heating and cooling energy use. For weekends and public holidays, a similar temperature-independence situation applies, with perhaps a greater temperature range occurring over these longer time spans.

The dependence of energy use on outside temperature within occupied buildings is thus expected to increase as temperatures fall below some "human comfort level", or threshold temperature range, and also to rise when outside temperatures increase above that level. When buildings are unoccupied, there is little need for maintaining comfort levels, so energy use can be then independent of outside temperature.

Generalised patterns of building energy use are illustrated in figure 7.1.

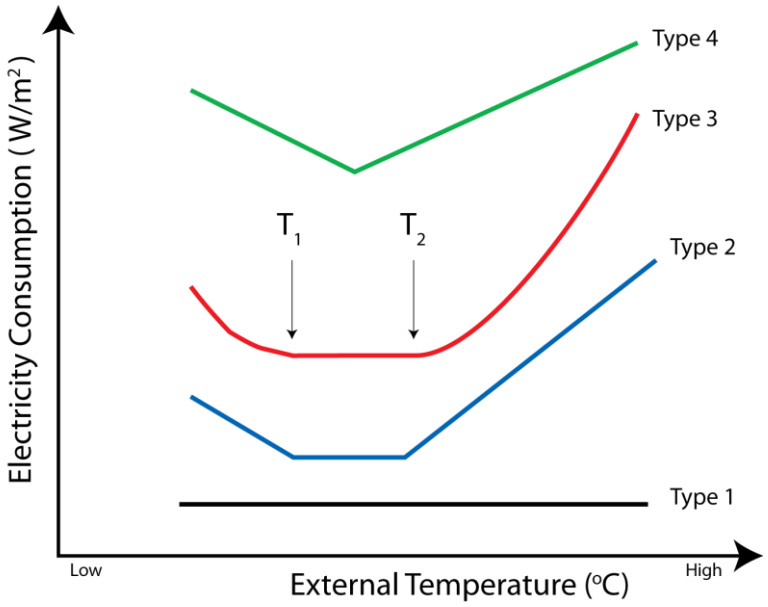

Figure 7.1 Schematic diagram illustrating some different responses of electricity consumption within buildings to external air temperature. The lines are plotted with arbitrary offsets on the vertical axis. T1 and T2 indicate temperatures between which there is no dependency of electricity consumption on temperature for types 2 and 3. The line designated Type-1 is where there is no dependence on outside temperature.

Data from different cities, and buildings within those cities, show pattern similar to the types 2-4. For instance, office building blocks in Tokyo (Ihara et al., 2008), and from Spain (Moral-Carcedo and Vicens-Otero, 2005), show linear increases in energy

consumption at both high and low air temperatures, with a flat response in the threshold temperature range (Type-2 response in the figure). Athens (Psiloglou et al., 2009) shows curvilinear responses at the high and low air temperatures, again with a flat response within the comfort level (Type-3). Data from London, by contrast, shows no flat response region, but linear increases in consumption either side of just one threshold temperature like for Type-4 (Psiloglou et al., 2009).

When air-conditioners are used to cool buildings, condensation often occurs in the air conditioner's coil, which reduces the cooling efficiency (Ihara et al., 2008). This impact becomes more significant when the specific humidity is high in the air. Sometimes, dehumidification is performed to achieve a good in-door comfort level. Thus, besides temperature, it is also found that building energy consumption is sometimes sensitive to specific humidity.

7.3 Data and Methodology.

Three office buildings in the Adelaide CBD were selected for examining their energy consumption response to weather conditions. The characteristics of these three buildings are summarized in Table 7.1, where they are labelled A, B, and C for anonymity.

Table 7.1 Information on the three buildings with sub-hourly electricity consumption data

Building ID	Floor area (m^2)	Electricity consumption data
A	16000	Half hourly, for months 3-4 and 6-12 of 2011
B	7000	15-minute, 21/6/2011-13/3/2012
C	20600	15-minute, 1/1/2011-13/3/2012

***** Only the total office floor area summed over all levels, is considered.

Sub-hourly electricity consumption data were available for the three buildings for about a year. Hourly weather data at the Kent Town station was obtained from the Bureau of Meteorology. Air temperature data from our temperature monitoring network (Chapter 2) was also available. Given that office electricity consumption primarily occurs during the

daytime, and that the temperature difference between the CBD and the surrounding area is smaller in the daytime (<=0.5^{o}C, Chapter 3), Kent Town weather data were used in the following analysis. (In this analysis, the effect of reducing energy consumption in winter due to a warming climate is not considered.)

Electricity consumption was averaged over three different time intervals: every half an hour, daytime (defined here as 8 AM- 6 PM local time), and daily (24 hours). Because electricity consumption of an office building mostly occurs in the daytime, it makes more sense to examine the relationship between electricity consumption and daytime temperature. A preliminary examination of the data showed that the electricity consumption within the three buildings follows the patterns outlined in the preceding section.

To quantify the dependence of electricity use within the buildings on certain meteorological variables, piece-wise linear regression models initially using air temperature and humidity as independent parameters were developed in the form:

$$E = b_0 + b_1 T + b_2 q \qquad \text{for } T<T_1 \text{ and } T>T_2 \qquad (1)$$

where E (W/m^2) is the energy consumption per unit floor area, T (^{o}C) is the outside air temperature, the range T_1 to T_2 (^{o}C) is the air temperature threshold range beyond which building electricity consumption varies with air temperature (Figure 7.1), and q (g/kg) is specific humidity. Equation (1) is applied for heating days ($T>T_2$) or cooling days ($T<T_1$) separately, with different numerical values for b_0, b_1, and b_2 for these cases. The regression coefficient b_1 has a unit of (W/m^2)/^{o}C, and a value which indicates how much the electricity consumption increases (if b_1> 0) or decreases (if b_1< 0) per degree increase of air temperature. The coefficient b_2 has a unit of (W/m^2)/(g/kg), and a value showing the rate of increase of electricity consumption with specific humidity.

7.4 Results.

7.4.1 Electricity consumption and its response to air temperature.

The half-hourly averaged electricity consumption of three buildings is plotted against air temperature in Figure 7.2, for both weekdays and weekends/public holidays. (At the

bottom of the weekday figures, the near horizontal bands of data come from overnight data when air-conditioning is usually running at a reduced rate.)

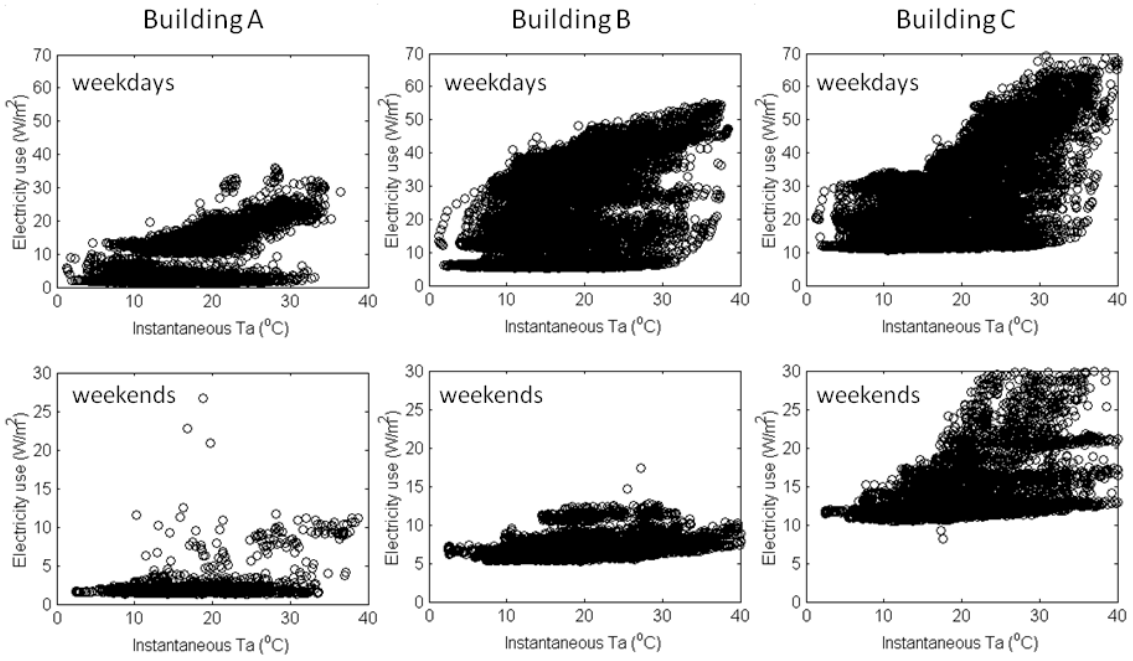

Figure 7.2 Average half-hourly specific electricity consumption vs. air temperature for the three building on weekdays (top row), and on weekends and public holidays (bottom row).

The three buildings show similar patterns in that daytime electricity consumption on weekdays is several times that at the weekends, that weekday consumption is dependent on temperature, and that the temperature dependency on weekends and holidays is weak or absent. (Albeit a variation to the different pattern for Building C is believed to be caused by some tenant occupancy during the weekends and holidays). There appears to be a temperature threshold beyond which weekday electricity consumption becomes temperature dependent. This threshold is between 15 and 20^{o}C (i.e. T_2 lies in this range).

In terms of actual values of instantaneous specific electricity consumption (W/m^2), the three buildings are quite different, increasing from building A to B, and to C. For building A, the specific electricity consumption is similar for night-time, weekends and holidays, within a range of 2-5 W/m^2. For weekdays, daytime electricity consumption is 10-30 W/m^2, part of which has little dependence of temperature.

Now we calculate three quantities for an easy comparison of the electricity consumption between buildings. They are the average electricity consumption for weekends and holidays (E_0), the average night-time electricity consumption for weekdays (E_n), and the average daytime electricity consumption for weekdays when the mean daytime temperature is below 17^{O}C (E_d), as shown in 7.4.2.

The three quantities for the three buildings are summarised in Table 7.2. From those results, the E_d values of buildings B and C are nearly 3 times of building A. And E_n for building B is about 5 times building A value, and 8 times for building C. These data indicate that the order of electricity-use efficiency increases from building C to B to A. (Effects of office occupant number density are not considered here).

Table7.2 Characteristics of the total electricity consumption for the three buildings

Buildings	Base consumption			Temperature dependency	
	Weekend	Night-time	Daytime	Daytime	24 hours
	E_0	E_n	E_d	$b_{1\text{-}d}$	$b_{1\text{-}dn}$
	W/m^2	W/m^2	W/m^2	W/m^2/^{O}C	W/m^2/^{O}C
A	2.01	2.26	11.93	0.81	0.38
B	7.03	10.42	32.20	0.62	0.39
C	13.07	17.66	30.14	1.34	0.82

7.4.2 Statistical modelling of the response of electricity consumption to weather conditions.

To better elucidate the electricity response characteristics for weekdays, daytime average and 24-hour average specific electricity consumption is plotted against daytime (8am-6pm) average air temperature (Figure 7.3). Buildings A and B show a typical response, but with no clear heating response. This latter could arise from the use of gas for heating for these two buildings, or that heating is not significantly used (see the next chapter for clarification of aspects of this) . Further exploration of this is beyond the scope of the present project. Building C has a response with no clear threshold range. For all three buildings, the average temperature threshold for cooling is visually estimated to be 17 ^{o}C.

This number is hence used for piece-wise linear regression for higher temperatures (Equation 1) for each building, with the results shown in Figures 7.4, 7.5, and 7.6.

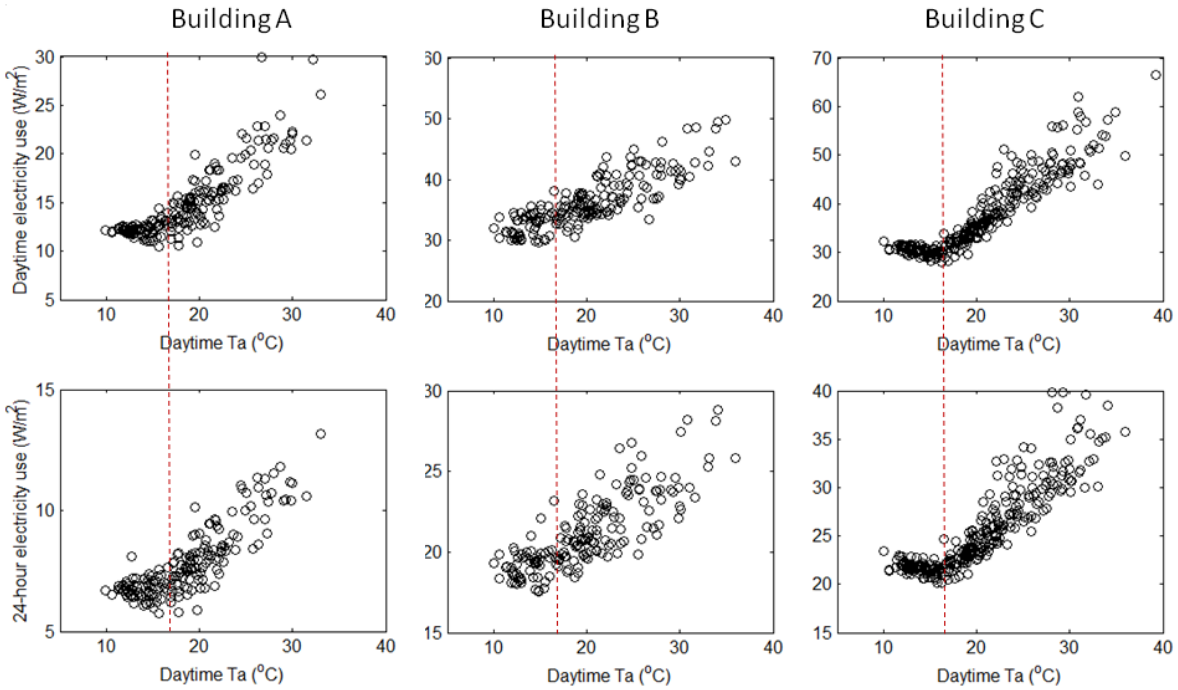

Figure 7.3 Weekday specific total electricity consumption averaged over daytime (8 AM – 6 PM, upper three panels), and over 24 hours (lower three panels) for the three buildings. Note the different electricity use scales. The red lines mark the threshould temperature (T2 in Figure 7.1), which is used for the regression modelling.

Generally, Equation 1 effectively captures 80-90% (based on R^2 values of the regressions) of the variability of mean daytime electricity consumption for the days with mean daytime air temperature exceeding 17^{o}C. Both air temperature and humidity are statistically significant in the regressions in interpreting the electricity consumption data. This indicates that for these warm days, air conditioning is operated to cool down and dehumidify the indoor air. The regression performs poorly, indicated by the low regression R^2 values, in interpreting the electricity consumption data for the days with mean daytime temperature below 17 ^{o}C.

The magnitude of the temperature dependency for temperatures higher than 17 ^{o}C varies between the three buildings, with the lowest value for building B, at 0.62 W/m^2/^{O}C, and the highest for building C, at 1.34 W/m^2/^{O}C. Building A is in between, with a value of 0.81 W/m^2/^{O}C (Table 2). It is interesting that building A has the highest electricity use

efficiency based on the base electricity consumption value, but does not have the lowest temperature dependence.

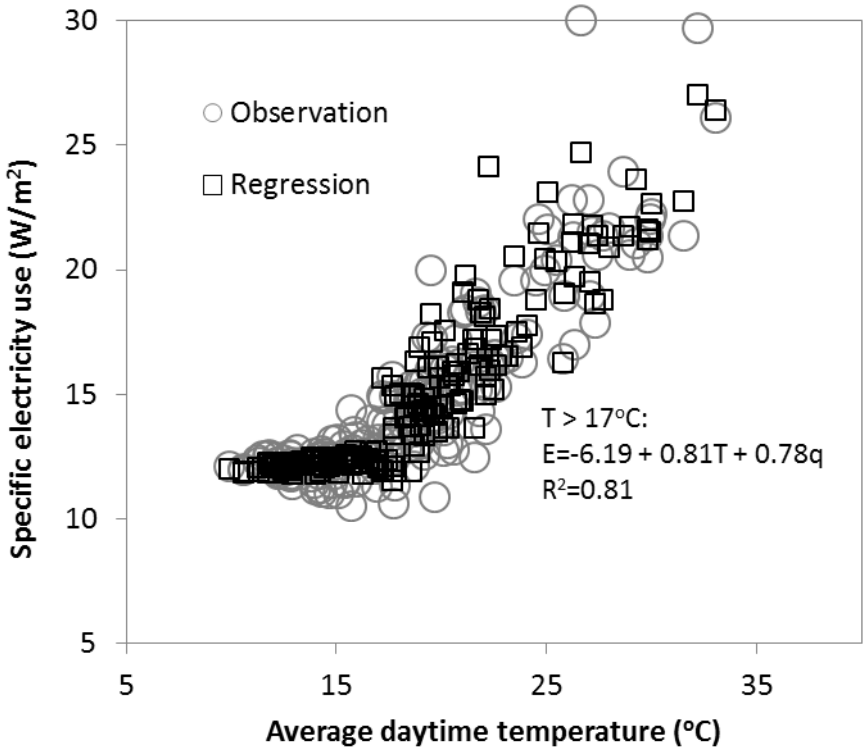

Figure 7.4 Observations and regression estimates of daytime specific electricity consumption for building A.

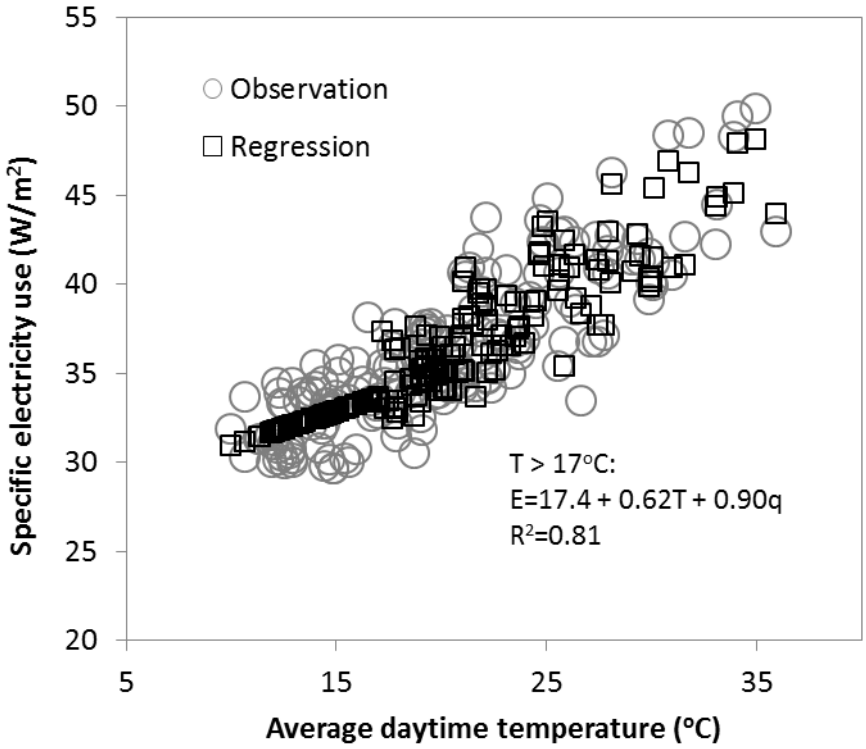

Figure 7.5 Observations and regression estimates of daytime specific electricity consumption for building B.

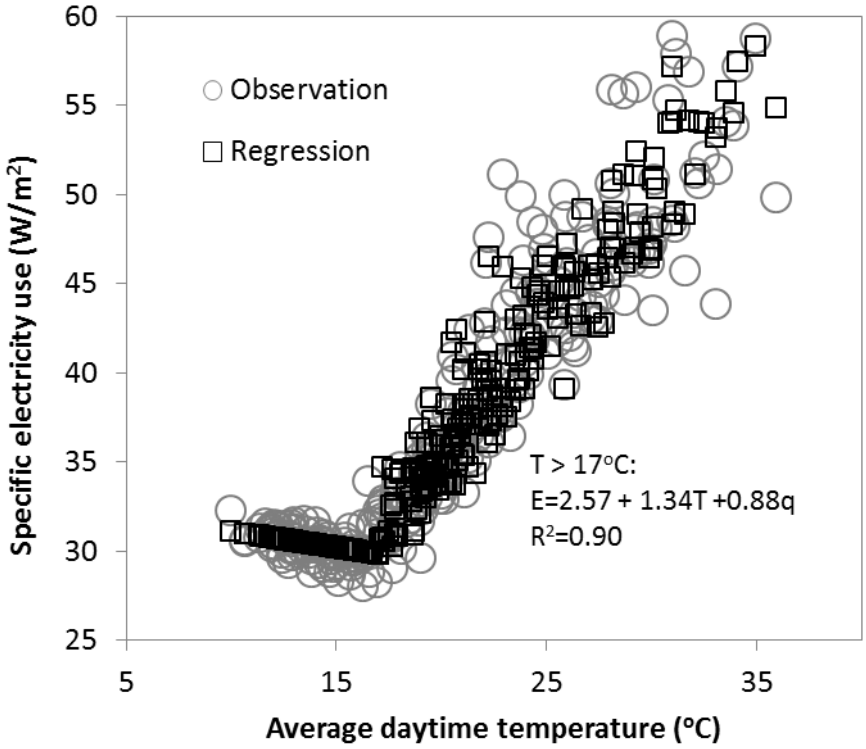

Figure 7.6 Observations and regression estimates of daytime specific electricity consumption for building C.

7.4.3 Comparison of the Adelaide office building electricity consumption with overseas examples.

How does energy performance of the three Adelaide buildings compare to those in other cities? The results for three office building blocks in Tokyo (Ihara et al., 2008) are chosen for comparison (Figure 7.7). In terms of energy use efficiency, indicated from the specific base daytime electricity consumption, buildings B and C are at a similar level to the Tokyo office buildings. Building A demonstrates a much higher efficiency, using only one half to one third that of the Tokyo office buildings. However, it should be noted that the difference in summer climate between the two cities (wet in Tokyo, and dry in Adelaide) may contribute to the difference in office building specific energy consumption.

In terms of temperature dependency, building C performs like the best Tokyo building, while buildings A and B are less sensitive to temperature, only one half of that of building C. This suggests that, in terms of energy use, office buildings in the Adelaide CBD may be more resilient to global warming than their counterparts in Tokyo.

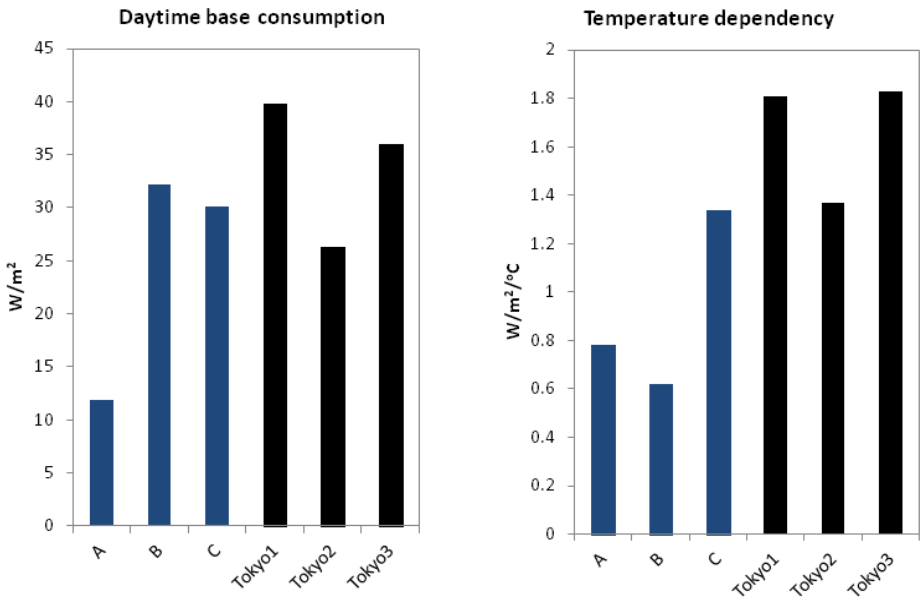

Figure 7.7 Comparison of specific total electricity consumption between the three buildings in Adelaide and three office building blocks in Tokyo.

7.4.4 The response of Adelaide CBD office buildings to climate change and heat waves.

The three Adelaide buildings behave differently in terms of both base electricity consumption and temperature dependency. To evaluate the effects of different energy performance on the total CBD office electricity consumption and associated CO_2 emission, calculations were performed for hypothetical CBD office buildings with average energy performance equivalent to building A, B, and C respectively. The total office floor area in the CBD is assumed to be 1,000,000 m^2, approximated from the current total office floor area there. The CO_2 emission factor is assumed to be 0.81 $kgCO_2$ emissions/kWh for electricity in South Australia (Australian Government, 2011).

The calculated annual electricity consumption for the total of all Adelaide CBD offices would be 54 million kWh if all office buildings had an energy performance similar to building A, but this would jump to 186 million kWh if all office buildings had an energy performance similar to building C. The corresponding annual CO_2 emission would jump from 43,000 tonnes for type A CBD office buildings, to 151,000 tonnes for type C buildings (Figure 7.8).

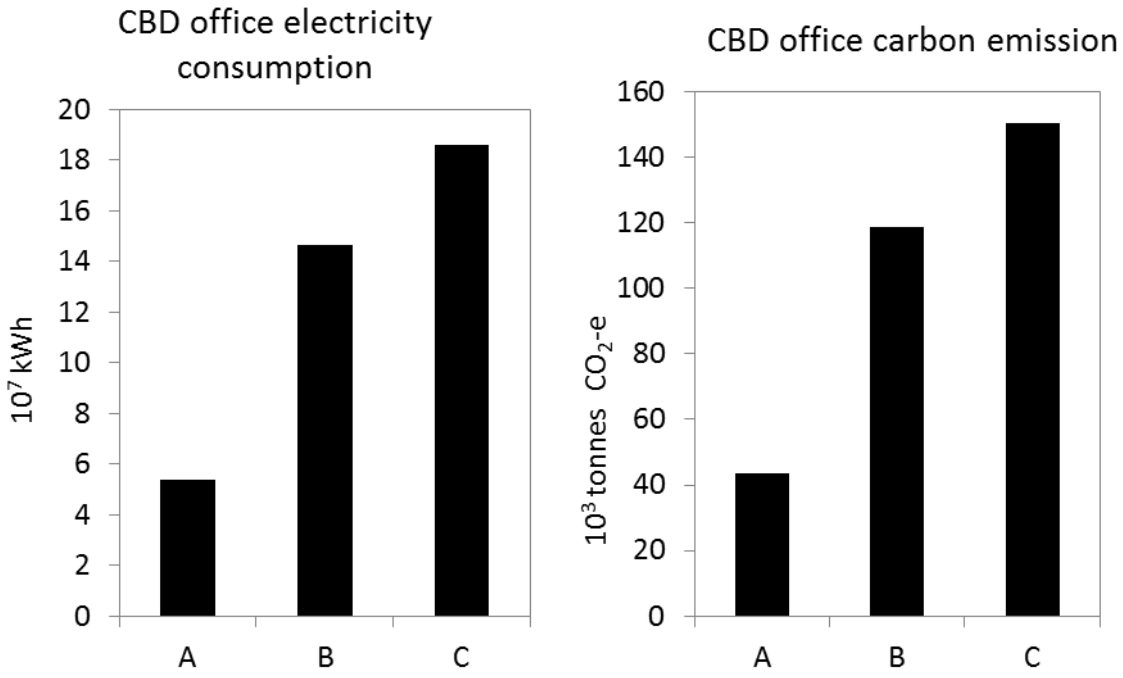

Figure 7.8 Estimated annual electricity consumption and associated CO_2 emission for Adelaide CBD office buildings (assuming a total 10^6 m^2 floor area) with hypothetical mean electricity consumption characteristics equivalent to buildings A, B, and C.

For such CBD office buildings, a one-degree increase of daytime air temperature, due to global warming or local urban development, would increase annual electricity consumption through an increase in the cooling energy demand in a range from 1.4 million kWh to 2.1 million kWh per year, depending on the building energy performance (Figure 7.9), with equivalent CO_2 emission from 1100 to 1700 tonnes.

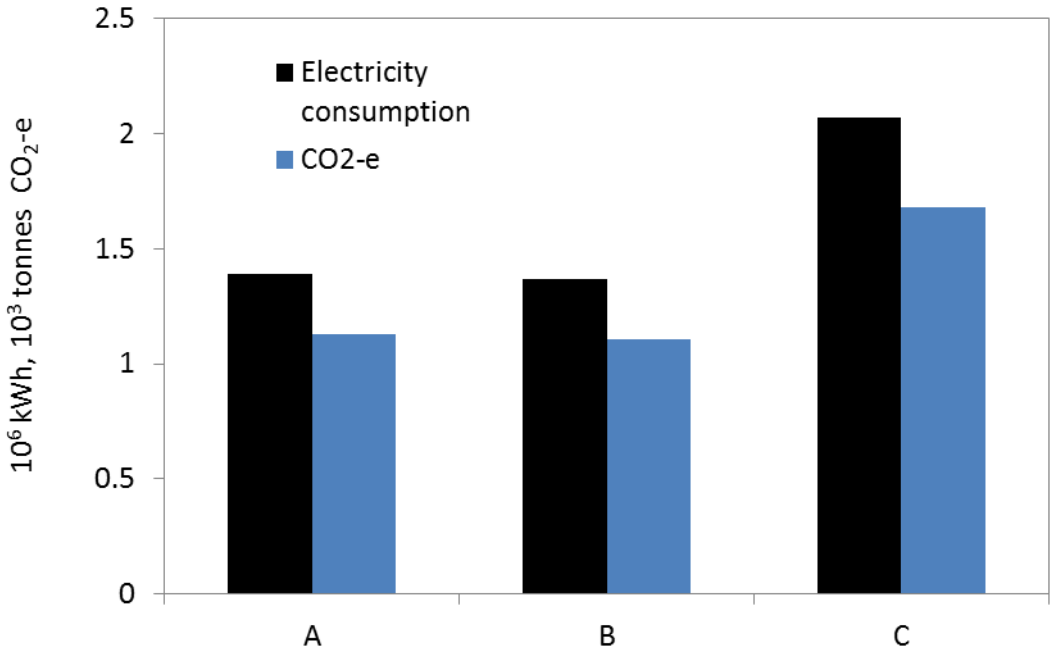

Figure 7.9 Increase of annual electricity consumption and associated CO_2 emission due to a one-degree temperature increase, for Adelaide CBD office buildings (assumed a total 10^6 m^2 floor area) with hypothetic mean electricity consumption characteristics equivalent to building A, B, or C.

The temperature dependency of office building electricity consumption indicates that electricity demand load will increase during any heat wave period. To examine this issue, the early 2009 heat wave (26/1-7/2/2009) is used as a forcing weather condition, in comparison to the average of two weeks prior to and two weeks after this heat wave event. The calculation is still based on the CBD office buildings with energy performance equivalent to building A, B, and C, respectively, irrespective of humidity levels. The results indicate that the daytime electricity demand for the office buildings in the CBD would increase by 9300, 7500, and 14800 kW, for building A-type, B-type, and C-type CBD office buildings respectively (Figure 7.10). This is about 78%, 23%, and 49% of base daytime electricity

demand for the three types of office buildings, respectively. It is interesting that the building with the highest overall energy use efficiency is more sensitive to heat wave events, in terms of its relative sensitivity to temperature.

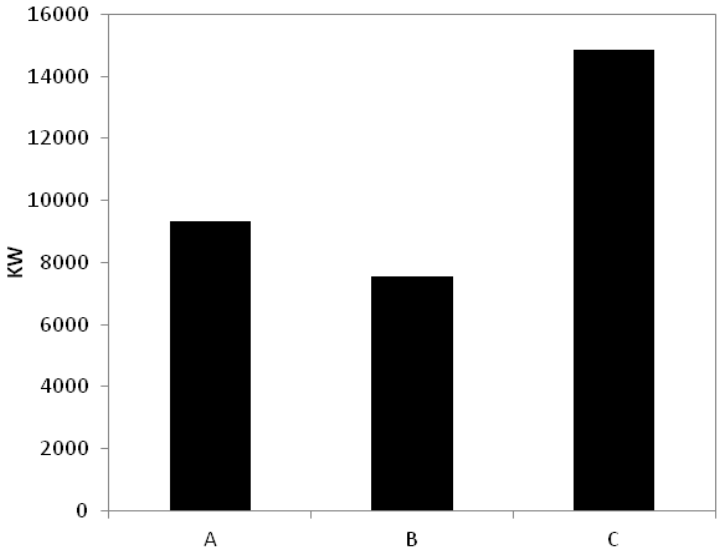

Figure 7.10 The projected increases in daytime electricity load during a heat wave event (similar to that in early 2009) for an Adelaide CBD office (assumed a total 10^6 m^2 floor area) with hypothetical mean electricity consumption equivalent to buildings A, B, and C.

7.5 Conclusions.

Based on these analyses, we conclude that the energy performance of the examined Adelaide office buildings is comparable to or better than those in Tokyo. For the Adelaide CBD office buildings as a whole, with energy performance similar to building B, the annual electricity consumption would be 150 million kWh, with associated CO_2 emission of 118,000 tonnes.

1) Electricity consumption of office buildings in the Adelaide CBD are sensitive to urban weather conditions, in particular, air temperature. There is a daytime mean temperature threshold of around 17 ^{O}C, above which, electricity consumption increases with air temperature. Below this, any temperature dependency is weak. This result indicates that electricity consumption, and associated economic and environmental impacts, are sensitive to climate warming and urban heat island intensities. The following points summarise the findings.

2) The weather dependency of office building electricity consumption can be modelled satisfactorily by linear regression, with both air temperature and humidity being significant predictor variables. The regression models are useful for predicting changes to electricity demand arising from future climate projections, as well as from shorter period heat wave conditions. However, they do depend on the selection of appropriate critical temperatures.
3) The base electricity consumption and temperature dependency vary by factors of 2-3 between the three buildings examined. This indicates that significant improvements to building energy performance should be attempted. A 2-3 times reduction in office building electricity consumption in Adelaide CBD, and associated CO_2 emission, can be achieved by improving the building energy performance –some approaches were outlined in chapter 6.
4) A warming of 1 ^{O}C daytime temperature may increase electricity consumption by 1.6 million kWh per year for the total office buildings in the Adelaide CBD. The corresponding increase of equivalent CO_2 emissions will be of the order of 1,300 tonnes per year.
5) Heat waves strongly influence electricity demand. For an event similar to the early 2009 heat wave, office building electricity demand may increase by 50% (averaged from the three examined buildings) from its base daytime electricity demand.

7.6 Recommendations for future work.

These recommendations are based on the findings of this chapter.

- **Analyse energy consumption in a wider range of buildings in the Adelaide CBD**. Given the large range in energy consumption and its temperature dependency found for the three buildings examined so far, it is prudent to examine more buildings in the Adelaide CBD to provide a better knowledge base for examining the reasons for the variability between CBD building electricity consumption.
- **Analyse energy consumption of residential buildings.** It is expected that residential buildings have quite different energy consumption patterns from office buildings,

and occur in a wide variety of styles, building materials, and energy use patterns. Inclusion of residential buildings would provide a more complete view of electricity consumption and demand, and help plan for appropriate responses to climate changes and urban development.

- **Establish the mechanisms underlying the different energy efficiencies and temperature dependencies of buildings**. Improving such understanding is important for improving building design to improve their thermal response to climate warming.
- **Construct forecasting models for electricity supply and allocation during heat wave events.** Knowing the quantitative relationships on the temperature dependence of electricity requirements for each electricity distribution zone, it is possible to forecast the peak electricity load demand and the peak time for the zone.
- **Analyze historical electricity data for each social-economic area to estimate the use of air conditioning systems.** Such and analysis would clarify whether and by how much heat-wave induced health problems are related to the affordability of air conditioning.
- **Develop sustainable urban heat island mitigation solutions, considering energy, water, and human health effects.**

Acknowledgements.

Discussions with Veronica Soebarto and Roger Clay, and editorial input from John Bennett improved the writing of this chapter.

References for Chapter 7.

Australian_Government, 2011. National Greenhouse Accounts Factors. Department of Climate Changes & Energy Efficiency, pp. 77.

Cancelo, J.R., Espasa, A., Grafe, R., 2008. Forecasting the electricity load from one day to one week ahead for the Spanish system operator. Int. J. Forecast., 24(4): 588-602.

CIE, 2007. Capitalising on the Builing Sector's Potential to Lessen the Costs of a Broad Based GHG Emissions Cut, Centre for International Economics.

DCCEE, 2012. Australia's Emissions Reduction Targets. Department of Climate Change and Energy Efficiency, Canberra.

DSEWPaC, 2011, The State of the Environment, Department of Sustainability, Environment, Water, Population and Communities, Canberra.

Eskeland, G.S., Mideksa, T.K., 2010. Electricity demand in a changing climate. Mitig. Adapt. Strateg. Glob. Chang., 15(8): 877-897.

Franco, G., Sanstad, A.H., 2008. Climate change and electricity demand in California. Climatic Change, 87: S139-S151.

Hirano, Y., Fujita, T., 2012. Evaluation of the impact of the urban heat island on residential and commercial energy consumption in Tokyo. Energy, 37(1): 371-383.

Ihara, T., Genchi, Y., Sato, T., Yamaguchi, K., Endo, Y., 2008. City-block-scale sensitivity of electricity consumption to air temperature and air humidity in business districts of Tokyo, Japan. Energy, 33(11): 1634-1645.

IPCC, 2007. Summary for policymakers. In: Parry, M.L., Canziani, O.F., Palutikof, J.P., van der Linden, P.J., C.E., H. (Eds.), Climate Change 2007: Impacts, Adaptation and Vulnerability. Contribution of Working Group II to the Fourth Assessment Report of the Intergovernmental Panel on Climate Change, . Cambridge University Press, Cambridge, UK, pp. 7–22.

Mirasgedis, S. et al., 2007. Modeling framework for estimating impacts of climate change on electricity demand at regional level: Case of Greece. Energy Conv. Manag., 48(5): 1737-1750.

Moral-Carcedo, J., Vicens-Otero, J., 2005. Modelling the non-linear response of Spanish electricity demand to temperature variations. Energy Econ., 27(3): 477-494.

Psiloglou, B.E., Giannakopoulos, C., Majithia, S., Petrakis, M., 2009. Factors affecting electricity demand in Athens, Greece and London, UK: A comparative assessment. Energy, 34(11): 1855-1863.

Ruth, M., Lin, A.C., 2006. Regional energy demand and adaptations to climate change: Methodology and application to the state of Maryland, USA. Energy Policy, 34(17): 2820-2833.

Thatcher, M.J., 2007. Modelling changes to electricity demand load duration curves as a consequence of predicted climate change for Australia. Energy, 32(9): 1647-1659.

Valor, E., Meneu, V., Caselles, V., 2001. Daily air temperature and electricity load in Spain. J. Appl. Meteorol., 40(8): 1413-1421.

Chapter 8 - Building Performance Modelling

Veronica Soebarto (University of Adelaide)
Sergey Zhukovskyi and Paul Davy (both formerly of Cundall)

8.1 Introduction.

The previous chapter discusses the relationship between electricity consumption and urban weather in Adelaide CBD. This is based on measured electricity use in three office buildings and analysing its relationship with outdoor air temperatures for an entire year. In this chapter, the impact of urban weather on the building energy use is further analysed through building performance simulations.

Three office buildings in the Adelaide CBD , the same as used in parts of chapter 6, are used as case studies here, shown in figures 8.1, 8.2 and 8.3 for buildings X, Y and Z respectively. Each building is simulated using Tas thermal simulation software (CADline 2013) whereby all the input data to the model are based on information from the building managements (for building envelope and HVAC data) and standard assumptions based on Specification JV of the National Construction Code/ Building Code of Australia (ABCB 2012) for internal gains, use profiles and various settings. For weather data over the buildings, the data from the Bureau of Meteorology site for Kent Town, SA, in the Test Reference Year (TRY) format was used. Although Kent Town is about 2 km from these three buildings in the Adelaide CBD, that data was used with a similar justification as in the preceding chapter.

To analyse the sensitivity of building energy use to changes in the urban weather, in particular to the outdoor temperatures, several scenarios are tested. They are:

Scenario 0. The reference state, with all buildings as they are, and weather as defined by Kent Town data.

Scenario 1. Increasing the outdoor temperatures by 2 degrees for the entire year.

Scenario 2. Testing a heat wave period between December and February, similar to the heat waves occurring from December 2008 to February 2009.

Scenario 3. Increasing the heights of surrounding buildings to the same height as the case study building, to analyse the impact of shading by other buildings.

Scenario 4. In addition, the building envelope was also modified to analyse the sensitivity of the building energy use to the envelope design. In the case of a building that is fully glazed the envelope is changed to only have 35% of the facade being glass, whereas for the other two buildings which currently are not fully glazed, the facade is modified to be 100% glazed.

8.2 Modelling Parameters.

8.2.1 Climate and weather data.

Adelaide is located at 34.9° south latitude and 138.5° east longitude, 42.7 meters above mean sea level. It has hot and dry summers, cool winters, and is pleasantly dry in the other seasons. Adelaide is considered a dry place with an average monthly rainfall of 66 mm during winter and only 23 mm during summer. The hottest months are January and February, with high temperatures continuing into March. There can be several very hot days with very warm nights (days with maximum temperature of over 38° C) in a year, and in general the diurnal range is quite significant (more than 10° C). In winter, a number of days with a maximum temperature of less than 13°C may occur. Summer average relative humidity is around 42% while in winter the average relative humidity is 68%. During summer 2008-2009, Adelaide experienced an extreme heat wave period (when there were 6 consecutive days with maximum temperatures above 40°C).

8.2.2 Site and adjacent structures.

The following sections provide details of each case study building and the modelling parameters used.

Figure 8.1 Building X: position in relation to surroundings (left,within the red frame, the yellow arrow denoting north); view from west (right)

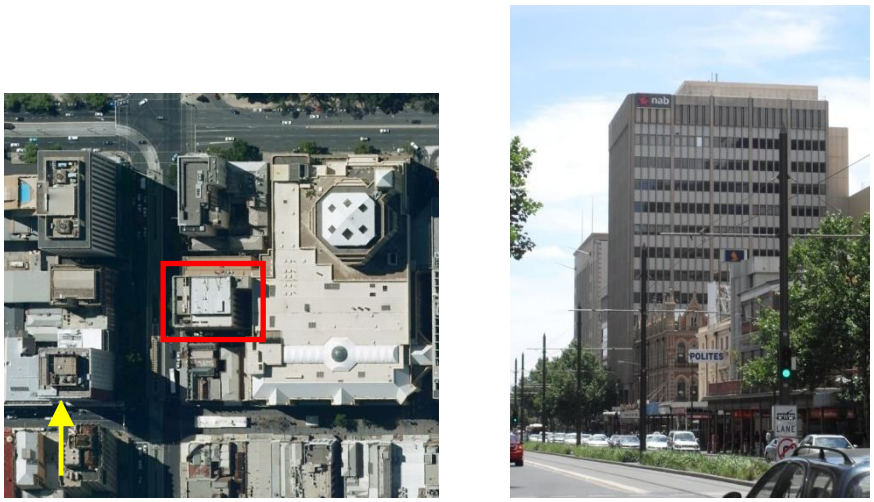

Figure 8.2 Building Y: position (left); view from south west (right)

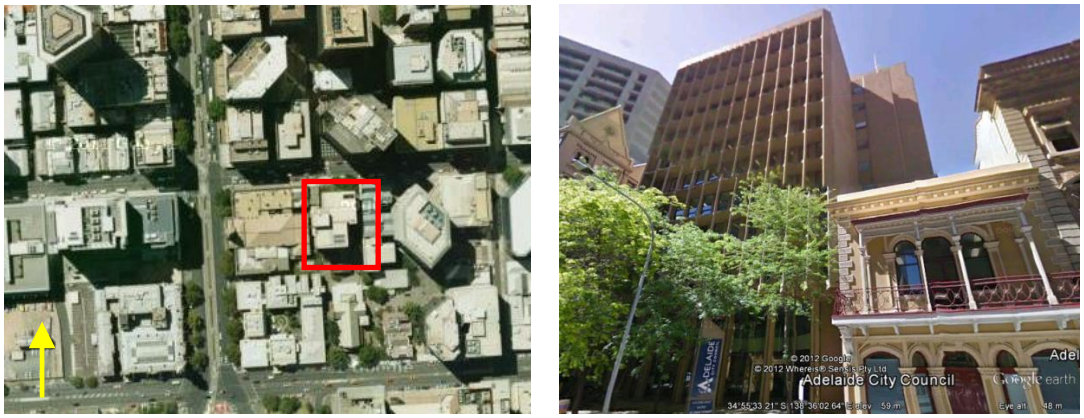

Figure 8.3 Building Z: position (left); view from north (right)

As surrounding structures will shade a building, they need to be accurately represented in each of the models. The geometrical data of the surrounding buildings are

obtained from Adelaide City Council. Figures 8.4 to 8.6 show the case study buildings together with the surrounding buildings. Environmental conditions such as ground reflectivity, temperature of external bounding surfaces, as well as air velocities across external surfaces are all assumed to be the same for all models and they are based on the wind speed and direction data from the Bureau of Meteorology data for Kent Town. It is however acknowledged that if measured data of such factors were available, they would have been included in the simulation models.

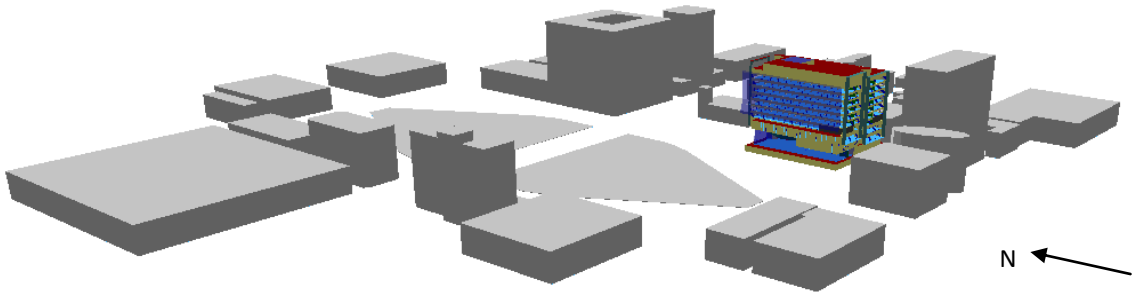

Figure 8.4 Building X and surrounding structures, as modelled. View from south west

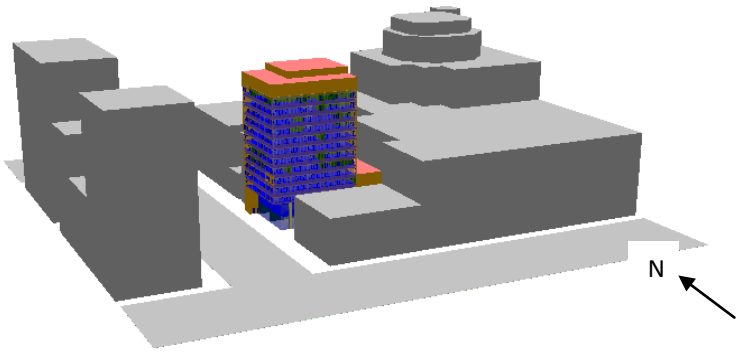

Figure 8.5 Building Y and surrounding structures, as modelled. View from south west

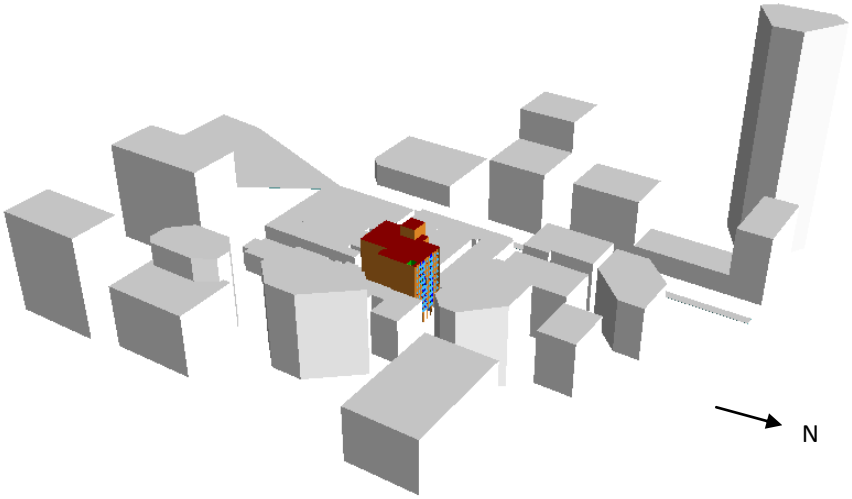

Figure 8.6 Building Z and surrounding structures, as modelled.
View from north east

8.2.3 Building envelopes.

Each building form has been modelled according to architectural drawings where available, or assumed based on the conservative approach and our experience. All rooms are modelled to the inside wall where appropriate. Some small details in the building form were varied to simplify the modelling, these variations having no significant impact on the modelling results. Details of the thermal properties of the building envelope are presented in section 8.3.

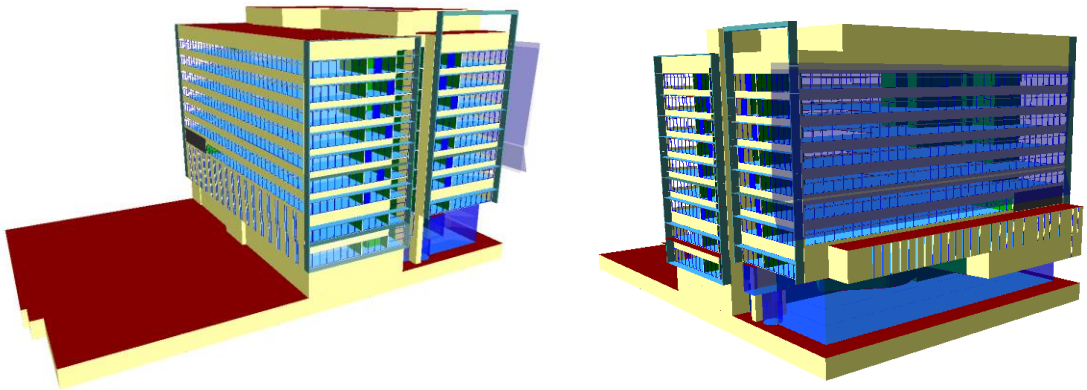

Figure 8.7 Building X model, viewed from the north-east (left) and north-west (right)

8.2.4 Internal thermal loads, energy use profiles and settings.

Internal loads, which typically consist of occupancy, lighting, and equipment or appliances, are the source of internal heat gains. The occupancy densities are modelled based on AS 1668.2-2012 (Standards Australia, 2012) while the metabolic rates are assumed to be the same as specified in Section JV3 of the Building Code of Australia (BCA), now called National Construction Code (i.e. 75 Watt per person for sensible heat and 55 Watt per person for latent heat). Lighting and equipment load densities are based on either the data from the building, where available, or based on Specification J6 of the BCA in 2011. Lighting and equipment energy use is then calculated in the simulation model by taking into account the load densities (Watt per m^2), use profiles and the floor area.

It is acknowledged that the models are not calibrated to the actual occupancy densities nor to the lighting and equipment load densities of the actual buildings as this is beyond the scope of the project.

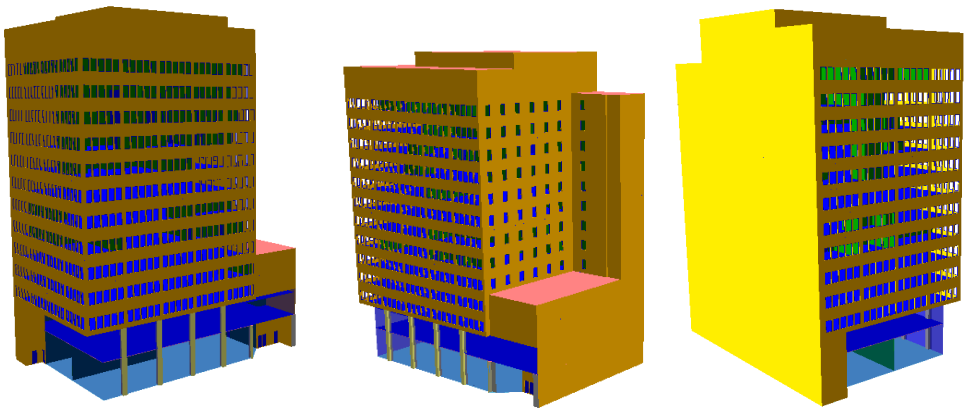

Figure 8.8 Building Y model: viewed from the south-west (left), the south-east (centre), and the north-west (right)

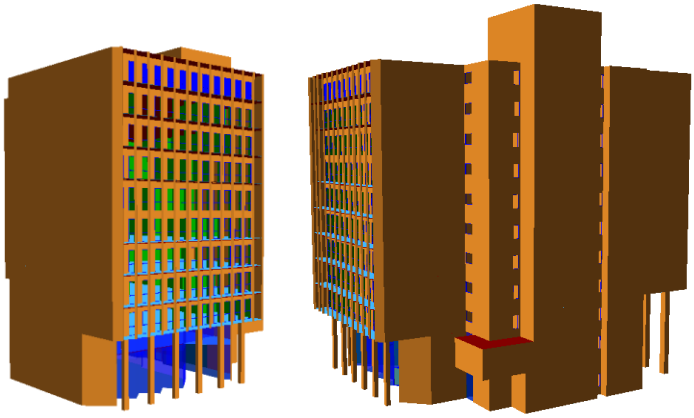

Figure 8.9 Building Z model: viewed from the north-east (left) and the north-west (right)

8.2.5 HVAC systems and settings.

Each floor of each building is zoned in the model to reflect how the HVAC (heating, ventilation and air-conditioning) systems are zoned in the actual building. Examples of the HVAC zones are presented in Figures 8.10 and 8.11. Note that the different colours in these figures are to represent different zones and do not represent specific types or usage of the zones.

It should be noted that all the air-handling equipment is assumed to be equipped with particulate filtration, and therefore the reduced airflow rate of 1 L/s per m^2 allowed by the standard specified concession was applied. Infiltration has been modelled as per provisions of JV3 (d) (F) of the BCA 2011. Allowance of 1.0 Air Changes per Hour (ACH) for perimeter zones and 0 ACH for centre zones was applied when pressurisation plant is operating and 1.5 ACH were applied for the whole building when pressurisation plant is not operating.

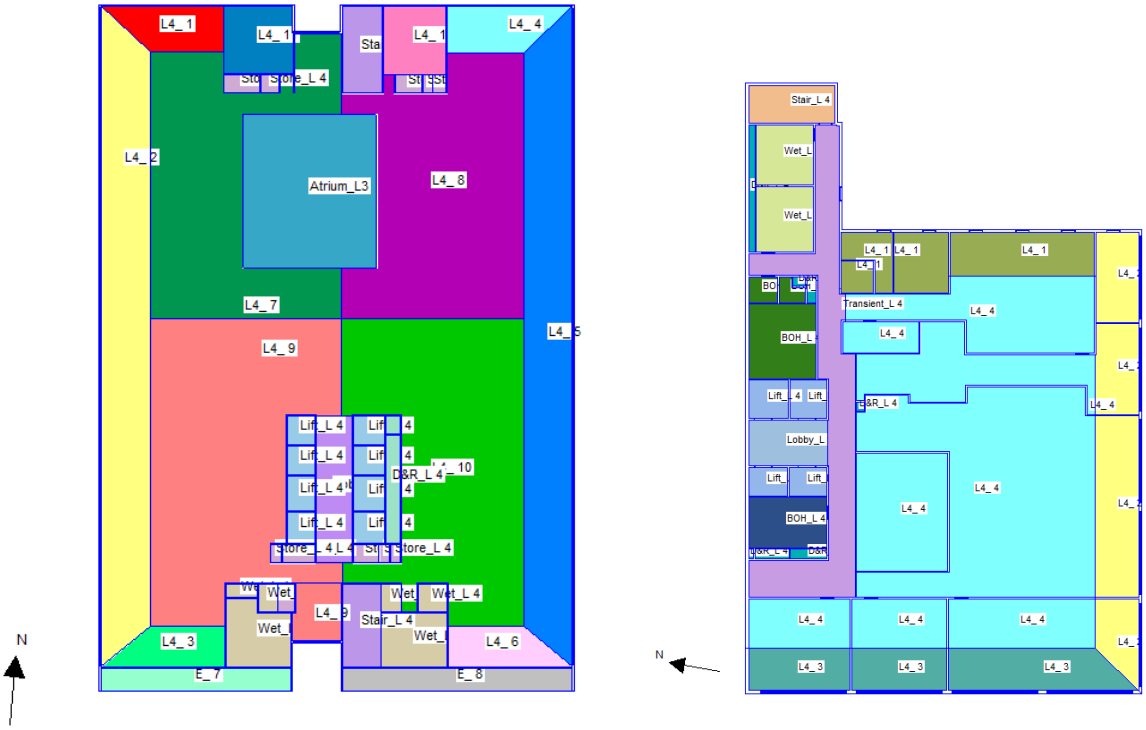

Figure 8.10 An example of zonings for the building X (left) and building Y (right)

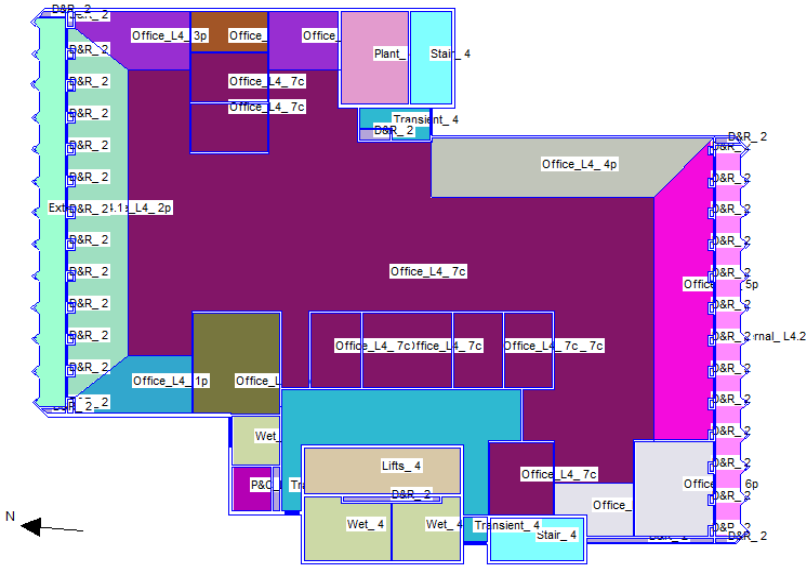

Figure 8.11 An example of zonings for building Z

8.3 Building Descriptions

8.3.1 Building X.

This is a multistorey office building comprising a car park on the basement for 130 cars, a publicly accessible ground floor, a mezzanine level with an Educational Centre, eleven floors for office tenants, and a plant room on the top floor. The total floor area is 34,590 m^2 (Table 8.1). This building has a large glazed facade facing west. A clear single glazing with DMS graphic (making the glazing not totally clear) is placed in front of this west facing facade to create a double-skin facade to reduce solar heat gains in the afternoon.

Table 8.1 Modelled Area Distribution of Building X

Area type	Floor Area (m^2)
Office and Supplementary	10,848
Labs	5,290
Commercial	4,469
Educational Centre	345
Retail and Lobby	1,264
Transient	1,136
Stair	908
Store	688
Lift	881
Wet	939
Plant rooms	3,147
Car park	4,675
TOTAL	**34,590**

The building geometry, envelope, orientation, shading, and lighting power densities are modelled according to the data from the actual building. Similarly, as-built equipment schedules and fan curves are used to model the pumps, boiler, Fan Coil Units (FCU), Air Handling Units (AHU) and fan operations. Note that the operations of Combined Heat Power (CHP) and absorption chillers were excluded from all the modelled scenarios as to pursue the most conservative approach. Table 8.2 and 8.3 show the details of modelling input parameters for this building.

Table 8.2 Modelling Input Parameters for building X

Item	Description	
Weather Data	Adelaide (SA) weather data has been used for this energy simulation based on a Test Reference Year (TRY), 1987.	
Building fabric	**Envelope Item**	**Thermal Properties**
	External walls (insulated)	R-value – 1.0 m² K/W
	Envelope walls (non-insulated 150 mm concrete)	R-value – 0.35 m² K/W
	Mid-level floors	R-value – 0.25 m² K/W
	Roof	R-value – 2.1 m² K/W
	Atrium ETFE (2 layer)	U-value – 1.8 W/ m² K
	Veil	Clear single glazing with DMS graphic 3mm dots (50% coverage)
	Glazing (N, S and E)	U-value – 1.8 W/ m² K, SC-0.41, VLT=48%
	Glazing (W)	U-value – 2.85 W/ m² K, SC-0.84, VLT=76%
External shading	Shading from overhangs, reveals and vertical structures have been incorporated into the 3D modelling based on the architectural design.	
Lighting Density	The lighting power densities for proposed services have been calculated based on the electrical reflected ceiling plans (where available) or applied conservative values based on Part J6 of the BCA	
Lighting Profile	As per default BCA 2010 (Specification JV) profiles	
Design Criteria Conditions	**Criteria**	**Design Value**
	Room Temperature Set	21°C - 24°C
	Occupancy load	75W/m² - sensible, 55W/m² - latent
	Minimum Outside Air (AS1668.2)	7.5 L/s per person. The increase above the minimal value required by the standard was applied where specified
	Lighting load	As per the lighting density nominated above.
	Equipment power load	15W/m² (BCA 2010)
Outside Air	Under normal operating conditions the building operates on 100% outside air between 8am to 6pm 5 days a week. The building operates on 150% of the minimum outside air requirements when ambient conditions are outside of the temperature range 16°C to 30°C.	
Infiltration	Allowance of 1 Air Changes per Hour (ACH) on perimeter zones and 0 ACH in internal zones when pressurisation plant is operating; allowance of 1.5 ACH to all zones when pressurisation plant is not operated	
Occupancy Density	The peak occupancy for each type of facility is shown below: Tenancy (office and supplementary) - 1 person per 10m² (BCA, Table D1.13) Wet areas, transitory and back of house – no occupant.	
Occupancy Profile	As per default BCA 2010 (Specification JV) profiles	
Equipment Profile	As per default BCA 2010 (Specification JV) profiles	
HVAC System	As per mechanical drawings and associated specifications (where available) or assumptions made by the modeller	
HVAC hours of Operation	As per default BCA 2010 (Specification JV) profiles	
HVAC Zoning	As per mechanical drawings and associated specifications	
Ancillaries	Ancillary system loads have been calculated from installation drawings and technical submissions	

Table 8.3 HVAC Input Parameters for building X

Item	Description
Wet areas (exhaust)	Exhaust Airflow -10L/s/m2 (AS1668.2) Exhaust Fan SFP – 0.65W/L/s (assumption)
Chillers	2 x Carrier 23XRV water-cooled chillers, each 1,400kW cooling capacity COP varies with part load only: • 10%: COP = 6.649 • 50%: COP = 11.752 • 100%: COP = 6.464
Condenser	Water flow rate = 0.054 L/s per KW Pump SPP = 301 W/L per second (ASHRAE 90.2) Pump Mechanical Efficiency = 60% Pump Electrical Efficiency – 95% Chiller Resistance = 35 kPa Flow Rate delta T = 6K Operation on demand
Cooling towers	Two cooling towers working in parallel Cooling tower fans controlled by VSD Design WBT = 22.5°C Design Range = 5.5°C Design Approach = 7°C Full Load Fan Performance = 3.2L/s (condenser water) per kW of fan power (BCA2011, J5.4 (f) p.497) Each CT comprises 9.9kW fan fit with VSD drive Operation on demand
Gas Boiler	Boiler Efficiency = 80% Distribution Efficiency = 90% Flow Rate delta T = 11K Operation on demand

8.3.2 Building Y.

Building Y is situated on the eastern side of King William Street on the north side of Rundle Mall. This 12,376 m^2 multistorey office building comprises of a basement, ground, mezzanine, eleven tenant levels, and a plant room on the top level (Table 8.4). The HVAC system in this building is currently being upgraded incorporating the following best practice technologies and techniques:

- efficient chillers,
- new chilled and condenser water pumps,
- introduction of air handling economy cycle strategy,
- implementation of induction Variable Air Volume (VAV) air distribution,
- BMS control strategy upgrade,

- outside air CO2 control, and energy sub-metering upgrade.

The building only has two facades with glazing (the eastern and southern facades) whereas both the northern and eastern facades have fewer openings as they are on the boundary with adjacent buildings.

Tables 8.5 and 8.6 show the modelling input parameters of this building. When not mentioned, other input parameters for this building are the same as for building X.

Table 8.4 Modelled Area Distribution of building Y

Area type	Floor Area (m^2)
Office and Supplementary	8,360
Retail and Lobby	576
Transient	565
Stair	243
Lift	314
Wet	428
Plantrooms	1,890
TOTAL	**12,376**

Table 8.5 Modelling Input Parameters for building Y

Item	Description	
Building fabric	**Envelope Item**	**Thermal Properties**
	External walls (insulated)	R-value – 1.2 m^2 K/W
	Envelope walls (non-insulated concrete)	R-value – 0.4 m^2 K/W
	Mid-level floors	R-value – 0.25 m^2 K/W
	Roof	R-value – 2.1 m^2 K/W
	Glazing	U-value – 2.9 W/ m^2 K

Table 8.6 HVAC Input Parameters for building Y

Item	Description
Wet areas (exhaust)	Exhaust Airflow -10L/s/m2 (AS1668.2) Exhaust Fan SFP – 0.65W/L/s (assumption)
Chillers	2 x Powerpax water-cooled chillers (assumed) COP varies with part load only: • 25%: COP = 11.07 • 50%: COP = 10.79 • 75%: COP = 7.55

Item	Description
	• 100%: COP = 5.29
Condenser	Water flow rate = 0.054 L/s per KW Pump SPP = 301 W/L per second (ASHRAE 90.2) Pump Mechanical Efficiency = 60% Pump Electrical Efficiency – 95% Chiller Resistance = 35 kPa Flow Rate delta T = 6K Operation on demand
Cooling towers	Heat rejection provided via cooling towers Two cooling towers working in parallel Cooling tower fans controlled by VSD Design WBT = 22.5°C Design Range = 5.5°C Design Approach = 7°C Full Load Fan Performance – 3.2L/s (condenser water) per kW of fan power (BCA2011, J5.4 (f) p.497) Operation on demand
Gas Boiler	Boiler Efficiency = 80% Distribution Efficiency = 90% Flow Rate delta T = 11K Operation on demand

8.3.3 Building Z.

Building Z is a multistorey office building that comprises a ground level, mezzanine, eleven office levels, and a plant room on the top floor, with a total floor area of 9062 m^2. Similar to building Y, this only has two facades with glazing, the northern and southern facades, whereas the other two facades are solid walls.

Tables 8.7 to 8.9 show modelling input parameters of this building. When not mentioned, other input parameters are the same as those of building Y.

Table 8.7 Modelled Area Distribution of building Z

Area type	Floor Area (m^2)
Office and Supplementary	7022.9
Transient	552.9
Stair	283.7
Lift	243.1
Wet	356.7
Plantrooms	602.3
TOTAL	**9061.6**

Table 8.8 Modelling Input Parameters for building Z

Item	Description	
Weather Data	Adelaide (SA) weather data has been used for this energy simulation based on a Test Reference Year (TRY), 1987.	
Building fabric	**Envelope Item**	**Thermal Properties**
	External walls (insulated)	R-value – 1.2 m² K/W
	Envelope walls (non-insulated concrete)	R-value – 0.4 m² K/W
	Mid-level floors	R-value – 0.25 m² K/W
	Roof	R-value – 2.1 m² K/W
	Glazing	U-value – 3.5 W/ m² K

Table 8.9 HVAC Input Parameters for building Z

Item	Description
Wet areas (exhaust)	Exhaust Airflow -10L/s/m2 (AS1668.2) Exhaust Fan Specific Fan Power (SFP) - 0.65W/L/s (assumption)
Chillers	2 x water cooled chillers COP varies with part load only (assumed): • 25%: COP = 5.6 • 50%: COP = 6.1 • 75%: COP = 6.4 • 100%: COP = 5.8

8.3.4 Estimation of Greenhouse Gas Emissions.

Results from simulating the different scenarios are converted into the Greenhouse Gas emission equivalent (GHG-e) values, with conversion coefficients as presented in Table 8.10.

Table 8.10 GHG-e Emission Factors for South Australia*

State	Electricity (kgCO2-e/kWh)	Gas (kgCO2-e/MJ)
SA	0.81	0.0512

* Based on National Greenhouse Account (NGA) Factors 2012 (Department of Climate Change and Energy Efficiency 2012).

8.4 Simulation Results.

As indicated in section 8.1, a number of scenarios were modelled to predict the sensitivity of the building design and its impact on the building energy use, with changes in the urban environment. In addition, a scenario covering a change to the building envelope is also examined to predict its impact on the building energy use. As a reminder, the scenarios are:

- S0 (Scenario 0): Base Case
- S1 (Scenario 1): 2°C increase of outdoor temperatures throughout the year
- S2 (Scenario 2): A heat wave period in summer
- S3 (Scenario 3): Shading by surrounding buildings or increase the height of surrounding buildings to be the same as the modelled building
- S4 (Scenario 4): External walls to be 35% glazing in building X and fully glazed for the other two buildings.

8.4.1 Simulation Results – Base scenario for each building.

Table 8.11 presents a summary of the simulated energy use (electricity and gas) of all three buildings before changes were applied. As the areas of these buildings are different, the results are normalised to the energy use per m^2 of floor area. It can be seen that the performance of buildings X and Y is similar, with around 125 kWh/m^2 per year of total energy use, or 50 kWh/m^2 per year for only the energy used for heating and cooling. The latter value is comparable with the average weather dependent (heating and cooling) energy use discussed in Chapter 7. Building Z, however, is predicted to have slightly higher energy consumption with 138 kWh/m^2 per year of total energy use and 60 kWh/m^2 per year of heating and cooling energy. Consequently, the predicted greenhouse gas emissions (GHG-e) from the energy used for heating and cooling (using the conversion factors in Table 8.10) in the X, Y and Z buildings is 31, 30 and 34 kgCO2-e/kWh per m^2 respectively.

Table 8.11 Simulated Base Energy Use of the Buildings

	X	Y	Z
Total floor area	34,590	12,376	9,062
Total Energy (Electricity & Gas), kWh	4,323,218	1,527,358	1,247,158
Total Energy in kWh per m^2	125	123	138
Total HVAC Energy (Electricity & Gas), kWh	1,764,538	611,082	546,199
Total HVAC Energy in kWh per m^2	51	49	60
HVAC GHG Emissions, (kgCO2-e/kWh)	1,081,219	367,755	306,627
HVAC GHG Emissions, (kgCO2-e/kWh) per m^2	31	30	34

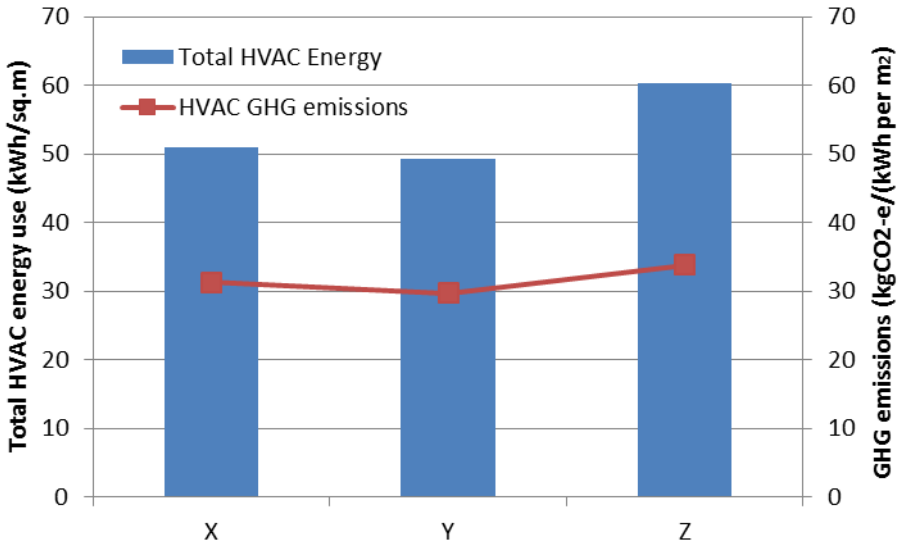

Figure 8.12 HVAC energy and green house gas emissions of the buildings in the Base scenario.

8.4.2 Simulation Results – Scenario 1.

Despite the common perception that an increase in external temperatures would increase building energy use due to the rise of cooling energy, the predictions here show that the total energy use of the three buildings would actually decrease. This is because, for Adelaide currently, the season for which heating is needed is longer than the season where cooling is required, as shown in Figure 8.13. The temperature range throughout the year falls mostly in and below the comfort zone. So a reduction in heating (due to an increase in

outdoor temperature from climate change) will outweigh the increase in cooling energy required in the warmer season, thus resulting in a reduction in total energy.

In all three buildings the gas use for heating in the cooler months is predicted to reduce by 50% due to the increase in the urban temperatures. Interestingly, the predicted GHG emission would increase because the rise in electricity consumption for cooling would produce more green gas house emissions than the decrease of the GHG emission due to the reduction in heating energy (due to the conversion coefficients for South Australia as presented in Table 8.10). Due to the increase in electricity use, the GHG emission from electricity in all 3 buildings would rise by 21%, whereas reduced gas use would result in decreasing GHG emission by 50%. In total, it is predicted that the 2-degrees rise of urban temperatures would increase the green gas house emissions in the three buildings by 10 to 12%.

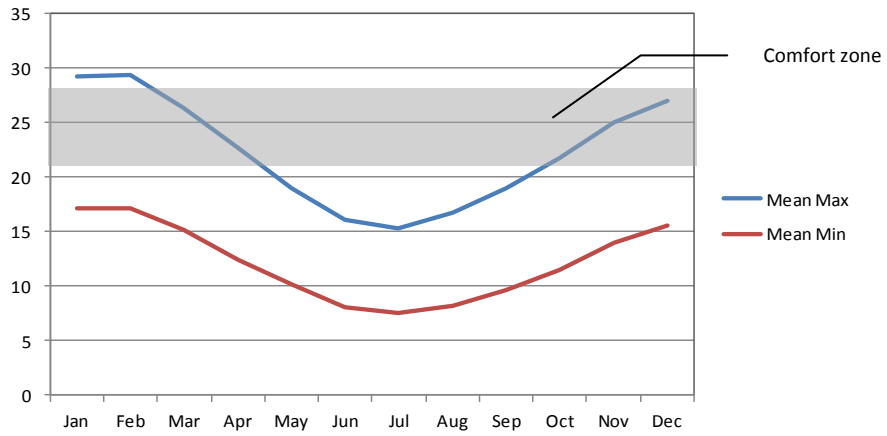

Figure 8.13 Adelaide monthly average temperatures and comfort zone in air-conditioned buildings

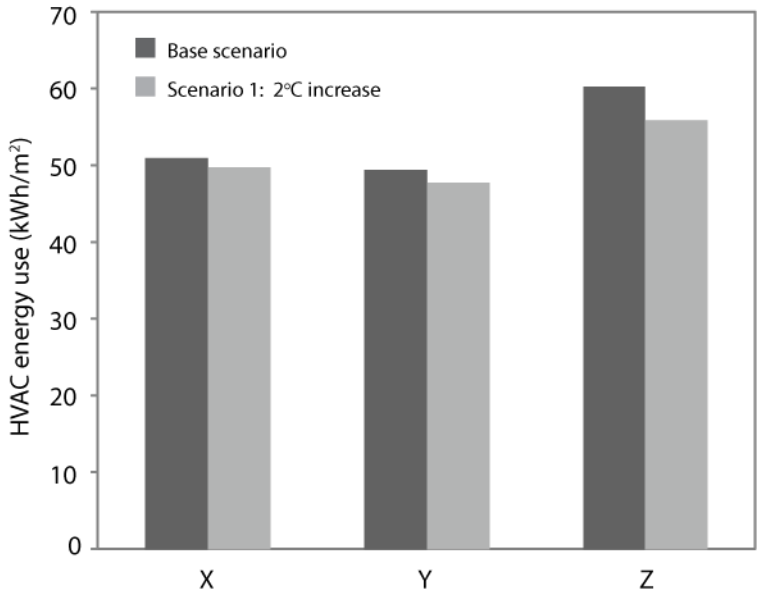

Figure 8.14 Comparison of predicted HVAC energy use of the three buildings for the base scenario and scenario 1.

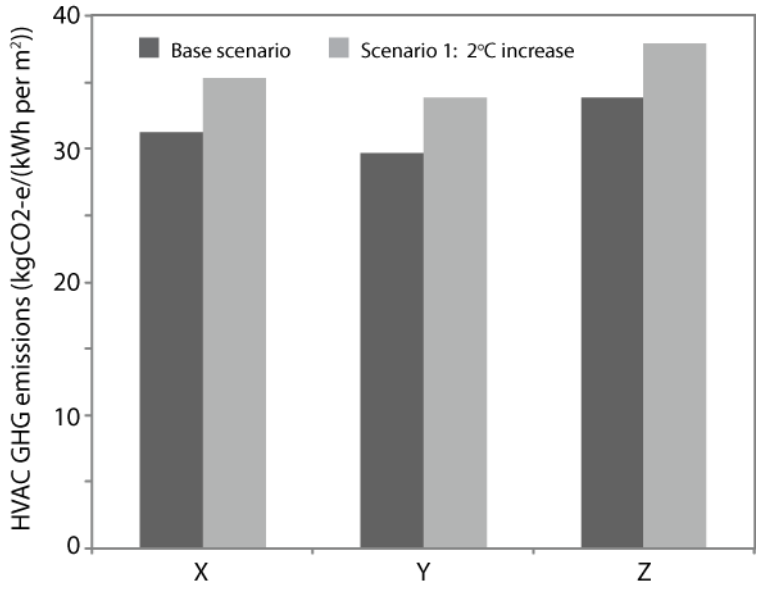

Figure 8.15 Comparison of predicted GHG Emissions from HVAC for the three buildings for the base scenario and Scenario 1.

8.4.3 Simulation Results – Scenario 2.

If there would be a period of heat wave in summer, such as the one that occurred between December 2008 and February 2009, it is predicted that the total energy consumption in all three buildings as well as the equivalent greenhouse gas emissions would

increase. The GHG emission due to the increase in cooling energy use is predicted to increase by around 8% in buildings X and Z, whereas the increase would be around 2% in building Y. The latter building has the smallest increase in the cooling energy during heat waves because most of the window glazing which faces west is shaded by the buildings across the street in the afternoon while the other large area of glazing faces south.

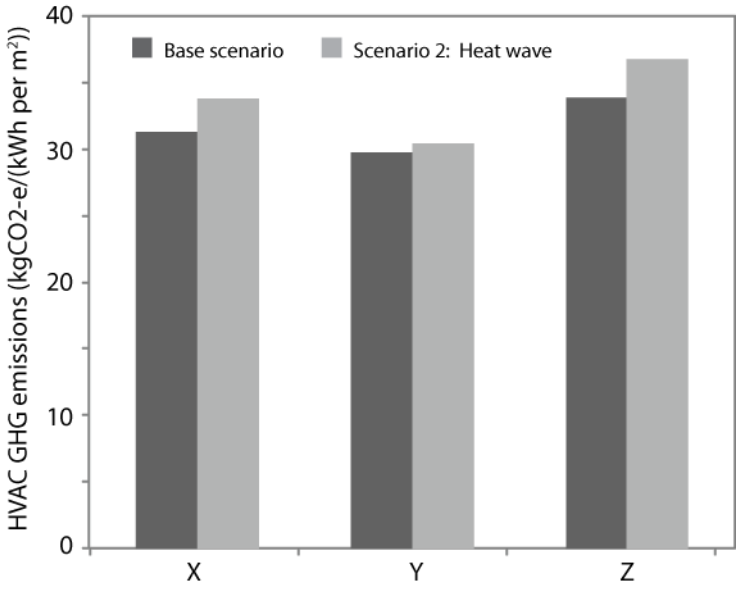

Figure 8.16 Comparison of the predicted GHG Emissions from HVAC for the buildings for the base scenario and Scenario 2.

8.4.4 Simulation Results – Scenario 3.

In the current condition, at least two sides of all three buildings are exposed to the elements, or have glazed wall surfaces. The other buildings adjacent to these three are either shorter or a distance away even though they are as tall as these buildings. In Scenario 3, it is assumed that adjacent or surrounding buildings are as tall as these buildings. The simulation is conducted to predict the impact of the change in the urban form due to future developments.

It is found that such an increase in the height of the surrounding buildings has minimal impact on the HVAC energy use of the three buildings or on their GHG emissions. While the energy use for cooling would decrease due to more shading provided by the surrounding buildings, the heating energy would increase at about the same rate. However, as there is more GHG emission per unit of electricity than per unit of gas use, the decrease

in the cooling energy would result in a reduction in the total GHG emission from the HVAC systems. It is predicted that in this scenario, the GHG emission would be reduced by around 2% for buildings X and Y while the reduction would be less than 1% for building Z. The impact on the latter building is much less as this building only has two facades with glazing while the longer facades are solid walls.

These results demonstrate that increasing building heights as a result of a drive to increase density in the city could actually have a positive benefit to the buildings and urban environment as the buildings would require less cooling due to the shading effects, hence there would be less GHG emissions produced by the HVAC systems. These results are similar to the findings by Williamson et al. (2009). It is however important to analyse further for any optimum building heights to ensure that the change in the urban form or building heights will not have an adverse impact due to the increase in heating energy. That is beyond the scope of this project.

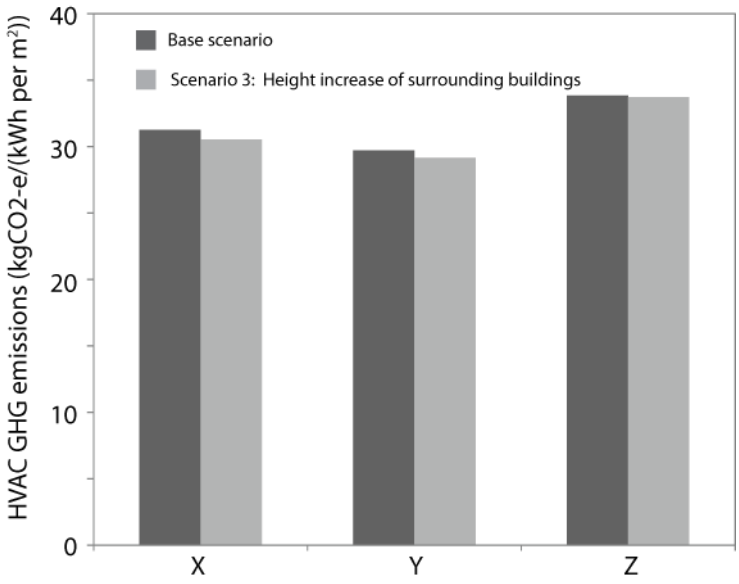

Figure 8.17 Comparison of the predicted GHG Emissions from HVAC of the buildings for Scenario 0 and Scenario 3.

8.4.5 Simulation Results – Scenario 4.

The final change applied was modifying the facades of these case study buildings. For building X, it was assumed that the east and west walls were only glazed at 35% of the total

wall areas, whereas for the other two buildings, the walls that in reality have only windows, would be 100% glazed.

In building X with the east and west facades only 35% glazed, the energy use for heating and cooling would be reduced by 2.3% while the equivalent GHG emission would decrease by 4%. As the reduction in the glazed area would mean less heat gain (hence less cooling energy), heating energy would increase though not as much as the reduction in the cooling energy. In building Y, increasing the glazed area to the east facade of the building (the west and south facades are already 100 glazed) would significantly increase both the HVAC energy use and greenhouse gas emission by 18% and 20% respectively. In the third building, Z, the increase is rather moderate with about 8% increase in HVAC energy use and GHG emissions. This moderate increase is due to the fact that only the north and south facades can be modified while the longer east and west facades would remain solid as they are on the boundaries of the site.

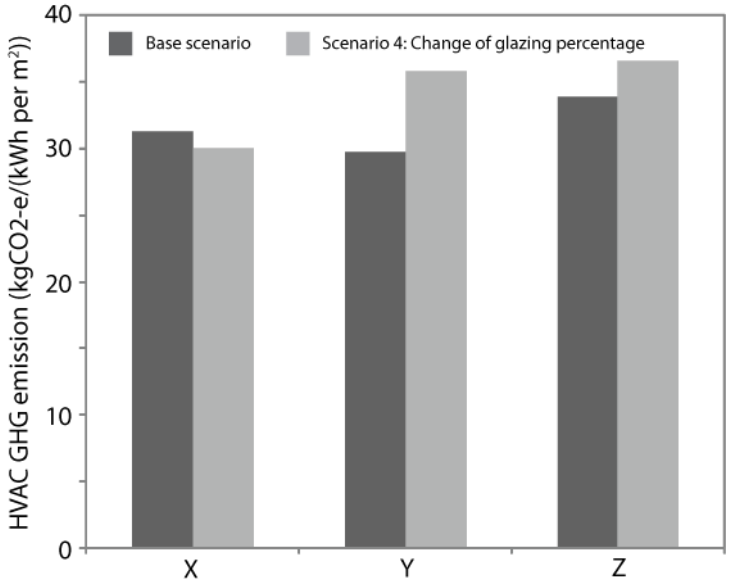

Figure 8.18 Comparison of the predicted GHG Emissions from HVAC of the buildings for Scenario 0 and Scenario 4.

These results demonstrate the importance of analysing the impact of the envelope designs on the building energy use during the design process. While changing the percentage of the window glazing in existing buildings is unlikely, these results suggest a possible solution to be implemented in retrofit projects of fully glazed buildings. Reducing

the glazed area for example by adding solid cladding panels would help reduce external heat gains, and hence reducing the need for cooling.

8.5 Summary.

Based on building performance simulation conducted with EDSL Tas program, this chapter establishes that the energy use and greenhouse gas emissions of the case study buildings are sensitive to changes in the urban climate. A 2 degrees increase in urban temperatures would result in an increase in greenhouse gas emissions, mainly due to the increase in cooling energy, even though the heating energy would decrease by 50%. If a period of heat waves occurred during summer, both the total energy and greenhouse gas emissions of all case study buildings are predicted to increase by up to 9%.

In the case of increased density of buildings in the city, created by an increase in building heights surrounding the case study buildings, it is found that total energy use and greenhouse gas emissions would be slightly reduced. That is because an increase in building heights means buildings would shade each other, thus reducing the solar heat gains through the building envelopes. This then leads to an important finding tested in the final scenario (4) in the study, which is from a changed building envelope. It is found that changing the building facades from a combination of solid walls and glazed windows to fully-glazed facades can significantly increase the building energy use and consequently increase the greenhouse gas emissions from the greater cooling energy required. This in particular is significant in the case of building Y. While the energy use per m^2 of floor area of this building in the base case scenario is comparable to that of the building X, its energy use per m^2 would surpass that of X if the facades were fully glazed. It is very important that this finding is considered by building owners and designers in making decisions about the building facades in new constructions, particularly as the current trend in new building designs leans toward those with fully-glazed facades in order to obtain as much daylight as possible to reduce electrical lighting costs.

Based on these findings, further research should be directed at:

1. Investigating the impact of increasing building heights together with fully glazing all building facades. This is because it is possible that the impact of having fully glazed

facades on cooling energy could be counterbalanced by the reduction in solar heat gains from shading by other buildings. Hence the modelled increase in cooling energy may not be as significant as shown in this study. However, increasing building heights may instead have more impact on increasing heating energy demands as buildings would now receive less solar heat gains in the cooler periods due to shading by other buildings, yet there would be more heat loss from the increased area of glazing.

2. Investigating the impact of increasing building heights and changes in the building envelope materials on urban climate. This is still unknown and needs further investigation. If changes in building densities, heights and envelope materials have a significant impact on the urban microclimate, then this in turn would impact on the heating and cooling energy use by buildings, and consequently on the greenhouse gas emissions from buildings.

References for Chapter 8.

ABCB (2012). National Construction Code, BCA Volume 1, Australian Building Codes Board, Canberra.

CADline (2013). Tas (Thermal Analysis Simulation) Software. Available from www.cadline.co.uk/Solutions/SustainableDesign/Tas.aspx

Department of Climate Change and Energy Efficiency (2012). "Australian National Greenhouse Accounts. National Greenhouse Accounts Factors". Commonwealth of Australia, Canberra.

Standards Australia (2012). AS 1668.2-2012. The use of ventilation and airconditioning in buildings. Part 2: Mechanical ventilation in buildings. *Standards Australia, Sydney*.

Williamson, T.J., Erell, E., and Soebarto, V. (2009). Assessing the error from failure to account for urban microclimate in computer simulation of building energy performance, *Proceedings of Building Simulation 2009, 11th International IBPSA Conference, International Building Performance Simulation Association, Glasgow, 27-30 Jul, 497-504.*

APPENDIX 8.1 Building X Modelling Results

Building X	Scenario Conditions				
	S0	S1	S2*	S3	S4
Small Power (Electricity)	1,527,731	1,527,731	1,527,731	1,527,731	1,527,731
Room Heating (Gas)	556,286	271,082	555,776	598,622	574,101
Room Cooling (Electricity)	328,570	466,526	380,496	299,304	290,831
Fans (Electricity)	672,254	673,430	672,285	672,205	672,234
Pumps (Electricity)	41,877	50,622	50,456	39,918	38,058
Lighting (Electricity)	1,030,950	1,030,950	1,030,950	1,030,950	1,030,950
Condenser Pumps (Electricity)	37,362	53,049	43,267	34,034	33,071
Cooling Tower Fans (Electricity)	128,189	204,005	167,961	121,782	116,365
Total Energy (Electricity & Gas), kWh	4,323,218	4,277,395	4,428,922	4,324,545	4,283,341
HVAC Energy (Electricity & Gas), kWh	1,764,538	1,718,715	1,870,241	1,765,865	1,724,661
HVAC GHG Emissions, from electricity (kgCO2-e)	978,684	1,172,583	1,064,717	945,467	931,954
HVAC GHG Emissions, from gas (kgCO2-e)	102,535	49,966	102,441	110,338	105,818
HVAC GHG Emissions, TOTAL (kgCO2-e)	1,081,219	1,222,549	1,167,157	1,055,805	1,037,772

* The S2 analysis was conducted for a modelled 'Heat wave' period representing a 13 day period occurred between the 26-Dec and 7-Feb 2009

APPENDIX 8.2 Building Y Modelling Results

Building Y	Scenario Conditions				
	S0	S1	S2*	S3	S4
Small Power (Electricity)	514,846	514,846	514,846	514,846	514,846
Room Heating (Gas)	203,333	95,505	192,940	206,435	229,047
Room Cooling (Electricity)	124,063	175,896	132,092	117,063	183,877
Fans (Electricity)	210,970	211,209	210,966	210,972	213,444
Pumps (Electricity)	14,632	17,577	15,136	14,342	19,468
Lighting (Electricity)	401,430	401,430	401,430	401,430	401,430
Condenser Pumps (Electricity)	14,107	20,001	12,746	13,311	20,909
Cooling Tower Fans (Electricity)	43,977	70,055	50,154	42,841	56,976
Total Energy (Electricity & Gas), kWh	1,527,358	1,506,519	1,530,310	1,521,241	1,639,997
HVAC Energy (Electricity & Gas), kWh	611,082	590,243	614,034	604,965	723,721
HVAC GHG Emissions, from electricity (kgCO2-e)	330,277	400,738	341,086	322,809	400,686
HVAC GHG Emissions, from gas (kgCO2-e)	37,478	17,603	35,563	38,050	42,218
HVAC GHG Emissions, TOTAL (kgCO2-e)	367,755	418,341	376,649	360,859	442,904

* The S2 analysis was conducted for a modelled 'Heat wave' period representing a 13 day period occurred between the 26-Dec and 7-Feb 2009

APPENDIX 8.3 Building Z Modelling Results

Building Y	Scenario Conditions				
	S0	S1	S2*	S3	S4
Small Power (Electricity)	382,557	382,557	382,557	382,557	382,557
Room Heating (Gas)	217,033	106,084	216,660	219,460	230,358
Room Cooling (Electricity)	85,020	125,594	100,817	83,700	102,372
Fans (Electricity)	185,237	185,251	185,238	185,237	185,237
Pumps (Electricity)	12,367	15,108	15,118	12,293	14,573
Lighting (Electricity)	318,401	318,402	318,402	318,402	318,402
Condenser Pumps (Electricity)	9,668	14,281	11,464	9,518	11,641
Cooling Tower Fans (Electricity)	36,872	59,686	49,576	36,533	42,850
Total Energy (Electricity & Gas), kWh	1,247,158	1,206,962	1,279,831	1,247,700	1,287,991
HVAC Energy (Electricity & Gas), kWh	546,199	506,003	578,872	546,741	587,031
HVAC GHG Emissions, from electricity (kgCO2-e)	266,624	323,934	293,392	265,098	288,905
HVAC GHG Emissions, from gas (kgCO2-e)	40,004	19,553	39,935	40,451	42,460
HVAC GHG Emissions, TOTAL (kgCO2-e)	306,628	343,488	333,326	305,548	331,365

* The S2 analysis was conducted for a modelled 'Heat wave' period representing a 13 day period occurred between the 26-Dec and 7-Feb 2009

Chapter 9. Summary

J.M. Bennett

This project focusses on examining the existence and repercussions of an urban heat island and warming generally, for Adelaide city. Adelaide is unique in having a CBD that is surrounded entirely by a band of parks of the order of 500 m wide, so might be expected to have thermal characteristics that differ from other national and internationl cities. The study clearly establishes the existence of an urban heat island with greatest intensity in the Adelaide CBD, measured relative to that unique parkland belt that encompasses it. As for other cities, it arises from the greater daytime absorption of solar energy by buildings and the slower release of that absorbed energy back to the atmosphere and space overnight, compared with more open sites, which for this study, are the surrounding Park Lands. That slower release partly arises from the greater thermal mass of CBD buildings compared to open soil and vegetated surfaces, and partly from higher radiative sky temperatures over the CBD than over the Park Lands. The Adelaide heat island is present in all seasons, and has a peak intensity which varies from day to night, and with the seasons. It is strongest at night under clear skies, becoming a maximum in the early morning before sunrise. Then, it has exceeded 9°C on occasions, but is typically less than a third of that. During the daytime, the difference between temperatures in the CBD and Park Land sites is about half that during the night, and displays a smaller variation.

The peak UHI intensity occurs in association with a greater concentration of buildings, but the location of the peak in the CBD shifts between day and night. In the day under clear skies, it is located towards the NW corner of the CBD. In the early morning before sunrise, again under clear skies, it sits more centrally in the northern section of King William Street. North Adelaide has a weaker UHII, corresponding to the lower density of tall buildings compared with the CBD.

The strength of the heat island is modulated by winds, with windspeeds higher than about 3-4 m/s rapidly lowering the intensity, finally anulling it above about 8 m/s. Clouds and rain also reduce the intensity. Annual and seasonal mean intensities are smaller than daily extremes because of these moderating influences. The circumstance of low winds, most often true at night, especially under clear skies that typically occur with anticyclonic

weather patterns, gives the strongest UHI intensity. This leads to CBD buildings having higher temperatures during the night than buildings in more open sites. The presence of an urban heat island consequently has repercussions on heating and cooling energy use in buildings for maintaining comfort levels for occupants. It also impinges on comfort levels in the open within the CBD. In summer, when the interior of building usually require cooling, the maintenance of higher building temperatures overnight because of higher CBD temperatures, may result in more energy being used for cooling during the following day.

Daytime UHII is smaller than at night by a factor of about 2, but in summer, contrary to the usual circumstance of winds reducing intensities, afternoon sea-breezes increase the UHII for Adelaide, as cool air is advected towards the CBD, even though that air has passed over approximately 12 km of heated suburban landscape prior to reaching the CBD. The parklands are deduced to cool more effectively than the CBD from this breeze, an aspect that is currently receiving further study. Any consequential reduction in temperatures in the CBD could be exploited to reduce cooling energy consumption at these times, and be used to improve comfort at street level.

Modelling shows that proximity to open space does lower CBD nighttime temperatures, even for constrained spaces like Victoria Square. Observations of building wall temperatures adjacent to open space indicate that cooling of more than a degree occurs compared to enclosed spaces. Such observations are supported by modelling the thermal behaviour of buildings on North Terrace. Other modelling here indicates that more generally, greater space between buildings leads to cooler surroundings. These results can be viewed as a result of greater sky-view factors at such sites, allowing more thermal radiation to be lost to space at night than in more enclosed sites.

Any UHI has repercussions on energy use. In winter time, having a warmer urban landscape is an advantage energy-wise, since less energy is used for heating than in a cooler landscape. In summer, when the interior of buildings usually requres cooling, the evidence provided by data on temperatures and energy use in buildings clearly shows that occasions of higher temperature are accompanied by greater daytime electrical energy use. The sensitivity of this energy use in buildings to external temperature however varies markedly from one building to another –by over a factor of 2 from the least to the most sensitive buildings examined, when increases in annual mean temperatures are considered. Over all

CBD office buildings, a 1 ^{o}C increase in daytime temperatures, together with an urban heat island, indicate increases of 1500 MWh per year in electrical energy use. The corresponding increase in equivalent CO_2 emissions will be of the order of one thousand tonnes per year.

For heat wave conditions like those encountered in February 2009, modelled building electrical energy use increases above base levels over the range of about 25% to 80% between different buildings. These variations indicate there is scope for reducing the energy impact of both climate warming and short term heat waves in new building designs. It follows also that increased energy commitments may be required by supply companies under climate warming and (shorter term) heat-wave scenarios.

Other modelling under limited test secenarios, of the effects of higher air temperatures on building energy use produced the counter-intuitive result that currently, a warming climate would lower the total energy use (both electrical and gas), through the decrease in energy used for heating in winter outweighing the greater energy use for cooling in summer. The total greenhouse gas emissions would increase, however, because most heating is gas-based, whereas cooling is electrically based. This result also depends on the fact that electricity production in SA is primarily based on coal and gas, not on solar geothermal, or wind, with many CBD buildings not yet especially employing these other energy sources. It is also clear that significant improvements can be made in energy building performance. Reductions of 200-300% in summertime cooling energy commitments appear achievable using methods that are simple to implement and incorporate in new buildings. It is also clear from modelling that reduction to building glazing can make a significant contribution to energy conservation. More detailed modelling is required to clarify the details and elucidate side effects, using actual building operation and occupancy schedules.

The report provides guidelines for predicting night-time urban heat island intensities in zones around sites, through an affective sky view factor (ESVF), based on urban geometry and surface absorptivity of solar radiation, under skies that range from completely clear to completely overcast. This effective sky view factor also provides guidance for likely energy use under changes in urban building density and climate. Based on projected increases to building heights, CBD nighttime temperatures are predicted to increase by up to 1°C, and daytime near-surface values to decrease in some places from the addiitonal shading that

such increases bring. (While one degree does not seem much, it has serious implications for cooling energy use within buildings, and for accompanying CO2 emissions. However, one energy modelling result indicated that increasing building heights would reduce energy consumption slightly, because more buildings would be shaded by adjacent ones. This aspect requires detailed work for full clarification).

While many of the results reported in this work provide a reliable base for decision making for planners, there are some which are indicative rather than definitive. Some arise from limitations to data –it would consolidate several observational deductions considerably to have nighttime airborne surface temperature flights spread throughout the seasons. Such flights would produce more reliable statisics of CBD-wide temperature patterns for comparison with the temperature sensor network, and help resolve some anomalies noted in temperature patterns. They would also improve the statistics for defining the connexions of UHI intensities with some urban morphology indicators like the frontal area index. Other limitations arise principally from incomplete thermal, moisture and flow data used in the several modelling approaches, and against which different model results could be compared. Exploration of model findings was limited by resources and time constraints also. Modelling of broad scale flow through the CBD was hindered by the absence of air flow data within urban canyons at various levels, against which numerical outcomes could be tested -for instance, while temperature differences between CBD and parklands were adequately modelled, it was not possible to clearly establish penetration distances and depths of cool park air into urban and suburban environments adjacent to the Park Lands, and on effects of summertime seabreezes on temperatures within the CBD. Modelling of the flow around buildings appeared realistic, but the thermal response of air less so, because of restrictions in the model physics itself, and perhaps from the absence of sufficiently detailed data on the thermal and moisture characteristics of building cladding, pavement and vegetated surfaces. Numerical modelling of individual building responses to environmental temperature changes was performed using “standard scenarios” rather than actual data, which for the CBD itself, does not currently exist, except for temperatures from the installed network. Clearly, some of these limitations could be reduced in future, and in several chapters, further work is suggested to address them.